UNIVERSITY OF TWENTE.

Deltares
Enabling Delta Life

SANTOSS sand transport model: Implementing and testing within the morphological model UNIBEST-TC

Harm G. Nomden

SANTOSS sand transport model: Implementing and testing within the morphological model UNIBEST-TC

Enschede, 15th March 2011

This master thesis was written by
Harm Gerrit Nomden

As fulfillment of the Master's degree
Civil Engineering & Management
University of Twente, The Netherlands

Under supervision of the following committee

Dr. Ir. J.S. Ribberink	(University of Twente)
Dr. Ir. J. J. Van der Werf	(Deltares / University of Twente)
Ir. W. M. Kranenburg	(University of Twente)

Title

SANTOSS sand transport model: Implementing and testing within the morphological model UNIBEST-TC

Client	**Pages**
Deltares	Main report: 70
University of Twente	Appendices: 35

Project number Deltares

120.2340 (2010)

120.4421.005 (2011)

Abstract

Due to the large (and increasing) amount of activities in coastal areas, predictions of the short-term and long-term morphological developments are becoming more and more important to ensure safety, navigation, recreation and ecology. To make these morphological predictions different modelling systems are developed including several sand transport formulations.

Recently, a new sand transport model was released by Ribberink et al. (2010), as a result of the research project SANTOSS (SANd Transport in Oscillatory flows in the Sheet-flow regime),. The model describes the sand transport within the wave boundary layer under (1) non-breaking waves with different shapes; (2) waves combined with currents; (3) for a large range of sand grain sizes; and (4) for both the ripple and sheet flow regime. The model is calibrated on detailed experiments in oscillatory flow tunnels and wave flumes and it explicitly accounts for unsteady (phase lag) and wave non-linearity effects (skewed and asymmetric waves) and for additional processes under real waves (e.g. boundary layer streaming, Lagrangian effects and vertical orbital velocities. Based on experiment results the SANTOSS sand transport model seems to predict the measured transport rates better in comparison with other transport models.

The goal of this research is to explore the applicability and behaviour of the SANTOSS transport model within a morphological model. This has been done by implementing the SANTOSS model within the morphological model UNIBEST-TC and comparing the results of a sensitivity analysis and two test cases with measurements and the results from the TRANSPOR2004 (TR2004) transport model, which was already implemented *(Van Rijn, 2007a*, *2007b)*.

The SANTOSS model was implemented successfully in the cross-shore profile model UNIBEST-TC. Some small adjustments to the SANTOSS code were necessary to make it more robust. Additionally, special attention is paid to the generation of representative orbital velocity time series which show both velocity skewness and acceleration skewness. Therefore, different theories are analyzed, tested and combined. Because the SANTOSS model does not cover the transport above the wave boundary layer, the current-related suspended load transport at higher levels is computed using the TR2004 formulations.

The sensitivity analysis focused on (1) predicted net transport rates and (2) the influence of several processes on the transport. It showed that the SANTOSS model reacts almost in the same way as the bed load and wave-related suspended load of TR2004 together. With the only difference that transport rates predicted by the SANTOSS model are lower over the whole range. In the ripple regime the transport rates predicted by SANTOSS are reduced to zero or become even slightly negative, mainly due to phase lag effects. The TR2004 model predictions are also almost reduced to zero when a phase lag factor is applied to the wave-related suspended load. In the sheet flow regime the increasing undertow velocity near the bed (due to partially breaking waves) and enhanced suspended sediment generate a high offshore directed current-related suspended load, which becomes dominant for both transport models.

The influence of different transport and hydrodynamic processes within the two transport models, like phase lag, acceleration and surface wave effects (only for the SANTOSS model) are analysed. Also influences of breaking waves and the use of different orbital velocity theories are explored for both models. Main conclusions are:

- In general, the two transport models react in the same way on changes in input or on exclusion of a certain process;

- Phase lag effects and surface wave effects (especially vertical orbital velocities) are of importance in the ripple regime. In the higher sheet flow regime the relative influence is low, because it is totally dominated here by the current-related suspended load.
- Acceleration effects are taken into account in a different way by the two transport models and has much more influence on the TR2004 predictions;
- The level from which the superimposed mean current velocity is extracted as input for the bed load transport is of large importance. The two transport models use a different level. This was shown to have a significant influence on the predicted transport rate.

To assess the performance of the two transport models on predicting morphological evolution, two test cases are used: LIP IID test 1B (erosive conditions, sand bar development) and test 1C (accretive conditions, onshore sand bar migration). For test 1B, modeled hydrodynamics agree in general well with measurements, but modeled concentrations of suspended sediment are overestimated offshore of the bar. Both transport models show a weak sand bar development and too much offshore bar migration (SANTOSS slightly more than TR2004). For test 1C there is some differences in modeled and measured hydrodynamics: velocity skewness of the orbital velocities and the undertow velocity in the trough onshore of the sand bar. This also explains the bad performance in morphological predictions by both transport models: small offshore bar migration instead of clear onshore migration.

In this research, especially the transport model formulations and the influence of several processes on the final net transport rates have been analysed. Based on the knowledge from the analyses, several recommendations are proposed for further research, changes to the transport formulations and necessary measurements to validate the influence of several processes.

Preface

This thesis represents the work that has been carried out at Deltares for my Master thesis project, relating the prediction of sand transport under coastal conditions by two transport formulations in a coastal morphological model. I really liked working with theories and models and it is something in I want to keep doing in the future, although it has also brought a lot of standard modelling frustration about theories that are hard to understand, are not perfectly implemented, do not work well in a specific case, the large uncertainties in this complicated modelling field and off course the endless debugging (also due to my own mistakes).

First, I would like to thank my three supervisors Jan, Jebbe and Wouter for introducing me in the world of sand transport, their interest in my work and their useful comments on my work. Especially my daily supervisor Jebbe, who I could interrupt at anytime, to discuss every strange topic or problem I had on my mind. I hope my work have contributed to their work and knowledge.

Next, I'm really grateful to have worked at Deltares, which gave me the opportunity to meet interesting and smart people and who gave me access to a tremendous amount of knowledge about hydrodynamic and sand transport modelling and coastal models. I would like to thank the people at the unit Marine and Coastal Systems and also Dirk Jan Walstra for answering the questions I had about the modelling and simulating part. I also want to thank Mr. Abreu for borrowing his code on wave form definition, which helped me a lot during my research.

I want to thank my fellow students at Deltares: Peter, Martijn, Sanne, Ingrid, Jorik, Rik, Kees, Giorgio (sorry again for calling you a student), Arnold, Brice and the students at Hydraulic Engineering for keeping me from my work, drinking coffee, chatting around and also discussing serious topics (football). Also I like to thank my housemates in Delft and in Enschede (sorry for the stress I brought home) and my friends of Pallet # for the great 7.5 years and for the phone calls when they were stuck in a traffic jam from work.

Last but not least, I thank my parents and brothers and especially my girlfriend Lianne for her contribution to my work, good advices, love and lots of encouragements.

I hope you will enjoy reading this report.

Harm Nomden

Enschede, March 2011

Content

1. Introduction 1
1.1. Context 1
1.2. Research definition 2
1.3. Research questions and methodology 2

2. Research background 5
2.1. Introduction 5
2.2. Hydrodynamic aspects 5
2.2.1. Wave propagation 5
2.2.2. Orbital motion 5
2.2.3. Currents 7
2.2.4. Boundary layer flow 7
2.3. Sediment transport aspects 7
2.3.1. Sediment properties 7
2.3.2. Transport regimes in oscillatory flow 8
2.3.3. Bed shear stress and wave form effects 8
2.3.4. Unsteady effects in oscillatory flow 9
2.3.5. Influence surface wave effects on sediment transport 9
2.4. Morphological aspects and modelling 9
2.5. Conclusions 10

3. Model descriptions 11
3.1. Introduction 11
3.2. UNIBEST-TC 11
3.2.1. Wave propagation module 11
3.2.2. Mean current profile module 12
3.2.3. Near bed orbital velocity module 12
3.2.4. Sediment transport module 12
3.2.5. Bed level change module 12
3.3. Two practical sediment transport models 12
3.3.1. TRANSPOR2004 sand transport model 13
3.3.2. SANTOSS sand transport model 15
3.3.3. Performance transport models (previous research on comparison transport predictions with experiment data) 17
3.4. Conclusions 18

4. Implementation SANTOSS model in UNIBEST-TC 19
4.1. Introduction 19
4.2. The SANTOSS sand transport code 19
4.3. Influence of bed-slopes on sediment transport 21
4.3.1. Slope effect on threshold of sediment transport 22
4.3.2. Slope effects on the transport rates and the direction 22
4.3.3. Including slope effects in SANTOSS formulations in UNIBEST-TC 23
4.4. Short wave flow velocity 24
4.4.1. Analysis available theories 25
4.4.2. Application SANTOSS in UNIBEST-TC 27
4.5. Wave group effect on near bed orbital velocity 29
4.5.1. Current application in UNIBEST-TC 29
4.5.2. Application SANTOSS in UNIBEST-TC 30

4.6. Superimposed current 30
4.6.1. Current application in UNIBEST-TC 30
4.6.2. Application SANTOSS in UNIBEST-TC 31
4.7. Suspended load transport above wave boundary layer 31
4.8. Conclusions 32

5. Sensitivity analysis transport models within UNIBEST-TC 33
5.1. Introduction 33
5.2. Set-up and standard settings 33
5.3. Model behaviour 34
5.3.1. Hydrodynamic exploration 36
5.3.2. Grain size variation 36
5.3.3. Wave period variation 38
5.3.4. Wave height variation 40
5.4. Comparison between orbital velocity theories 42
5.5. Conclusions 45

6. Application of SANTOSS model to test cases 47
6.1. Introduction 47
6.2. Description LIP IID experiments 47
6.3. Hydrodynamic calibration 47
6.4. Transport predictions and morphology 50
6.5. Conclusions 51

7. Conclusions, discussion and recommendations 63
7.1. Introduction 63
7.2. Conclusions 63
7.3. Discussion 65
7.4. Recommendations 66

8. References 69

List of Symbols 73

List of Figures and Tables 75

A. UNIBEST-TC with TR2004 and SANTOSS 1
A.1. UNIBEST-TC: General user-defined input and boundary conditions 1
A.2. UNIBEST-TC: Wave module 3
A.3. UNIBEST-TC: Current profile module 7
A.4. UNIBEST-TC: Orbital velocity module 12
A.5. UNIBEST-TC: Sediment transport modules 14

B. Different orbital velocity theories 23
B.1. Current options and proposed changes to orbital velocity module 23
B.2. Analysis formula Abreu et al. (*2010*) 23
B.3. Generation of necessary wave form parameters 27

C. Description FORTRAN codes 33

1. Introduction

This research focuses on the implementation and testing of the new SANTOSS sand transport model in the coastal morphologic modelling system UNIBEST-TC. This chapter describes the research objective, research framework and the research questions, but first provides a short context of the research.

1.1. Context

Due to the large (and increasing) amount of activities in coastal areas, it is becoming more and more important to be able to predict short-term and long-term morphological developments in coastal areas and to increase knowledge of important hydrodynamic and sand transport processes. Points of interest are for example the development of the coastline, the impact of sea level rise on coastal development, the design of sea harbours, the planning and design of sand nourishment schemes to protect the land and other coastal defence measures or policies in order to the conserve or protect the coastal environment and ecosystem.

The transformation of waves, local currents, and the resulting sediment transport in the nearshore depend strongly on the bathymetry. If sediment flux gradients modify this bathymetry (e.g., onshore or offshore sandbar migration), subsequent wave and current patterns change as well. This, in turn, leads to further modifications of the bathymetry (See Figure 1-1). The complexity lies in the prediction of the strong variability in time and space and the feedback between the processes.

Morphological modelling systems are used to compute the hydrodynamics and the resulting sediment transport and morphological evolution. Field and lab research during the last decades resulted in better knowledge of waves and currents and their (combined) influence on the sand transport. Based on this knowledge more accurate practical sand transport models were developed. The current state of the art sand transport model is TRANSPOR2004 (*Van Rijn, 2007a*, *2007b; Van Rijn, Walstra, et al., 2007*), which is implemented in the morphological models of Deltares.

Recently, as a result of the research project SANTOSS (SANd Transport in Oscillatory flows in the Sheet-flow regime), a new sand transport model was released by Ribberink et al. (*2010*). They showed that the new transport model is able to predict the transport rates more accurately than existing transport models for the detailed transport measurements in laboratory experiments with coastal conditions.

The SANTOSS transport model explicitly accounts for the most important physical processes through parameterizations based on the experimental data and sound

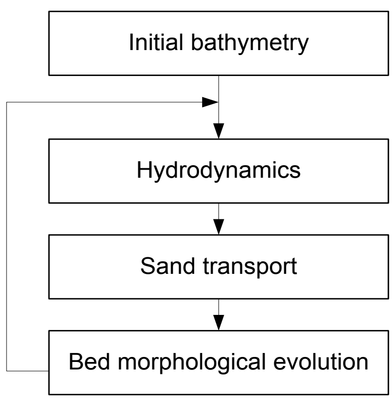

Figure 1-1: The morphodynamic loop

understanding of the physical processes (*University of Twente, 2010*). Due to new measurements under asymmetric oscillating flows (at the Oscillating Flow Tunnel in Aberdeen) and under progressive surface wave (at the Groβer Wellenkanal in Hannover) they were able to develop a new formula with a focus on unsteady, non-linear and surface wave effects.

1.2. Research definition

The next step in the development of a sand transport model is to test it in a morphological modelling system. Although the transport formulations of the SANTOSS model only focus on regular and non-breaking waves it is interesting to check whether it is possible to implement the formulations in a coastal morphological model, to test the behaviour under changing conditions and test for a few selected morphological test cases.

The objective of this research is:

> *To explore the applicability and behaviour of the SANTOSS sand transport model within the framework of the cross-shore profile model UNIBEST-TC in comparison with TRANSPOR2004.*

The choice for the cross-shore profile model UNIBEST-TC (TC: Time-dependent Cross-shore) is primarily based on correspondence with the focus of this research (the SANTOSS model focused on wave-dominated transport predictions) and relative simplicity of the model (assumes cross-shore profile is uniform alongshore).

A new version of UNIBEST-TC including the TR2004 formulations is used as starting point for this research. This gives the opportunity to use the TR2004 predictions as a reference point and also make a detailed comparison between the two sand transport models. Further, the hydrodynamic theories used in this version are assumed to give a good representation of the hydrodynamics. Only if necessary, changes are made to these theories.

This research focuses on non-cohesive uniform sediment. Effects on transport rates due to gradation, flocculation, clay coating, packing or biological and organic material effects are not taken into account.

1.3. Research questions and methodology

For this research five research questions are stated. Next to the implementation of the SANTOSS sand transport model and the application, also the influence of several important processes is explored in more detail:

1. *What are the main characteristics of UNIBEST-TC and the sand transport models and what are necessary changes for the implementation of the SANTOSS model in the UNIBEST-TC environment?*

This question is answered by first summarizing the recognized hydrodynamic, sediment transport and morphological processes (Chapter 2). The focus lays here also on the cross-shore transport. Next, the main aspects of the morphological model UNIBEST-TC and the two transport models are discussed and how the important processes are included (Chapter 3). The necessary changes made to the SANTOSS model and to UNIBEST-TC to make implementation possible are extensively discussed (Chapter 4).

2. *What are the differences in total sand transport rates predicted by the two sand transport models under a large range of conditions (e.g. grain size, wave height, wave period, wave shape)?*
3. *What is the relative influence of the specific transport aspects (e.g. bed forms, wave asymmetry, surface wave effects and phase lag effects) on the sediment transport rates?*

For the second and third research question a sensitivity analysis of the UNIBEST-TC versions with TR2004 and SANTOSS is executed (Chapter 5). Not only the total transport rates are compared but also the different sediment loads (bed-load, wave-related suspended load and current-related suspended load and the loads predicted by SANTOSS) are separately discussed. During the sensitivity analysis the influence of the different processes is defined by excluding these processes individually.

4. *To what extent is it possible to predict morphological changes using the UNIBEST-TC version with the SANTOSS model and what is the performance compared to TR2004?*
5. *What is the relative influence of specific hydrodynamic and transport aspects (e.g. bed forms, wave asymmetry, surface wave effects and phase lag effects) on the morphological behaviour?*

It is tried to answer the final two research questions by applying the both transport models to two test cases. The two test cases are used to assess the performance of the models on predicting morphological changes (Chapter 6) and to check what kind of effect the different specific processes have on the morphological evolution.

This report concludes with answering the research questions and recommendations for further research.

2. Research background

2.1. Introduction

In this research several hydrodynamic and transport processes, which are of large importance, are described in this chapter. In the first paragraph a description of hydrodynamic aspects is given, followed by sediment transport aspects in the next paragraph. At the end of this chapter, it is described how the transport and hydrodynamic aspects influence sediment transport and thus also cross-shore morphology.

2.2. Hydrodynamic aspects

2.2.1. Wave propagation

Waves near the coast can be divided into three classes based on their wave period (*Dean & Dalrymple, 2002*). The first class consist of wind waves and swell with typical periods of 1-25 seconds and varying in wave height. These short waves travel in wave groups which propagate with the wave group velocity. In deep water the wave group velocity is equal to half the celerity of individual waves. Waves propagate into more shallow water slow down until their velocity is equal to the wave group velocity. The waves lengths get shorter, the waves change direction (refraction) towards the normal of the coast line, become higher (shoaling) and change in shape (non-linearity). Meanwhile, the waves loose energy smoothly due to dissipation by bed friction and in a short period of time by breaking in really shallow water.

A second class of waves is formed by “low-frequency waves” (infra-gravity waves). They are generated at open sea by group-behaviour of wind waves. Their periods range between 20-100 seconds. Low-frequency waves include both free and forced waves. In the surf zone low-frequency waves become free, because the wind waves that cause the forcing are decaying there. At the shore these long waves reflect and can even get trapped in the surf zone.

The third class of waves is formed by tidal waves. In the Netherlands the important tidal components are within the diurnal and semi-diurnal regime in which the most important constituent is the semi-diurnal lunar contribution (a period of 12 hours and 25 minutes).

2.2.2. Orbital motion

The orbital motion of the water particles under waves change when water becomes shallow. From a circular movement at deepwater to elongated ellipses (and “purely” horizontal motion near the bottom) at shallow water. The orbital motion changes together with the waves, which means that the near-bed orbital velocity also shows non-linearity.

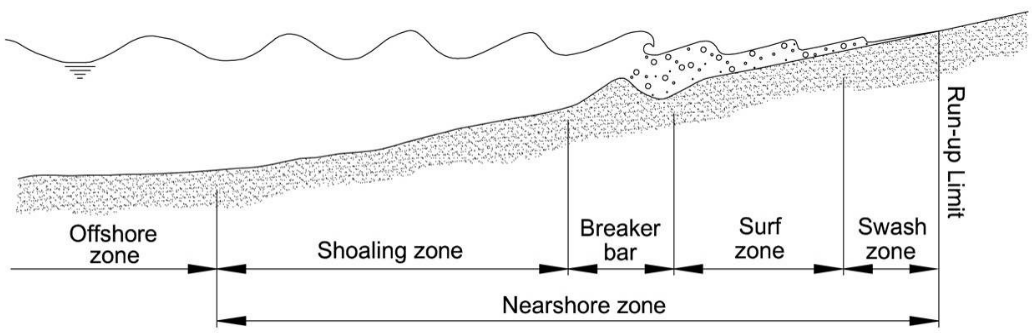

Figure 2-1: Simple example of a cross-shore profile + terminology

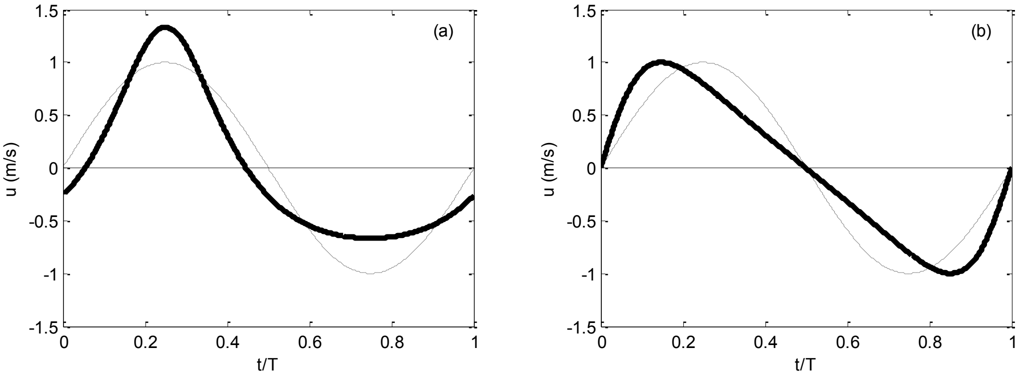

Figure 2-2: Free-stream velocity under skewed (a) and asymmetric (forward leaning) wave (b) compared to a sine wave.

Non-linearity consists of wave skewness (velocity skewness) and wave asymmetry (acceleration skewness), which are shown in Figure 2-2. Under skewed waves, the crest velocities become higher and the crest period shorter, while the trough velocities are lower and the trough period longer. Under asymmetric waves the acceleration and deceleration periods are not of equal length. There are two methods used to define the skewness and asymmetry of the orbital flow velocity. The first method is used in the SANTOSS formulations and states the skewness R and the asymmetry β as:

$$R = \frac{u_{w,\max}}{u_{w,\max} - u_{w,\min}} \quad \beta = \frac{a_{w,\max}}{a_{w.\max} - a_{w,\min}} \tag{2.2.1}$$

Where $u_{w,max}$ ($u_{w,max}$) = the maximum velocity under the crest (trough) and $a_{w,max}$ ($a_{w,min}$) = the maximum acceleration (deceleration). For realistic conditions the values of both R and β range between 0.5 – 0.8, where both are 0.5 for sinusoidal waves. The other method is to use the time-averaged third power of the velocity scaled by the third power of the standard deviation to define the velocity skewness Sk (used by different authors like:

$$Sk = \frac{\left\langle u_w^{\;3} \right\rangle}{\left\langle u_w^{\;2} \right\rangle^{1.5}} \quad As = \frac{\left\langle H\left(u_w\right)^3 \right\rangle}{\left\langle u_w^{\;2} \right\rangle^{1.5}} \tag{2.2.2}$$

The acceleration skewness (asymmetry of the wave: As) is defined using the same expression only replacing u_w in the numerator by its Hilbert transform. For natural

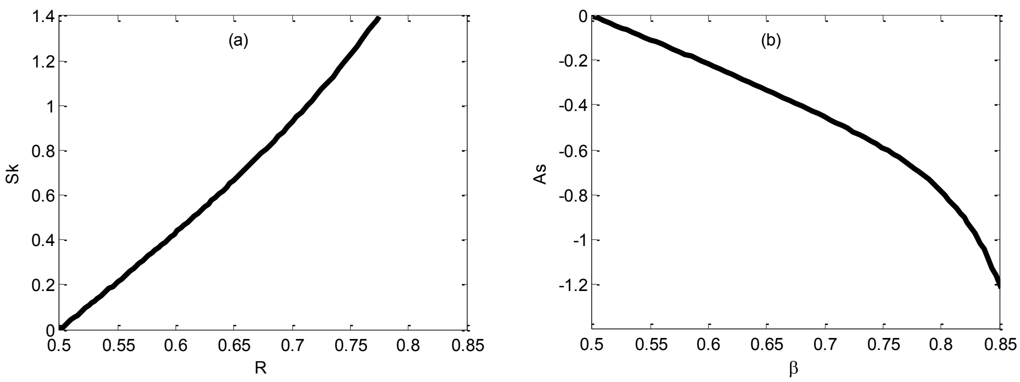

Figure 2-3: Relation between the wave form parameters using the formula of Abreu et al. (2010, see par.4.4 and Appendix B): (a) skewness R and Sk for only skewed (non-asymmetric) waves; (b) asymmetry β and As for only asymmetric (non-skewed) waves.

conditions the range of Sk lies between 0 → 1.4 and the range of As between 0 → -1.4 (Figure 2-2). Thus, both Sk and As are 0 for sinusoidal waves and for forward leaning wave asymmetry As becomes negative. Further in this report the parameters for skewness (R and Sk) and for asymmetry (β and As) are used several times, so these should be remembered very well and not be mixed up.

2.2.3. Currents

Waves induce a net transport of water towards the coast in the upper water layers, which induces set-up near the coast and currents. Different types of nearshore currents can be distinguished like wave-driven longshore currents, which are induced by waves approaching the coast under an angle (refraction of waves induce a long-shore momentum). Another type is a cross-shore current that is uniform in the longshore direction and which takes place in the lower layers (undertow). Especially under breaking waves this undertow can become high. The water that is transported towards the coast can also be returned by rip currents (non-uniform in longshore direction). The magnitude of these different currents lies in the order of 1 m/s.

2.2.4. Boundary layer flow

In shallow waters the near bed orbital velocity under waves is basically horizontal. At the bed the flow velocity is zero and due to viscosity the flow velocity above the bed is reduced due to the bed. The transition zone, between the bed and the point where the flow velocity is not anymore influence by the bed is called the boundary layer. Because most of the sediment transport takes place near the bed this process plays an important role in sediment transport (*Dohmen-Janssen, 1999*).

The thickness of the boundary layer depends on the Reynolds number ($Re = U_w * A_w / v$) and the relative roughness (k_s/A_w) in which U_w is the orbital velocity amplitude, A_w is the amplitude of the horizontal orbital displacement, v is the kinematic viscosity and k_s is the bed roughness height. As a result the wave boundary layer for short waves is really small (order of centimetres) and for tidal waves the flow profile has almost a logarithmic profile like for currents.

Due to the lower velocities within the wave boundary layer, the flow in the boundary layer contains less inertia and reacts faster to varying pressure gradients. This is why the flow velocity in the boundary layer is ahead in phase to the free-stream velocity (for laminar flow 45º, for rough turbulent flow <45º).

A final important point about the hydrodynamics in the wave boundary layer is the streaming that is present. Despite of a mean velocity above the wave boundary layer there might be a different mean velocity present within the wave boundary layer. This may have two causes:

- Wave skewness causes a difference in generated turbulent energy between the two half-cycles, which leads to differences in the velocity profile in the wave boundary layer and a possible net streaming.
- The vertical and horizontal orbital velocities are not exactly 90° out of phase in the boundary layer as they would be in a frictionless flow (leads to an onshore-directed mean velocity close to the bed (*Longuet-Higgins, 1953*)).

2.3. Sediment transport aspects

2.3.1. Sediment properties

Beside hydrodynamic parameters also sand characteristics are important for correct predictions of cross-shore transport. Sediment density (2650 kg/m^3 for sediment from North Sea), shape (assumed to be spherical, although this not the case) and the grain size are important factors. This study focuses on non-cohesive sand, which means that the grain sizes diameter is higher than 0.1 mm. If the sediment consists of a mixture of sand with different grain sizes, the grains of different sizes may influence each other. As said before, this research focuses on uniform sediment, so gradation effects are assumed to be low and thus not considered in this study.

2.3.2. Transport regimes in oscillatory flow

The different transport regimes in oscillatory flows are characterised by the bed forms and can be predicted based on the mobility number:

$$\psi = \frac{u_{\max}^2}{(s-1)gD_{50}} \tag{2.3.1}$$

In which u_{max} = maximum orbital velocity, s = sediment specific gravity (2,65 for sand), g = acceleration due to gravity and D_{50} = sediment grain size for which 50% of the sediment sample is finer. The ripple regime is found for $\Psi<190$: bed forms are developed, ranging from small vortex ripples to large mega-ripples and dunes. At small vortex ripples twice every wave cycle a vortex is formed in the lee of the crest of the ripples, which results every time in sediment taken into suspension. Also 2D- and 3D ripples are observed which are linked to respectively large (<0.2 mm) and small grain sizes (>0.3 mm). The sheet-flow regime can be found for $\Psi>300$: at high orbital velocities the small ripples are washed out and the bed becomes plane. A thin layer with high sand concentrations is moving in a "sheet" over the bed. In the transition zone $190<\Psi<300$ the bed is really sensitive.

Based on ripple dimension measurements under irregular waves it was recommended by O'Donoghue et al. (*2006*) to use the mean of the one tenth highest near bed velocities for the calculation of the mobility number. Furthermore, it must be mentioned that the dimensions of the bed forms cannot be predicted very well. Extensive measurements on bed forms under oscillatory flows have been taken place in oscillatory flow tunnels, but the influence of the realistic conditions (e.g. surface wave conditions and combination with currents) is not totally clear.

2.3.3. Bed shear stress and wave form effects

Sediment gets into motion due to bed shear stresses. The non-dimensional bed shear stress is defined by the Shields parameter θ:

$$\theta = \frac{0.5f \cdot u^2}{(s-1)gD_{50}} \tag{2.3.2}$$

In which f = friction factor, which positive related to the orbital diameter and negatively related to the bed roughness height. This relation with the velocity above the bed would have explained the net bed-load transports under skewed waves. The roughness height depends largely on the sediment grain size and the ripple dimensions, but also a sheet flow (mobile-bed) increases the roughness. Overall, wave skewness is already taken into account quite well by different transport models. Due to the higher onshore velocities higher bed shear stresses are found under the crest and lower bed shear stresses under the trough.

A second example is that acceleration of the near bed velocity leads to a smaller wave boundary layer and thus a higher velocity gradient near the bed and a higher bed shear stress. For non-skewed but asymmetric waves (forward leaning in this case) this would lead to a higher onshore bed shear stress under the crest and a lower offshore bed shear stress under the trough compared to sinusoidal waves. Nielsen (*2006*) introduces a sediment mobilising velocity which shows that the bed shear stress is quadratic related to a linear combination of the velocity and the acceleration. As a result, wave asymmetry leads to higher onshore bed shear stresses under the crest and lower offshore bed shear stresses under the trough. The same conclusions were made based on measurements in fixed bed flow tunnel experiments within the SANTOSS project (*Van der A, et al., 2008*) and based on extensive model studies of sediment transport processes under combined skewed and asymmetric waves using the PointSand Model (fully developed U-tube conditions) by Ruessink et al. (*2009*).

2.3.4. Unsteady effects in oscillatory flow

In steady flow the sand transport rate is proportional to a power (>1) of the near bed velocity. Many sediment transport models assume that the sediment transport in oscillatory flows also reacts instantaneously to the near bed orbital flow velocity or to the bed shear stress which is in some way related to the near bed flow velocity.

Unsteady effects are recognized when the phase lag between bed shear stress and concentration profiles (so no instantaneous reaction) leads to a change in sediment transport (*Dibajnia & Watanabe, 1998; Dohmen-Janssen, 1999*). Phase lag effects are especially of importance when the vertical sediment pick-up and settling processes take place at a time-scale of the same order as the wave period (in rippled-bed conditions or in sheet flow conditions for fine sediments, high orbital velocities and short wave periods). Due to phase lag effects net transport rates might be reduced or even change direction.

Ruessink et al. (*2009*) concluded also using their PSM modelling studies that phase lag effects are an essential mechanism for predicting transport rates. The wave-induced transport rates under velocity skewed waves reduce due to phase lag effects. They conclude that this reduction goes to zero, which means that the sediment transport is only determined by the current-related negative sediment transport.

2.3.5. Influence surface wave effects on sediment transport

Progressive surface waves induce Lagrangian and Eulerian effects (*O'Donoghue & Ribberink, 2007; Schretlen, et al., 2008*), which might lead to a large difference in transport rates compared to the same conditions in Oscillating Flow Tunnels, going up to a factor 2.5 (*Dohmen-Janssen & Hanes, 2002*). The Eulerian effects are already mentioned before (streaming due to skewness and Longuet-Higgins streaming) of which the Longuet-Higgins streaming is not present in an oscillatory flow tunnel, but also leads to an additional mean bed shear stress (*Longuet-Higgins, 2005*). The Lagrangian effect leads to extra onshore directed transport due to two processes that also count up to a certain amount for sediment particles:

- A fluid particle in a wave move with larger forward velocities at the top of its orbit compared to the backward velocities at the bottom.
- The fluid particles move with the wave during its forward motion and against it during its backward motion, and they thus experience a longer crest period and a shorter trough period.

2.4. Morphological aspects and modelling

Waves, current and sediment transport in coastal areas depend strongly on the bathymetry. Spatial gradients in sediment transport rates modify the bathymetry, which leads to feedback to the wave and current patterns and the resulting sediment transport. A strong feedback is visible in a coastal system and due to the ever changing wave conditions the system keeps trying to find a new equilibrium. Examples of changes are migration or deformation of sand dunes, trenches, and erosion/accretion of beaches. Especially in the nearshore zone of sandy beaches changes in morphology are clearly visible (e.g. on- or offshore migration of sand bars).

Three different beach types are distinguished: reflective beaches (steep slope, incoming waves are reflected), dissipative beaches (incoming waves become totally dissipated) and moderate dissipative (an intermediate beach type). The Dutch coast can be placed in the moderate dissipative beach type (average wave height at deep water is about 1 m, peak wave period is about 6 s, the tidal range is 1.5-3.0 m, sediment grain sizes of about 300 μm and the near shore zone has a width of several hundreds of meters and a bottom slope of about 1:200). A large part of the Dutch coast is further characterized by 2 or 3 adjacent sand bars parallel to the shore line.

The generation and decay of a sandbar happens slowly over time and shows a cyclic cross-shore behaviour, arising near the shoreline and slowly (on average 0.01 m/day) moving through the surf zone and finally decaying in the outer nearshore zone at depths of 5-7 m (*Grasmeijer, 2002*). Superimposed on these long-term changes are weekly and monthly on- and offshore fluctuations (with the order of 1 m/day).

Morphological process models have problems to reproduce the natural behaviour of coasts on timescales of a few days to weeks and have shown high uncertainty on longer terms (*Ruessink, et al., 2007*). Most of these models predict the amount of beach erosion pretty well. Beach erosion, for example offshore migration of sand bars, takes place during storms when large waves break on the bar. The feedback between breaking waves, undertow, suspended sediment transport, and the sandbar are important here.

On the other hand, the models have trouble to predict the recovery of the beach profile under calm conditions (*Ruessink, et al., 2007; Van Rijn, et al., submitted*). Accretion, for example onshore bar migration, is predicted for energetic and (almost) non-breaking wave conditions (especially swell conditions). Important in accretive conditions is the feedback between near-bed wave skewness, bed-load transport, stokes drift, and the sandbar, with negligible to small influence of bound infra-gravity waves.

2.5. Conclusions

This chapter summarized several hydrodynamic- and sediment-related processes which play a significant role in wave-dominated coastal cross-shore sand transport. It is made clear that there is a strong interaction between the different processes and that they all have an influence on the net transport rate (onshore or offshore directed depending on the conditions). Furthermore, it is made clear that morphological changes due to gradients in sediment transport rates results in a strong feedback towards the hydrodynamics and resulting transport rates. Later in this report, several of the processes described in this chapter are point of discussion or mentioned again, so it is assumed that the reader understands these processes.

3. Model descriptions

3.1. Introduction

This chapter gives a description of the three different models used in this research. First, a short description is given of the morphologic model UNIBEST-TC followed by a description of the two sand transport models TRANSPOR2004 (*Van Rijn, 2007a*, *2007b*) and SANTOSS (*Ribberink, et al., 2010*). At the end of this chapter a previous comparison between the performances of the two sand transport models is discussed, which focused on the prediction of transport rates measured during experiments.

3.2. UNIBEST-TC

UNIBEST-TC is the cross-shore sediment transport module of the program package UNIBEST, which stands for UNIform BEach Sediment Transport (*Bosboom, et al., 2000*). All modules of this package consider sediment transports along a sandy coast which locally may be considered uniform in alongshore direction. UNIBEST-TC (TC: Time-dependent Cross-shore) is designed to compute cross-shore sediment transports and the resulting profile changes along any coastal profile of arbitrary shape under the combined action of waves, longshore tidal currents and wind. The model allows for constant, periodic and time series of the hydrodynamic boundary conditions to be prescribed. The UNIBEST-TC software can be used for several coastal problems, e.g.:

- Dynamics of cross-shore profiles;
- Cross-shore development due to seasonal variations of the incident wave field;
- Bar generation and migration;
- To check the stability of beach nourishments;
- To estimate the impact of sand extraction on the cross-shore bottom profile development.

The UNIBEST-TC model is a parametric cross-shore profile-model, which is based on coupled, wave-averaged equations of hydrodynamics (waves and mean currents), sediment transport and bed level evolution. The formulations are divided over 5 modules: (1) the wave propagation module, (2) the mean current profile module, (3) the wave orbital velocity module, (4) bed load and suspended load transport module, and (5) bed level change module. For each predefined time step the modules are called in succession to calculate the hydrodynamic and transport rates over a whole profile after which the bed level changes define the new bathymetry, which is used as input for the next time step.

3.2.1. Wave propagation module

The wave propagation model consists of three first-order differential equations. The first one is the time-averaged wave energy balance of Battjes and Janssen (*1978*) extended with a breaker delay concept *(Roelvink, et al., 1995)*. For the maximum wave height (based on wave height to depth ratio), the breaker coefficient γ of Ruessink et al. (*2003*) is used. The second differential equation is the balance equation for the energy contained in surface rollers of Nairn et al. (*1990*). The third differential equation describes the horizontal momentum balance from which the mean water level set-up is computed. The refraction of the waves is computed using Snell's law. The three coupled equations are solved by numerical integration over the cross-shore profile. These equations generate the input required by the local models for the vertical velocity profile, the concentration vertical and the bed-load transport.

3.2.2. Mean current profile module

Based on the local wave forcing, mass flux, tide and wind forcing, a vertical distribution of the longshore and cross-shore velocities is calculated, taking into account the near-bed streaming. The vertical distribution of the flow velocities is determined with the Quasi-3D approach of Reniers et al. (*2004*). Based on the local wave forcing, the mass flux, tide and wind forcing, a vertical distribution of the longshore and cross-shore velocities is calculated. The near-bed streaming is included in the calculations. In this module the Eulerian current velocities are also adjusted to get the GLM velocities (including Stokes drift) using the method of Walstra et al. (*2000*).

3.2.3. Near bed orbital velocity module

The near bed velocity signal ($u_b(t)$) is constructed to have the same characteristics of short-wave velocity skewness, amplitude modulation ($u_{nl}(t)$), bound infragravity waves ($u_{bw}(t)$), and mean flow ($u_{mean}(t)$) as a natural random wave field. The near bed velocity is the sum of these three components: $u_b(t) = u_{nl}(t) + u_{bw}(t) + u_{mean}(t)$.

Several theories (*Rienecker & Fenton, 1981; Isobe & Horikawa, 1982; Van Thiel de Vries, 2009; Ruessink & Van Rijn, in preparation*) are available to develop a short wave (regular wave) velocity time series including skewness and asymmetry. These models consist of a combination of sines and cosines with certain amplitudes which represent the right wave shape (in more detail discussed in paragraph 4.3).

An amplitude modulation is taken place to include the effect of wave groups, with the focus on the preservation of velocity skewness. The bound long wave velocity is calculated using the method of Roelvink and Stive (*Bosboom, et al., 2000*) (In more detail discussed in paragraph 4.5).

3.2.4. Sediment transport module

The transport formulations for both bed load and suspended sediment load of Van Rijn (*2007a*, *2007b*) are already implemented including the Bagnold approach to account for bed slope-induced transport (see paragraph 4.3 for further explanation of slope effect).

Problems can be noticed with the wet-dry boundary. In UNIBEST-TC an approach is used in which the most landward wet computational grid point at each time step is taken as the grid point where the non-dimensional wave period ($T_p/(gh)^{0.5}$) exceeds a certain factor (TDRY = 20-40) for the first time. For the range of wave periods considered in the present erosion cases, this implies that no hydrodynamic and transport computations are carried out in depths less than about 0.1 m (small-scale) and 0.5 m(large-scale test) respectively. The sediment transport rate at the last wet grid point is translated into an offshore or onshore advection of the dry grid points by extrapolation over part of the dry beach and dune profile (horizontal extent of the extrapolation is based on local run-up.)

3.2.5. Bed level change module

At the end of each time step the bed levels are updated through:

$$\frac{\partial z_b}{\partial t} = \frac{\partial\left(q_b + q_{s,w} + q_{s,c}\right)}{\partial x} \qquad (3.2.1)$$

3.3. Two practical sediment transport models

Because of their relative simplicity, practical sand transport models instead of process-based models, are used in practice for sediment transport predictions. Three classes of practical sand transport models can be distinguished:

- Time-averaged models use the wave-averaged values of velocity an concentration. The transport always takes place in the direction of the mean current.

- Quasi-steady models relate the instantaneous sediment transport rates to some power of the instantaneous near bed flow velocity or bed shear stress *(Ribberink, 1998; Nielsen, 2006)*.
- Semi-unsteady models account for unsteady (phase lag) effects without modelling the detailed time-dependent horizontal velocity and vertical concentration profiles (*Dibajnia & Watanabe, 1998; Dohmen-Janssen, et al., 2002*).

The two transport models considered in this study (SANTOSS and TRANSPOR2004) are different concerning this subdivision and include or exclude several effects discussed in Chapter 2. Below, the transport models are shortly described after which a previous comparison between the two sediment models (*Ribberink, et al., 2010; Wong, 2010*) is shortly discussed. An extensive description of the two transport models can be found in Appendix A.5.

3.3.1. TRANSPOR2004 sand transport model

TRANSPOR2004 makes a division between bed-load transport and suspended-load transport. The bed load transport is modelled in a quasi-steady way (the bed load transport is instantaneously related to the bed shear stress), and the suspended load is based on a time-averaged approach. An improvement towards hydrodynamic and morphological modelling was the introduction of a bed roughness predictor within the TR2004 model, which predicts bed forms and the experienced roughness by the flow over the bed.

Bed roughness predictor

TR2004 distinguishes wave-related and current-related bed roughness. The current-related roughness ($k_{s,c}$) is computed from the roughness heights induced by ripples ($k_{s,c,r}$), mega-ripples ($k_{s,c,mr}$) and in case of estuaries or rivers also dunes ($k_{s,c,d}$, not for coastal waters). For coastal areas: $k_{s,c} = [k_{s,c,r}^2 + k_{s,c,mr}^2]^{0.5}$. The wave-related bed roughness is only linked to the ripples due to the small length-scale of the orbital motion ($k_{s,w} = k_{s,c,r}$). The bed roughness induced by these bed forms is linked to the non-dimensional mobility number Ψ_{TR2004} based on both the depth-averaged current and the orbital motion:

$$\psi_{TR2004} = \frac{\left(V_R^2 + U_{w,R}^2\right)^{0.5}}{(s-1)gD_{50}} \tag{3.3.1}$$

In which V_R = the representative depth-averaged velocity based on the velocity in the lowest computational layer (assuming logarithmic profile) and $U_{w,R}$ = the representative peak orbital velocity amplitude = $(0.5U_{w,on}^3 + 0.5U_{w,off}^3)^{1/3}$. Mega-ripples are expected for Ψ_{TR2004}< 550 leading to a roughness of the order of $k_{s,w,mr}$=0.01h_d, ripples are highest for Ψ_{TR2004}< 50 ($k_{s,c,r}$=150D_{50}) and are degrading until Ψ_{TR2004}> 250 into the sheet flow regime ($k_{s,c,r}$ = 20D_{50}). The bed roughness is calculated together with the current profile (iterative process) and is further used for the suspended load transport rates.

Bed-load transport

In TR2004 the bed-load transport rates (q_b) for sand (d_{50}>62μm) are instantaneously related to the instantaneous bed shear stress due to both currents and waves. The result is a quasi-steady method which calculates the net sediment transport using a intra-wave approach. The formula is equal to the proposed formula of Van Rijn (1993), only is slightly modified and calibrated on experiments on bed-load transport under sheet-flow conditions in a large-scale wave tunnel *(Ribberink, 1998; Van Rijn, 2000)*. The bed load transport formula is also verified on field data under river (48 data sets from three rivers), tidal (two data sets from two tidal banks based on ripple migration) and coastal flow conditions (1 dataset from one field site based on mega-ripple migration under waves+currents conditions).

$$q_b(t) = \frac{1}{2}\rho_s D_{50} D_*^{-0.3} \left[\frac{\tau'_{b,wc}(t)}{\rho_w}\right]^{0.5} \left[\frac{\tau'_{b,wc}(t) - \tau_{b,cr}}{\tau_{b,cr}}\right] \tag{3.3.2}$$

In which $\tau'_{b,cw}$ = bed shear stress related to the free-stream velocity near the bed and the grain friction coefficient = $0.5\rho_w f'_{cw}(U_{\delta,cw})^2$, ρ_s = sediment density, ρ_w = water density, and D_* = the dimensionless particle size = $D_{50}[(s-1)g/v^2]^{1/3}$. $U_{\delta,cw}$ is the instantaneous velocity due to currents and waves.

Three comments can be made on the bed load transport formulations in UNIBEST-TC:

- For the wave-induced orbital velocity the free-stream velocity is used. Van Rijn *(Van Rijn, 2007a)* states that the current velocity at the edge of the wave boundary layer together with an additional representative streaming velocity. In UNIBEST-TC a different approach is used for the superimposed current, because the quasi-3D approach (*Reniers, et al., 2004*) is used for the mean current profile module. The mean current profile already includes the near bed streaming. This is why the mean velocity in the lowest computational point is used as superimposed current velocity which is added to the orbital velocity time series.
- As suggested by Van Rijn (*2007a*) the influence of acceleration effects is included by replacing the orbital velocity component by a "sediment mobilising velocity" $U_\theta(t)$ according to the time domain filter method of Nielsen and Callaghan *(2003)*. This aspect was not yet implemented in the UNIBEST-TC version that was provided in this research and is included in the formulations.
- In UNIBEST-TC the phase lag effects on the bed load transport (recognized by Dohmen-Janssen (1999)) are not included, as recommended by Van Rijn (2007a).

Suspended-load transport

The suspended-load transport formulations in TR2004 are based on a time-averaged approach and divide the suspended-load into current-related transport and wave-related transport. The current-related suspended-load transport is based on the time-averaged vertical distribution of the concentration and fluid velocities:

$$q_{s,c} = \frac{\int_a^{h+\eta} \bar{U}\bar{C}dz}{(1-p)\rho_s} \tag{3.3.3}$$

In which $q_{s,c}$ is the current-related suspended load transport (m^2/s), U(z) is the local time-averaged velocity at height z, C is the local time-averaged sediment concentration at height z (kg/m^3), p is the porosity (=0.4) and ρ_s is the sediment density (kg/m^3).

The wave-related suspended sediment transport is defined as the transport of the sediment particles by the oscillating fluid component and is based on the amount of sediment in the suspension layer above the bed and a velocity skewness factor.

$$q_{s,w} = \lambda f_{pl} \left[\frac{U_{w,c}^4 - U_{w,t}^4}{U_{w,c}^3 + U_{w,t}^3}\right] \frac{\int_a^{\delta} \bar{C}dz}{(1-p)\rho_s} \tag{3.3.4}$$

where the term $[(U_{w,c})^4-(U_{w,t})^4]/[(U_{w,c})^3+(U_{w,t})^3]$ = the velocity skewness factor. $U_{w,c}$ and $U_{w,t}$ are the peak orbital velocities under respectively the crest and the trough. δ is the thickness of suspension layer near the bed (≈ 6 x thickness of the wave boundary layer thickness) and λ= 0.1 =a constant; and f_{pl} = a phase lag factor (between +1 and -1).

In TR2004 the suspended sediment concentration profile over the whole depth is determined using a reference concentration close to the bed and an advection-diffusion equation for the distribution over the depth. In the advection-diffusion equation the fall velocity of suspended sediment and mixing coefficient due to waves and current play a vital role. The suspended transport rates and concentration profiles are extensively validated on river, tidal and coastal data (304 datasets from 9 rivers and tidal estuaries and 54 datasets from the Egmond beach along the coast of the Netherlands). The model is even validated on measurements under partial breaking waves.

The phase lag factor predicts the reduction in the wave-related suspended transport due to phase lag effect or even changes the transport into offshore direction and is computed using:

$$f_{pl} = -\tanh\left[100\left(P - P_{cr}\right)\right] \qquad P = \frac{k_{s,w,r}}{w_s T_p} \qquad P_{cr} = 0.1 \tag{3.3.5}$$

The phase lag factor is not standard implemented and is an extra feature that is mentioned by Van Rijn, Walstra et al. (*2007*) and which is added in the UNIBEST-TC formulations.

3.3.2. SANTOSS sand transport model

The other sand transport model is the SANTOSS model (*Ribberink, et al., 2010*) which is based on the semi-unsteady model concept of Dibajnia and Watanabe (*1998*). The concept uses a half-cycle approach (Figure 3-1): it divides a wave cycle into a crest period (onshore velocities) and a trough period (offshore velocities) and defines per half-cycle the entrained and transported sediment and the amount of sediment, which is not yet settled down at the end of the half-cycle and is mainly transported during the next half cycle. The total sediment transport in the wave boundary layer is calculated according to:

$$\Phi_b = \sqrt{|\theta_c|}\,\frac{T_c}{T_p}\left(\Omega_{cc} + \frac{T_c}{2T_{cu}}\Omega_{tc}\right)\frac{\vec{\theta}_c}{|\theta_c|} + \sqrt{|\theta_t|}\,\frac{T_t}{T_p}\left(\Omega_{tt} + \frac{T_t}{2T_{tu}}\Omega_{ct}\right)\frac{\vec{\theta}_t}{|\theta_t|} \tag{3.3.6}$$

In which Φ_b = the non-dimensional sediment transport = $q_b/[(s-1)gD_{50}^3]^{0.5}$, s = relative density = ρ_s/ρ_w and g = the gravitational acceleration. The concept divides a wave cycle into two half-cycles (a crest and trough) and uses the representative shear stresses (θ_c and θ_t, based on combination of orbital velocity and mean current, Figure 3-2), the representative entrained loads (Ω_c and Ω_t) and the total (T_c and T_t) and acceleration periods (T_{cu} and T_{tu}) per half cycle to calculate the sediment transport. A phase lag approach defines which part of an entrained sediment load is also transported during the same half cycle (Ω_{cc} and Ω_{tt}) or during the next half-cycle (Ω_{ct} and Ω_{tc}).

Several modifications have taken place compared to the original model concept of Dibajnia and Watanabe (*1998*):

- Ripple dimensions are based on the formulations of O'Donoghue et al. (*2006*) and depend only on the orbital flow velocities;
- The bed shear stress is used as driving parameter instead of the near-bed velocity;
- The influence of different wave shapes (velocity- and/or acceleration-skewed) is accounted for by including asymmetry effects in the friction factor (*Van der A, et al., 2008*) and in the definition of the phase lag parameter.
- The effects of flow unsteadiness (phase-lags) are modelled in a modified way using a phase lag parameter based on the necessary time for the stirred sediment to fall back to the bed. The sheet flow layer or ripple height is used as reference height and the deceleration periods as critical time periods.
- The model is capable of dealing with waves and currents under an angle. The current velocity not only affects the absolute shear stresses during a

wave cycle but also influences the half cycle and acceleration periods and maximum velocities.

- Specific effects of progressive surface waves are included in the model:
    - Additional bed shear stress in the direction of wave advance due to boundary layer streaming;
    - Adaptation of half-cycle periods due to the Lagrangian effect and;
    - Vertical orbital velocities which enhance/oppose the settling of sediment and thus decrease/increase phase lag effects.

The empirical formulations of the recognized processes are calibrated on extensive measurements of net transport rates in oscillatory flow tunnels (OFT's) and wave flumes (e.g. GWK), where the processes related to surface waves were relatively excluded and included. In the oscillatory flow tunnel experiments also measurements in the ripple regime were used (more about the data set can be found in the next paragraph).

Ribberink et al. (*2010*) stated that the SANTOSS model should cover all the wave- and current-related sediment transport rates within the wave boundary layer (thickness in the order of centimetres).

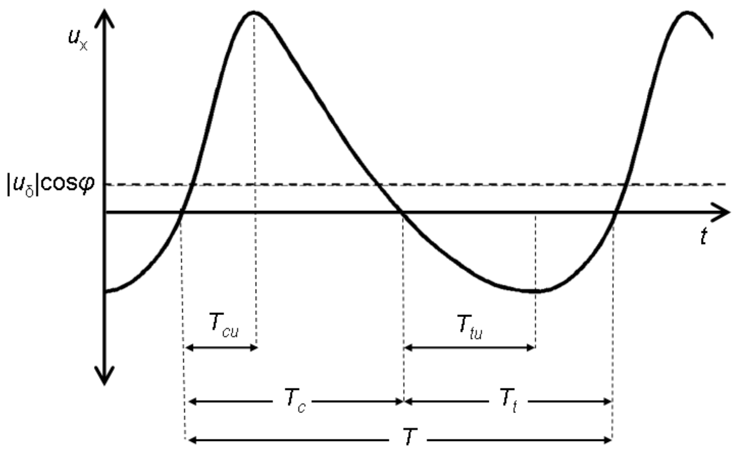

Figure 3-1: Velocity time series in wave direction. Tc and Tt are respectively the crest and trough periods, Tcu and Ttu are the crest and trough acceleration time lengths. The current shifts the time series up or down and affects both the maximum velocities and the periods (Ribberink, et al., 2010).

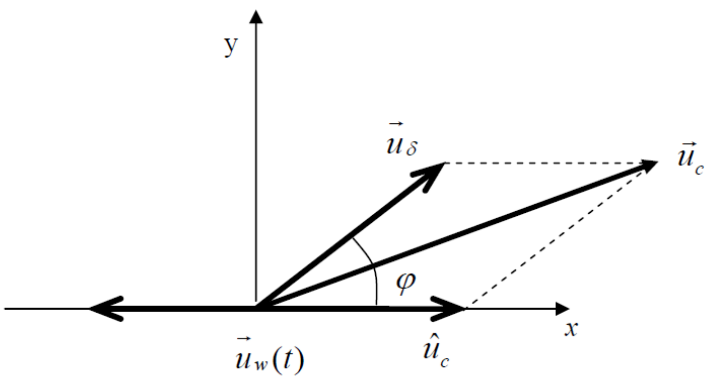

Figure 3-2: Illustration of wave and current velocity vectors $\vec{u}_w(t)$ and $\vec{u}_\delta$. The vector $\vec{u}_c$ is the resultant velocity vector at maximum velocity under the crest of the wave (Ribberink, et al., 2010).

3.3.3. Performance transport models (previous research on comparison transport predictions with experiment data)

The SANTOSS formulations have been compared to the TR2004 formulations in a previous research (*Ribberink, et al., 2010; Wong, 2010*), which primarily focused on the reproduction of a large amount of detailed transport measurements under different conditions. In total 221 transport wave-dominated measurements from the SANTOSS database (*Van der Werf, et al., 2009*) were used, among which skewed waves, asymmetric waves, waves+currents and surface waves (flume tunnel experiments). Measurement in both sheet-flow and rippled-bed regimes were present and all cases are for non-breaking waves conditions. Detailed data about the near bed orbital velocities and the current velocities were used as input.

For the comparison measured near-bed orbital velocity time series and current velocities were used and applied to the total formulations of SANTOSS. The same input is used for the bed-load transport formulations of TR2004 (*Van Rijn, 2007a*) including the filter method of Nielsen and Callaghan *(2003)* and the near-bed streaming as proposed in Van Rijn (*2007a*).

Table 3-1 shows the different subsets together with the performance of the two transport formulations on transport rate predictions. The overall performance of the SANTOSS model is better; especially for velocity skewed waves, acceleration skewed (asymmetric) waves, and for the rippled-bed regime in general, the prediction of the SANTOSS model is much better. Interesting is that for the few (realistic) conditions (the surface waves) the two models show exactly the same performance.

A few discussion points towards this comparison are:

- The SANTOSS model is calibrated on the data sets that are used to compare the predictions of the models in contrast to the Van Rijn model, which can explain the differences in performance.
- Only the bed-load transport formulations of TR2004 are used for the comparison. This while especially in the ripple regime (high roughness) and in case of high orbital velocities also sediment gets into suspension (according to the formulations of Van Rijn (*2007b*)).
- Finally, the TR2004 formulations are especially designed to perform well in morphological models under all possible conditions (the models demand relative simple and especially robust formulations).

Table 3-1: Comparison of the performance of TR2004 and SANTOSS on large amount of sand transport measurements (Ribberink, et al., 2010; Wong, 2010)

	Number of data	**TR2004 (bed-load)**		**SANTOSS**	
	211	**Factor 2**	**Factor 5**	**Factor 2**	**Factor 5**
Overall performance	221	43%	64%	77%	93%
Data sub-set: type of bed-form					
Sheet flow regime	155	54%	79%	83%	96%
Rippled-bed regime	56	13%	20%	61%	84%
Data sub-set: Type of flow					
Velocity skewed waves (no currents)	94	27%	46%	69%	89%
Acceleration skewed waves (no currents)	53	38%	60%	79%	98%
Waves with currents	50	66%	90%	86%	92%
Surface waves	14	86%	100%	86%	100%

3.4. Conclusions

This chapter gave a description of the coastal modelling system UNIBEST-TC and the two transport models that are of interest in this study: TR2004 and SANTOSS. The two transport models are calibrated on partly the same experimental data. The TR2004 formulations are based on extensive experiment measurements, but are also verified on field data (good agreement with river, tidal and coastal flow conditions). The SANTOSS model is calibrated on a large amount of detailed tunnel and flume experiments for both the ripple and sheet flow regime, but no field data are used for calibration or validation.

The two transport models use different concepts. The TR2004 formulations consist of three parts of which the bed roughness predictor has a direct interaction with the hydrodynamics in the model (influences the input). The bed-load is defined using a quasi-steady intra-wave approach, while the suspended load is defined in at time-averaged way using a suspended concentration and velocity profile. The suspended load consists of a wave-related (taking place in a small layer above the bed) and current-related suspended load (over the whole depth). Wave boundary layer streaming and acceleration effects are included in the bed load formulations, while phase lag effects can be included in the wave-related suspended load. The effects of wave asymmetry and phase lag effects were not yet implemented in the provided UNIBEST-TC version and are added for further analysis in this research.

The SANTOSS model is more process-based and includes all transport components in the wave boundary layer (which is in principal the bed load and wave-related suspended load). The half-cycle model concept also includes wave form effects, unsteady (phase lag) effects and the recognized surface wave effects, although their formulations are different compared to TR2004.

The previous comparison between the bed load formulations of TR2004 and the SANTOSS model showed that the SANTOSS model performs better on the prediction of the transport rates measured in different experiments. Some comments can be made on this comparison, especially about the data used for the comparison (SANTOSS model is calibrated on this data) and the comparison with only the bed load formulations of TR2004. A detailed comparison between the SANTOSS model and the total TR2004 formulations can give more insight in the model behaviour under changing conditions. Therefore, in Chapter 5 a comparison between the total transport rates predicted by the two models is executed.

4. Implementation SANTOSS model in UNIBEST-TC

4.1. Introduction

This chapter gives an extensive review about the implementation of the SANTOSS transport formulations in the coastal modelling system UNIBEST-TC. Several issues are reviewed and choices made during the implementation are substantiated. In the first paragraph a few changes to the original SANTOSS transport formulations are mentioned. Next, some theories about slope effects are mentioned and how this is taken into account in the SANTOSS model (par. 4.3). Then, theories about the orbital flow velocity induced by short waves are explored (par. 4.3) followed by the influence of wave groups (par. 4.5) and how a superimposed current is included (par. 4.6). Finally, it is discussed how possible suspended load transport above the wave boundary layer is included (par. 4.7).

4.2. The SANTOSS sand transport code

The SANTOSS Matlab code (provided by Ribberink et al. (*2010*)) can make sediment transport predictions for different conditions: e.g. currents alone, oscillating horizontal motion (U-tube) with or without currents and surface waves with or without currents. Only the part for surface waves with superimposed currents has been copied and translated into FORTRAN 77 language (in which UNIBEST-TC is written), taking into account that the near-bed orbital motion can also become zero (for example at deeper water with small wave period).

First a stand-alone version of the SANTOSS code in FORTRAN was made to check whether the code has any errors. For all possible conditions the predictions made by the FORTRAN code has been compared to the Matlab code to check whether the model gives exactly the same results.

Some small changes to the SANTOSS code have been made, which were necessary before implementation of the code was possible, which are discussed in this paragraph.

Coordinate system

The coordinate systems used by the SANTOSS model and UNIBEST-TC are different. The sand transport model assumes waves propagate in x-direction with currents at angle φ counter-clockwise from this direction. In UNIBEST-TC the waves propagate at angle θ counter-clockwise from the cross-shore (x-) direction, and the net current $\vec{v} = \{u, v\}$ has a component in cross-shore and alongshore (y-) direction. Using the following formula solves the discrepancy:

$$\varphi = \operatorname{atan}\left(v/u\right) - \theta \qquad (4.2.1)$$

Furthermore, SANTOSS computes the net transport rates in the direction of wave propagation ($q_{b,wa}$) and normal to this direction ($q_{b,\perp wa}$), which are related to the UNIBEST-TC coordinate system in the following way:

$$\begin{aligned} q_{b,x} &= q_{b,wa}\cos\theta - q_{b,\perp wa}\sin\theta \\ q_{b,y} &= q_{b,wa}\sin\theta + q_{b,\perp wa}\cos\theta \end{aligned} \qquad (4.2.2)$$

Definition of the half-cycle periods and the acceleration periods

The SANTOSS Matlab code uses two wave form parameters (skewness R and asymmetry β (equation (2.2.1)) to define the half-cycle periods and the acceleration periods. In fact, the skewness parameter R is used to define the half-cycle periods in case of skewed waves (based on second-order Stokes waves). The asymmetry parameter β is used to define the acceleration periods in case of asymmetric waves (*Malarkey, 2008*).

Two problems arise considering the input delivered by UNIBEST-TC. The first issue is that when waves are both skewed and asymmetric, the method used in the Matlab code to define the periods based on R and β does not lead to exact results. Besides, UNIBEST-TC delivers a time series as input. Another issue is that UNIBEST-TC generates an orbital flow velocity time series of multiple waves, which can be of different shape and length in case of wave group simulation (see for more details par 4.5).

These issues resulted into the choice to write an extra function which extracts numerically from a time series of a wave train the zero-crossings, maxima and minima. From these data it defines for an arbitrary amount of half-cycles the half-cycle periods, the acceleration periods and the maximum flow velocities. In a later stage, the Shields stresses and the entrained loads are calculated per half-cycle. The phase lag effect is applied over the wave train in which a part of the entrained load of a half-cycle is given to the next half-cycle in the wave train (the last half-cycle gives to the first one).

Combination of high current with low oscillatory velocities

The proposed half-cycle approach for waves in combination with a current can lead to problems when the component of the current velocity in the direction of the wave propagation becomes too high compared to the orbital velocity. In this case one of the half-cycles (crest or trough) can get really small and eventually disappear, which brings problems to the phase lag factor. Especially when (a part of) the waves break, a strong current can be generated, which can induce this problem.

The actual problem lies in the model concept of SANTOSS. Entrained sediment can only be transported in the same half-cycle or in the next. It is not possible to transport sediment over several half-cycles, while this might be the case especially when one of the half-cycles becomes really small or when (small) sediment is entrained to high levels.

To avoid errors while running the model, the code is changed in such a way that if a half-cycle disappears, the load that is directed to this half-cycle from the previous half-cycle, is directed to the next half-cycle. So for example: when a crest disappears, the load that is coming from the previous trough should be directed to the next trough. This is a simple modification and it must be mentioned that (under phase lag dominated situations) this does not lead to a smooth transition zone in net transport rates around the point where a half-cycle disappears. On the other hand, these conditions are not common for coastal areas and in case of for example a high undertow due to breaking waves, the sediment transport is dominated by current-related suspended transport.

Redefinition of experienced periods (Lagrangian grain motion)

For surface waves conditions (realistic conditions) sediment grains move in the direction of wave propagation under the wave crest and against the wave under the wave trough (Lagrangian motion). In this way they experience a longer crest period $T_{c,sw}$ (= $T_c + \Delta T_c$) and a shorter trough period $T_{t,,sw}$ (= $T_t - \Delta T_t$). The extension / reduction of the half-cycle period depend on the ratio of the wave propagation velocity c and the horizontal grain displacement during the half wave-cycle (orbital diameter) d_g and can be written as:

$$\Delta T = \frac{d_g}{c} \tag{4.2.3}$$

In the SANTOSS formulations the crest-period extension and trough period reduction is estimated assuming a sinusoidal wave shape for the half-cycle horizontal grain motion:

$$\Delta T_c = \frac{d_g}{c} = \left(\frac{c}{\zeta \hat{u}}\pi - 2\right)^{-1} T \qquad \Delta T_t = \frac{d_g}{c} = \left(\frac{c}{\zeta \hat{u}}\pi + 2\right)^{-1} T \tag{4.2.4}$$

Where u = the representative orbital velocity amplitude and the reduction factor ζ = 0.55 = the ratio of the horizontal grain-velocity amplitude and the free-stream velocity amplitude u. Because of the numerical definition of an arbitrary amount of half-cycles with possibly different time lengths and an arbitrary superimposed current it is not recommended to use the total wave period in this approximation. It is better to replace the wave period in formula (4.2.4) with twice the measured half-cycle period:

$$\Delta T_c = \frac{d_g}{c} = \left(\frac{c}{2\zeta \hat{u}_{w,c}}\pi - 1\right)^{-1} T_c \qquad \Delta T_t = \frac{d_g}{c} = \left(\frac{c}{2\zeta \hat{u}_{w,t}}\pi + 1\right)^{-1} T_t \tag{4.2.5}$$

This is physically more correct and it does not lead to extra problems with disappearing half-cycles as mentioned above. The factor ζ might need to be recalibrated, but the difference in period change is not large.

Vertical flow velocity for ripple-cases

One discussion point considering the calibration of the SANTOSS model is the influence of the vertical velocity on the settling velocity of the suspended sediment. Vertical velocities affect therefore the phase lag parameter for both crest (lower phase lag parameter, less phase lag effect) and trough (larger phase lag parameter, more phase lag effect). The influence of vertical velocity is only calibrated for sheet flow conditions, because the full-scale surface wave experiments in flumes focused all on sheet flow transport. As a result the settling/fall velocity is therefore corrected with the maximum vertical velocity at 3 times the height of the sheet flow layer thickness above the bed (under the crest the fall velocity is enhanced due to downward flow velocity and under the trough the fall velocity is reduced).

For ripple conditions the influence of vertical velocities cannot be calibrated, but according to Ribberink et al. (*2010*) vertical velocities at the level of 3 times the ripple height should be chosen for ripple conditions.

4.3. Influence of bed-slopes on sediment transport

Most transport formulas are based on transport measurements for (nearly) horizontal beds. The bed slope may affect the transport rates in three ways:

- The bed slope influences the local near-bed flow velocity.
- The bed slope influences the threshold conditions for initiation of motion
- The bed slope can change the transport rates and/or direction, once the sediment is in motion.

The influence of a slope on the hydrodynamics and the resulting influenced shear stresses are hard to measure and probably also small, which is why this is not taken into account any further. Only when the chosen near-bed orbital velocity theory takes into account the slope (*Elfrink, et al., 2006*), this is used. Experimental studies primarily focused on a steady flow (rivers), which is why also the influence of the bed slope on other sediment transport processes in coastal areas are unknown, like the dimensions of ripples, thicknesses of the sheet flow layer and possible changing to phase lag effects.

In the application of bed slope effects in a transport formula it is necessary to define the bed slope in the direction of flow velocity (more precise the direction of the bed shear stress and called the longitudinal slope angle) and the slope normal to this direction (the lateral/transverse slope angle). Important in the influence of the bed slope on both the threshold conditions and the transport rates and direction is the natural angle of repose φ_r of the sediment grains, which is for sand grains mostly around 30º-35º.

Besides a better prediction of the physics, slope effects also add to stability of morphological results. Slope effects induce diffusive behaviour of for example bars and trenches. Including slope effects should therefore always enhance down slope transport.

4.3.1. Slope effect on threshold of sediment transport

Both a longitudinal and a lateral slope influence the critical Shields parameter. In case of only a longitudinal slope (β_{sl}) the critical Shields parameter has been corrected by the Schocklitsch factor:

$$f_{cr,Schocklitsch} = \frac{\theta_{b,cr,sl}}{\theta_{b,cr,0}} = \frac{\sin(\varphi_r + \beta_{sl})}{\sin\varphi_r} \qquad \beta_{sl} = a\tan\left(\frac{dz_b}{ds}\right) \tag{4.3.1}$$

In which $\theta_{b,cr,0}$ = the nominal critical Shields parameter (horizontal bed), $\theta_{b,cr,sl}$ = the critical Shields parameter after slope correction, dz_b/ds = the local bed slope in the direction (s) of the bed shear stress and φ_r = the angle of repose of the sediment. Positive values of the slope refer to up sloping beds, negative values to down sloping beds. The correction due to only a lateral slope (normal to the direction of the wave-and-current-induced bed shear stress) is called the Leitner-factor (for β_{sl} = 0):

$$f_{cr,Leitner} = \frac{\theta_{b,cr,slope}}{\theta_{b,cr,0}} = \cos\gamma_{sl}\left[1 - \left(\frac{\tan\gamma_{sl}}{\tan\varphi_r}\right)^2\right]^{0.5} \qquad \gamma_{sl} = a\tan\left(\frac{dz_b}{dn}\right) \tag{4.3.2}$$

With dz_b/dn = the local bed slope normal to the direction of the fluid induced bed shear stress. Both factors are found by different authors. Van Rijn (*1993*) proposes to multiply the factors in case of both longitudinal and lateral slopes. Walstra et al. (*2007*) modified a formula of Dey (*2003*) into a simple formula which agrees really well with measured data:

$$f_{cr,Dey^*} = \frac{\theta_{cr,slope}}{\theta_{cr,0}} = \left(1 - \frac{\tan\beta_{sl}}{\tan\varphi_r}\right)^{0.75}\left(1 - \frac{\tan\gamma_{sl}}{\tan\varphi_r}\right)^{0.37} \tag{4.3.3}$$

Apsley and Stansby (*2008*) use basic mechanical principles to include gravitational influence on slopes of arbitrary orientation and come to the next factor to correct the critical Shields parameter (leads also to both Schocklitsch and Leitner factor):

$$\vec{\theta}_{cr,A\&S} = \frac{\sin\beta_{sl,\max}\cos\psi + \sqrt{\cos^2\beta_{sl,\max}\tan^2\varphi_r - \sin^2\beta\sin^2\psi}}{\tan\varphi_r}\theta_{cr,0} \tag{4.3.4}$$

In which $\beta_{sl,max}$ = the angle between the slope with the horizontal (maximum slope) and Ψ is the angle between direction of the bed shear stress and upslope direction.

A short comparison made for up and down sloping cases with or without lateral slopes showed that the formula of Apsley and Stansby (*2008*) predicts approximately the same correction terms as proposed by Van Rijn (*1993*). In contrast, the adapted formula of Dey (*2003*) predicts much lower values for upslope cases and for small negative slopes (down slope).

4.3.2. Slope effects on the transport rates and the direction

In case of a sloping bed not only the effects on the initiation of motion have to be taken into account, but also the transport directly induced by gravity when the grains have been set in motion. Two kinds of solutions are found in previous studies.

The effect of slopes on the sediment transport rates is in UNIBEST-TC modelled by the Bagnold parameter β_s is used in UNIBEST-TC (*Bosboom, et al., 2000*) which increases the non-dimensional instantaneous bed load transport in case of down-slope transport and decreases it in case of upslope transport according to the next formula:

$$\Phi_{b,slope} = \beta_s \Phi_b \quad \text{with} \quad \beta_s = \frac{\tan\varphi_r}{\tan(\varphi_r) + \dfrac{dz_b}{ds}} \tag{4.3.5}$$

In which the dz_b/ds = again the slope in flow direction/bed shear stress. In TR2004 this method is implemented by using the intra-wave transport calculations.

Apsley and Stansby (*2008*) take into account the down-slope component of the particle weight. This does not only affect the critical bed shear stress, but also the magnitude of the bed shear stress and the direction (when bed shear stress is not directed upslope or down-slope). The component of (buoyancy-reduced) weight down the slope is defined as:

$$\tau_{w,downslope} = (s-1)\rho g V \sin\beta_{sl,\max} \cdot \hat{\mathbf{b}} \tag{4.3.6}$$

In which s is the relative sediment density, V is the volume of the particle and the vector **b** is the vector down slope. This means that the effective stress is the sum of this down slope term and the bed shear stress induced by the near bed flow velocity. These two terms might be directed into different directions. The non-dimensional effective stress is then finally defined as:

$$\vec{\upsilon}_{eff} - \vec{\upsilon} + \frac{}{\tan\varphi_r}\sin\beta \cdot \hat{\mathbf{b}} \tag{4.3.7}$$

4.3.3. Including slope effects in SANTOSS formulations in UNIBEST-TC

As said before, the numerical stability is very important in numerical modelling and thus also in UNIBEST-TC. Sediment transport takes especially place in the near shore where on- and off-shore directed sediment fluxes meet; which leads to growth, migration or diffusion of sand bars. The diffusion of sediment transport is controlled by slope effects and it is recommended to calibrate on this behaviour. In UNIBEST-TC with the TR2004 formulations it is chosen to only use the Schocklitsch factor (only longitudinal slope is taken into account) for only the bed-load transport. This has been done because the high bed shear stresses is primarily directed in cross-shore direction. Furthermore, the tangents of the angle of repose $\tan(\varphi_r)$ can this way easily be used for calibration (unrealistic low values are for example found by *Ruessink, et al., 2007*). Also inclusion of the slope effects to the reference concentration c_a and the suspended sediment fluxes would lead to more numeric instability.

Using the method of Apsley & Stansby (*2008*) for the SANTOSS formulations in UNIBEST-TC leads to a problem, caused by the phase lag concept. Adding the down slope component of the sediment particle weight to the bed shear stress leads to higher shear stresses down slope and lower shear stresses upslope. Under conditions where phase lags are not dominant this leads to a higher net down slope transport, which is expected behaviour.

On the other hand, when phase lags are dominant (for example when ripples are present) the higher amount of entrained sediment during the down slope half-cycle (due to the higher shear stress) is transported in the next half-cycle upslope, which can lead to enhanced upslope transport. This implies that in reality not only the bed shear stresses is affected by slopes, but also other processes like phase lag parameters, suspended loads, hydrodynamics, etc.

Finally it is chosen to use only the Schocklitsch factor together with the Bagnold parameter in the application of the SANTOSS formulations. This provides in an easy way a gradient-diffusion-like behaviour, which enhances numerical stability. The transport formula of the SANTOSS model is redefined into:

$$\vec{\Phi} = \beta_{s,c}\sqrt{|\theta_c|}\frac{T_c}{T}\left(\Omega_{cc} + \frac{T_c}{2T_{tc}}\Omega_{tc}\right)\frac{\vec{\theta_c}}{|\theta_c|} + \beta_{s,t}\sqrt{|\theta_t|}\frac{T_t}{T}\left(\Omega_{tt} + \frac{T_t}{2T_{ct}}\Omega_{ct}\right)\frac{\vec{\theta_t}}{|\theta_t|} \quad (4.3.8)$$

$$\beta_{s,c} = \frac{\tan\varphi_r}{\tan(\varphi_r) + \frac{dz_b}{ds_c}} \quad (4.3.9)$$

$$\beta_{s,t} = \frac{\tan\varphi_r}{\tan(\varphi_r) + \frac{dz_b}{ds_t}} \quad (4.3.10)$$

In which $\beta_{s,c}$ and $\beta_{s,t}$ are the slope corrections for the sediment loads transported under respectively the crest and the trough, dz_b/ds = the slope in the direction of the bed shear stress/flow velocity (in this case the representative crest velocity and trough velocity). The formulations have been tested for different slopes and only in cases where the critical shear stress is just exceeded the high phase lags can enhance upslope transport. In the test-cases it does not lead to any numeric instability.

Finally it should be mentioned that the SANTOSS model calculates the total amount of transported sediment which consists of bed load transport and suspended load transport in the wave boundary layer. This means that a slope also influences (a part of) the suspended load, while in the current version of UNIBEST-TC only the bed load transport is affected by the slope.

4.4. Short wave flow velocity

Wave-related transport is essential in the near shore and is linked to onshore transport rates. A good representation of the near bed orbital velocities is necessary as input for the sand transport models. However, there seems to be a lot of different theories developed which formerly focused only on representing skewness. Two general accepted theories are:

- Rienecker & Fenton (*1981*): Stream function theory, 8-order theory which shows only skewness.
- Isobe & Horikawa (*1982*) adjusted by Grasmeijer and Van Rijn (*1998*): Second-order Stokes wave: shows only skewness and wobbles under high non-linear waves.

Only in the last years also the influence of asymmetric waves is noticed and three theories also represent these:

- Elfrink et al. (*2006*): used empirical expressions to predict the peak orbital velocities and the half cycle and acceleration periods: shows skewness and asymmetry, but shows discontinuities in acceleration and skewness is not exactly represented. Was also recommended by Ribberink et al. (*2010*) to use in combination with SANTOSS
- Ruessink & Van Rijn (*in preparation*): is also applied by Van Rijn et al. (*in preparation*): shows both skewness and asymmetry but also wobbles under high non-linear waves. Root-mean-square velocity is based on linear wave theory.
- Van Thiel de Vries (*2009*): Combination of the stream function theory of Rienecker & Fenton and the Skewness and Asymmetry theory of Ruessink & Van Rijn: overestimates both skewness and asymmetry and no wobbles.

It is expected that asymmetry has a large influence on transport rates and thus the focus lay on the latter three theories of which only Elfrink et al. (*2006*) was not yet implemented in UNIBEST-TC. These theories are extensively analysed in this research due to the facts that the theory of Ruessink & Van Rijn (*in preparation*) shows unrealistic wobbles (which gives problems with the half-cycle concept) and the theory of

Van Thiel de Vries (*2009*) was not correctly implemented (a typing error in the formula was found in a later stage).

4.4.1. Analysis available theories

Below, the three theories are discussed shortly. The two theories of Ruessink & Van Rijn (*in preparation*) and Elfrink et al. (*2006*) are slightly modified. In the next sub-paragraph the results of the three theories are compared.

Elfrink et al. (2006)

Elfrink et al. (*2006, to this theory will be referred with "Elfrink"*) analysed field measurements at Terschelling (the Netherlands, NOURTEC project), Duck (USA, SandyDuck97 experiments) and Egmond aan Zee (the Netherlands, Coast3D project). They determined the characteristic velocity parameters (acceleration and half-cycle periods and the peak orbital velocities) based on 3 independent dimensionless wave parameters: normalized wave height H*, wave length L* and the local Irribarren number ξ:

$$H^* = \frac{H}{h_d} \quad L^* = \frac{L}{h_d} \quad \xi = \frac{\tan\beta_{sl}}{\sqrt{H_{rms}/L_0}} \tag{4.4.1}$$

In which H = the local wave height, h_d is the local depth, L = the local wave length, β_{slope} = average slope angle over the length of 2 local wave length offshore of the point and L_0 = the wave length at deep water. Elfrink et al. (*2006*) used empirical expressions to calculate the peak orbital velocities (for crest $U_{w,c}$ and trough $U_{w,t}$) and the partial periods (half-cycle periods T_c and T_t and the acceleration periods $T_{w,cu}$ and $T_{w,tu}$).

They developed time series for the orbital flow velocity on a relatively simple way by combining the defined points under the condition that the average velocity is kept zero. The result is a time series showing discontinuities in acceleration, which gives problems with the calculation of transport rates with TR2004 (uses acceleration) and also with the determination of wave asymmetry (As and β). Due to these reasons the formula of Abreu et al. (*2010*) is used to develop a smooth time series.

Abreu, et al. (*2010*) defines a near bed orbital flow velocity time series without any unrealistic wobbles and without any discontinuities in velocity or acceleration. This formula is has his origins in the formula defined by Drake & Calantoni (*2001*) but Abreu et al. (*2010*) found a way to rewrite a formula of an infinite number of higher harmonics into a simple formula:

$$u(t) = U_w f \frac{\left[\sin(\omega t) + \dfrac{r_{Abreu}\sin\phi_{Abreu}}{1+f}\right]}{\left[1 - r_{Abreu}\cos(\omega t + \phi_{Abreu})\right]} \tag{4.4.2}$$

In which U_w = the amplitude of the orbital velocity (defined as $(U_c+U_t)/2$), the variable f = $(1- r_{Abreu}^2)^{0.5}$ = a dimensionless factor allowing the velocity amplitude to be equal to U_w, ω = the angular frequency, r_{Abreu} = an index of non-linearity and ϕ_{Abreu} = a phase which determines if the non-linearity consists of skewness or asymmetry. The two wave form parameters r_{Abreu} and ϕ_{Abreu} are really easy in use and can be easily interpreted: when r_{Abreu} = 0 it gives a sinusoidal form (for every ϕ_{Abreu}), when r_{Abreu} becomes higher non-linearity increases and it depends on ϕ_{Abreu} if this leads to skewness or asymmetry: ϕ_{Abreu}=-0.5π gives skewed waves, ϕ_{Abreu}=0 gives non-skewed, forward leaning asymmetric waves.

Abreu et al. (*2010*) shows a method to find the values for r_{Abreu} and ϕ_{Abreu} using the skewness R together with asymmetry β (Eq. (2.2.1)) or instead of β using the wave skewness parameter α (see Appendix B.2 for further details and analysis of the Abreu function). α is defined as the ratio between two times the acceleration period of the crest T_{cu} and the total wave period:

$$\alpha = \frac{2 \cdot T_{cu}}{T} \tag{4.4.3}$$

From the wave characteristics defined by Elfrink the values of the skewness R ($=U_{w,c}/(U_{w,c}+U_{w,t})$) and the wave form parameter α ($2T_{w,cu}/Tp$) can be calculated which leads to the (r,ϕ_{Abreu}) combination (according to method describe above). The other 2 input parameters for the formula of Abreu et al. (*2010*) (see equation (B.2.1)) can be easily derived ($U_w = (U_{w,c}+ U_{w,t})/2$ and $\omega = 2*\pi/T$).

Ruessink & Van Rijn (in preparation)

In the theory developed by Ruessink & Van Rijn (*in preparation, to this theory will be referred as "R&vR"*) the time series is based on three parameters: (1) skewness Sk, (2) asymmetry As and (3) the root-mean-square orbital velocity based on linear wave theory. They parameterized the wave skewness Sk and wave asymmetry As as a function of the Ursell number defined as:

$$Ur = \frac{3}{8}\frac{H_s k}{\left(kh_d\right)^3} \tag{4.4.4}$$

In which H_s = the significant wave height (average of 1/3 highest waves) = $1.41*H_{rms}$, H_{rms} = root-mean-square wave height, k = the local wave number and h_d the depth. The parameterization is optimized by applying a nonlinear least square fit procedure to more than 30.000 measurements at Egmond aan Zee and Terschelling during several measurement campaigns. They calculate the total non-linearity B and phase $\phi_{R\&vR}$ by:

$$B = \frac{0.7939}{1+\exp\left[\frac{-0.6065-\log(Ur)}{0.3539}\right]} \tag{4.4.5}$$

$$\phi_{R\&vR} = -\frac{\pi}{2}+\frac{\pi}{2}\tanh\left(\frac{0.6373}{Ur^{0.5995}}\right) \tag{4.4.6}$$

With $B = \sqrt{Sk^2 + As^2}$ and $\phi_{RvR} = \tan^{-1}\left(As/Sk\right)$ these result in:

$$Sk = B\cos\phi_{RvR} \tag{4.4.7}$$

$$As = B\sin\phi_{RvR} \tag{4.4.8}$$

It is noted that equation (4.4.5) contains a typing error in the paper of Ruessink & Van Rijn (*in preparation*). The only problem is the translation of these wave form parameter into a time series that is proposed by R&vR. For high asymmetric waves the time series shows some unrealistic wobbles, because they use only a second-order harmonic function.

The definition of the skewness and asymmetry seems to be promising. Therefore, it has been tried to use another method to generate time series. Also in this case the formula of Abreu et al. (*2010*) is used. A relation that was found was the relative simple relationship between the wave form parameter r_{Abreu} and ϕ_{Abreu} and the skewness Sk and asymmetry As. The phase ϕ_{Abreu} can be directly related to the ratio Sk/As:

$$\phi_{Abreu} = \tan^{-1}\left(\frac{Sk}{As}\right) \quad \text{with} \quad -\pi < \phi_{Abreu} < 0 \tag{4.4.9}$$

$$Sk = -B\sin\left(\phi_{Abreu}\right) \tag{4.4.10}$$

$$As = -B\cos\left(\phi_{Abreu}\right) \tag{4.4.11}$$

The non-linearity index r_{Abreu} can be directly related to the total non-linearity B according to (using least-square-fitting):

$$\left|r_{Abreu}\right| = -0.2926\cdot B^2 + 1.015\cdot B \quad \text{with } B = \sqrt{Sk^2+As^2} \tag{4.4.12}$$

According to Ruessink & Van Rijn the time series should have the same root-mean-square velocity as defined by linear wave theory. This can be realized by adjusting the amplitude U_w in Eq. (4.4.2) in such a way that the predefined U_{rms} can be used. After least-square-fitting the next relation was found between U_w and U_{rms}:

$$U_w = \frac{\sqrt{2}\cdot U_{rms}}{\left[-0.3\left|r_{Abreu}\right|^3 + 0.087\left|r_{Abreu}\right|^2 - 0.045\left|r_{Abreu}\right| + 1\right]} \tag{4.4.13}$$

This means that using the formula of Abreu et al. (*2010*) a representative time series can be easily generated based on Skewness (Sk), the Asymmetry (As) and the root-mean-square velocity U_{rms}.

Van Thiel de Vries (2009)

Van Thiel De Vries (*2009, to this theory will be referred as "vTdV"*) extended the Rienecker & Fenton (*1981*) theory in which the short wave velocity form is described by the weighted sum of eight sine and cosine functions:

$$u_{bed}(t) = \sum_{i=1}^{8} wA_i \cos(i\omega t) + (1-w)A_i \sin(i\omega t) \tag{4.4.14}$$

In which $u_{bed}(t)$ is the near bed short wave flow velocity, i refers to the i-th harmonic, ω is the angular wave frequency, A_i is the amplitude of a specific harmonic (computed from stream function theory) and w is a weighting function affecting the wave shape. When w=1 the wave form is purely skewed and when w=0 purely asymmetric. Van Thiel de Vries (*2009*) found a relation between the ratio of skewness Sk and asymmetry As on the one side and the weighting function w on the other side. The total non-linearity B is independent of w but depends on ratio of the amplitudes obtained with stream function theory as proposed by Rienecker & Fenton (1981). On contrary the phase $\phi = \tan^{-1}(As/Sk)$ can be related to w as follows:

$$w = 0.2719 \ln\left(\left|\frac{\phi + 1.8642}{0.2933 - \phi}\right|\right) \tag{4.4.15}$$

Where must be mentioned again that there was a typing error in this equation in the doctoral thesis of Van Thiel de Vries (*2009, equation 6.18*), which was why it was wrong implemented in UNIBEST-TC. The phase ϕ is first taken from measurements and this was a good way to define the bore intervals. Later, the phase $\phi_{R\&vR}$ (4.4.6) from the theory of Ruessink & Van Rijn *(in preparation)* is used. It must be mentioned that this does not lead to the same rate of skewness and asymmetry as Ruessink & Van Rijn, but generally leads to higher non-linearity with the same ratio (As/Sk).

4.4.2. Application SANTOSS in UNIBEST-TC

When comparing the three theories the first thing that can be noticed is that R&vR and vTdV do not take into account the effect of different slopes. According to the theory of Elfrink et al. (*2006*) a higher slope decreases the skewness and the maximum onshore velocity and slightly increase the offshore velocity and the asymmetry (As).

In Figure 4-1 several examples of near bed orbital flow velocity time series are given for the three considered theories. The figures at the left show the orbital velocities under three waves with different wave lengths, while the relative wave height H/h_d (0.4) and the slope (1/40) are kept constant. A change in relative wave length (L/h_d) means in this case (constant depth) that the wave period changes. Two remarks can be made about these figures:

- Overall, the three theories all show that an increase of relative wave length, leads to an increase in non-linearity. At “deep water” (small ratio L/h_d) the wave form is (almost) sinusoidal, and maybe slightly skewed. With increasing relative wave length this first leads to an increase of skewness and later a shift appears from skewness to asymmetry. Remarkable is that according to Elfrink the waves lean slightly backwards when the ratio L/h_d is really small.

- Important differences between the three theories are the maximum and root-mean-square velocities. The velocity time series of R&vR are based on the root-mean-square velocity according to linear wave theory, which increase with increasing relative wave length (with increasing period). The flow velocities calculated by vTdV and Elfrink become relatively lower when the non-linearity increases.

The figures at the right are examples of a change in relative wave height (H_{rms}/h_d). The ratio L/h_d (=15) and the slope are kept constant. The next conclusions can be drawn:

- The influence of the relative wave height is clearly visible: an increase in relative wave height directly increases the maximal velocities under both the crest and the trough.
- According to Elfrink the wave height only influences the amplitude and has only a marginal effect on the wave form (both skewness and asymmetry). This is in contrast to R&vR and vTdV, who relate the wave form to the Ursell number and thus also to the relative wave height.

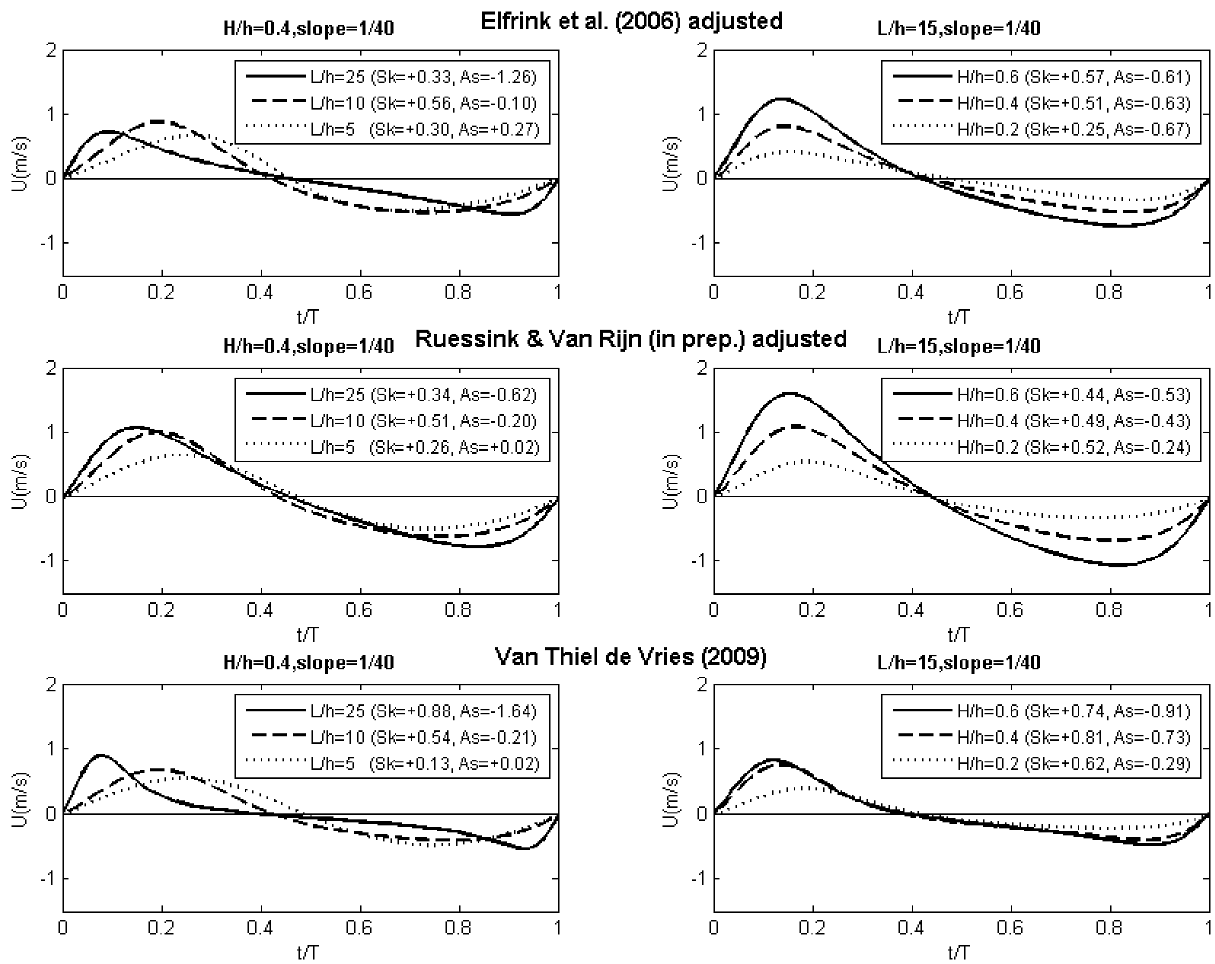

Figure 4-1: Comparison of three near-bed orbital velocity theories: Elfrink et al. (2006) adjusted with Abreu et al. (2010); Ruessink & Van Rijn (in preparation) adjusted with Abreu et al. (2010) amplitude based on linear wave theory; and Van Thiel de Vries (2009). Plots are based on a depth of 2 meters. On the left side the influence of a change in L/h_d is visible and on the right side the influence of a change in H_{rms}/h_d.

- A remarkable aspect of the theory of vTdV is that it seems to be limited to the ratio H/h_d=0.5, which might be due to the theory of Rienecker & Fenton and/or the implementation in UNIBEST-TC. For H_{rms}/h_d>0.5 the amplitude does not chance any more, only the phase φ (and thus the asymmetry and skewness) changes slightly.
- R&vR relates the amplitude to linear wave theory which seems to overestimate the amplitudes which are predicted by vTdV and Elfrink.

The lower amplitudes under non-linear waves are earlier recognized (*Rienecker & Fenton, 1981; Grasmeijer & Van Rijn, 1998*) and Grasmeijer & Ruessink (*2003*) found the following correction factor for the local orbital velocity amplitude based on small- and large scale experiments and field measurements:

$$U_w = \frac{U_{w,c} + U_{w,t}}{2} = r \cdot U_{orb,linear} \tag{4.4.16}$$

$$r = -0.4\frac{H_w}{h_d} + 1 \tag{4.4.17}$$

When for the theory of R&vR this relation is used instead of equation (4.4.13), the results agree much better with the orbital velocity characteristics of Elfrink.

Eventually, it is chosen to use in this research the theory of R&vR with this last modification because it gives a representation of the near bed orbital velocities that (in theory) agrees with extensive measurements of skewness, asymmetry and maximum velocities in the field. In Chapter 6 the SANTOSS and TR2004 model are tested in two cases, where the representations of the orbital velocities are compared with measurements. Because the choice for an orbital velocity theory seems to be of large importance, the resulting transport rates from the different theories under different conditions are charted in paragraph 5.4.

It must be mentioned that a quick analysis of the measurements of the orbital velocities of the experiments by Dohmen-Janssen-2002 and Schretlen-2010 (see *Van der Werf, et al., 2009*) does not confirm the results of equations (4.4.16) and (4.4.17). This might be influenced because these were experiments with regular waves. It can be concluded that more studies might be useful on this topic.

4.5. Wave group effect on near bed orbital velocity

Waves travel often in wave groups (mostly groups of 7 individual waves), which leads to alternating high and low waves. Because of the differences in wave height the individual waves should have different wave forms (see previous paragraph for influence of wave height on skewness and asymmetry). Due to the wave height variation in the group, the radiation stresses vary as well, being highest under the highest waves. This results in a time-varying set-up in the shoaling zone, with the largest depression under the highest waves (180° out of phase with the wave group). The effect of this is a long wave motion on the scale of the wave group. The long wave has the length and the frequency of the wave group and it travels with the group at the wave group speed. The velocities under the long waves are 90° out of phase with the bound long wave (positive). After breaking of the short waves the long waves can be released and does not have to be 180° out of phase with the group.

4.5.1. Current application in UNIBEST-TC

In UNIBEST-TC a representative wave group time series is developed using a simple formula, which combines 2 regular wave time series with one slightly out of phase, which leads to wave group behaviour over 7 waves. In the way this time series has been constructed, only skewness is represented, but no asymmetry (for more details Appendix A.4). The bound long wave velocity time series (amplitude and phase compared to the wave group) is calculated using the method of Roelvink and Stive (*Bosboom, et al., 2000*).

4.5.2. Application SANTOSS in UNIBEST-TC

Two problems are identified when applying the wave group effects to the SANTOSS formulations. First, the asymmetry of the short waves is not taken into account any more using the method in UNIBEST-TC, which is predicted to have an important influence on the wave-related transport prediction by SANTOSS. It was tried to make representative wave group behaviour, but this was not really possible and led to even more debatable results. Secondly, the SANTOSS formulations demand a clear definition of the half-cycles, which can become difficult for the combination of small waves in combination with long wave flow velocities and superimposed currents (earlier mentioned in paragraph 4.2).

Finally, it has been chosen to only use a single representative orbital motion as input for the SANTOSS model, which is based on root-mean-square wave height and peak wave period. For comparison the same orbital velocity time series is off course used as input for the TR2004 formulations of the bed-load. To take into account the influence of high waves the significant on- and offshore velocities are computed using the significant wave height (H_{sig} = 1.41*H_{rms}) and used for the prediction of ripples and the concentration profiles.

The choice to use only a regular wave on simplicity of application but can be supported by conclusions of others. Grasmeijer (*2002*) concluded for example that the low-frequency waves cannot be ignored in predicting the flow field in the nearshore, but that it only has a marginal effect on the total transported load in the near shore zone. On the other hand

The use of the significant wave height (average of one-third highest waves) as input for a representative orbital motion is based on earlier studies which use also the significant orbital velocities as input (*Dibajnia & Watanabe, 1998; Grasmeijer & Ruessink, 2003*).

4.6. Superimposed current

Beside an orbital motion induced by short waves near the bottom there is also a mean velocity present directed in an arbitrary direction. Due to the stresses induced over the whole water column by waves the mean current profile is not logarithmic like in cases of current-alone. An undertow and near-bed streaming are the processes under waves, which also become important. In this paragraph it is first described how the TR2004 formulations implemented in UNIBEST-TC take into account the near bed mean velocity. Then the way how SANTOSS has been implemented is given.

4.6.1. Current application in UNIBEST-TC

Van Rijn (*2007a*) states to use the current velocity at the edge of the wave boundary layer for the bed-load transport and add a certain streaming velocity which depends on the orbital amplitude U_w, the wave propagation velocity and the wave-related roughness height. This method has been used when only a depth-averaged velocity for the undertow is known (in models like CROSMOR, etc.).

In UNIBEST-TC (*Bosboom, et al., 2000*) the Quasi-3D formulations of Reniers et al. (*2004*) are implemented, which describes the vertical structure of the mean velocity profile over the whole depth below the trough level. The formulations include presence of wind, wave stresses, pressure gradients, turbulent eddy viscosity and a wave boundary layer.

In the Quasi-3D formulations, Instead of linking bed roughness to real depth-averaged mean velocity, it is linked to a representative depth-averaged mean velocity ($\bar{u}_R$) based on the mean velocity in the lowest computational layer (z=a), assuming a logarithmic velocity profile. Important is to notice that due to near-bed streaming ($\bar{u}_R$) can be positive while the real depth-averaged current velocity might be negative (compared to wave propagation direction). Several iterations are used to determine the equilibrium between roughness and strength of the near bed mean velocity. It is assumed and checked (*Reniers, et al., 2004*) that the current profile is modelled in a correct way and that the velocity in the lowest layer can be used as input as for the bed load model.

4.6.2. Application SANTOSS in UNIBEST-TC

The SANTOSS formulations use the magnitude (u_c) and direction (angle compared to the wave propagation direction) of the mean current velocity at (or closely above) the edge of the wave boundary layer for calculating the bed shear stress and the resulting sediment transport. The measurement should take place above streaming because the influence of the streaming is already included in the SANTOSS formulations.

In the model applications and calibrations a constant level (20 cm above the bed) has been used from which the current velocity was taken, which was for all the measurements well above the boundary layer. While along a cross-shore profile currents and waves of different scales are present, it is in practice recommended to estimate a more suitable level for the edge of the wave boundary layer for each combination. Ribberink et al. (*2010*) recommends the expression proposed by Sleath (*1987*):

$$\frac{\delta_w}{k_{s,w}} = 0.27\left[\frac{A_w}{k_{s,w}}\right]^{0.67} \tag{4.6.1}$$

In which δ_w = the height at which the difference between the horizontal flow velocity and the free-stream velocity is less than 5%, A_w = characteristic orbital excursion amplitude and $k_{s,w}$ = wave-related roughness height.

A few comments are made on the implementation of the SANTOSS formulations considering a superimposed current:

- There are more formulas for describing the wave boundary layer thickness. Van Rijn (*2007b*) uses for example a formula which results into thicker wave boundary layers and even uses a factor 20 to take into account irregular waves (FACDEL = 20).
- Especially different transport rate predictions can be expected when the superimposed current velocity is high and opposed (e.g. undertow becomes large under breaking waves) or in the same direction as wave propagation. The higher level at which the mean velocity is measured by SANTOSS and thus the higher shift of the orbital time series that are used as input lead to a larger effect on the transport rates (changing half cycle periods and changing maximum orbital velocities).
- The Eulerian current velocities are used as input for the SANTOSS model, because the SANTOSS formulations already include an adaptation for the Lagrangian effect (grain motion).

4.7. Suspended load transport above wave boundary layer

According to Ribberink et al. (*2010*) the SANTOSS transport formulations includes all wave- and current-related sediment transport in the wave boundary layer. They also state that under non-breaking waves and small superimposed currents all sand transport takes place inside the wave boundary layer, so the SANTOSS transport model should in these cases cover all the transport.

On the other hand, for strong superimposed currents and breaking waves sediment may get into suspension to levels above the wave boundary layer, which should then be covered with another transport model for current-related suspended transport. The wave-related suspended transport defined in TR2004 does not have to be included, because this should be covered by the SANTOSS formulations. This despite the fact, that the wave-related suspended load is based on the suspended sediment within a thicker layer. As lower level for the integration of the suspended transport the level defined by equation (4.6.1) is used.

4.8. Conclusions

The SANTOSS transport model is implemented successfully in the UNIBEST-TC model by aligning the output of the current profile and orbital velocity modules to the necessary input for the SANTOSS model. Several small modifications to the SANTOSS model code were necessary to make it more robust and to extract the necessary velocity characteristics from the near-bed orbital velocity time series that are provided. Further, a relative simple method, almost the same as which was already used in UNIBEST-TC, is used to take into account the slope effects. Herein, just like in the bed load formulations of TR2004, the natural angle of repose (tanϕ) can be used to calibrate the stability of possible bars.

Next to the changes to the SANTOSS model are some choices and changes made to the input that is provided by UNIBEST-TC. This focuses on the orbital velocities and the current velocity from which the two conclusions can be drawn:

- The wave-current interaction is a complex element, especially due to the non-logarithmic current profile under real waves and the influence of wave irregularity on the wave boundary layer. In case of a superimposed current, the SANTOSS model uses the current velocity at the edge of the wave boundary layer as input. The TR2004 model on the other hand, uses the current velocity in the lowest computational point, which is why is expected that the transport predictions by the SANTOSS model are in general more influenced by a superimposed current than bed load transport of the TR2004 model. The influence of an undertow induced by breaking waves is tested in the next chapter.
- The SANTOSS model concept requires explicitly a good representation of the orbital velocity time series (including skewness and asymmetry and without unrealistic wobbles and discontinuities). To answer this criterion two theories available in the UNIBEST-TC version are modified and two are added. Especially the combination of three theories (*Grasmeijer & Ruessink, 2003; Abreu, et al., 2010; Ruessink & Van Rijn, in preparation*), leads to an orbital velocity time series which should (in theory) make a good representation of skewness, asymmetry and orbital amplitudes. It was chosen not to include wave group effects (irregularity of wave heights and the bound long wave) and use a representative (based on root-mean-square wave height and peak wave period) regular wave for the orbital velocities. In the test cases in Chapter 6 the results of the different orbital velocity will be compared with measurements.

The SANTOSS model covers in principal all the sediment transport in the wave boundary layer. It has been chosen to let the SANTOSS model predictions replace the bed load, the total wave-related suspended load and the current-related suspended load within the wave boundary layer. Thus, only the current-related suspended load above the wave boundary layer was not covered by the SANTOSS model.

5. Sensitivity analysis transport models within UNIBEST-TC

5.1. Introduction

To explore the differences between predictions of net transport rate under waves of the TR2004 and the SANTOSS model an extensive sensitivity analysis is executed for realistic conditions. Important is to understand that due to interaction between different processes, variation of one variable influences several processes. In the analysis a one-point approach is used and each time one variable is varied while keeping other variables constant.

In the first paragraph the standard settings of the analysis are described, followed by an analysis of hydrodynamic input for the considered range of conditions (paragraph 5.3). Next, the effect of variation of respectively grain size, wave period and wave height on the transport loads is examined. The influence of several processes is analyzed by turning them off. Finally, the differences in transport predictions calculated with the different orbital velocity theories are shown and discussed (paragraph 5.4). In the conclusion the influence of different processes are summarized.

5.2. Set-up and standard settings

The use of 1 grid cell gives the possibility to simulate each condition and extract information needed. Important is to mention that because of the one-point approach there is no spatial distributed process involved. In UNIBEST-TC the only spatial distributed process is the delayed breaking of waves (wave breaking concept with breaker delay) so the breaker delay has been turned off. For the wave breaking parameter γ the formula of Ruessink et al. (*2003*) which uses only local conditions instead of deep water conditions.

The in some way independent variables that define a specific wave condition are: the water depth (h_d), the significant wave height (H_{rms}), peak wave period (T_p), the angle between wave direction and normal of coast line (θ_{wave}), the sediment grain size (D_{50}), the bottom slope (slope) and a superimposed tide velocity (V_{tide} and φ_{tide}). For the

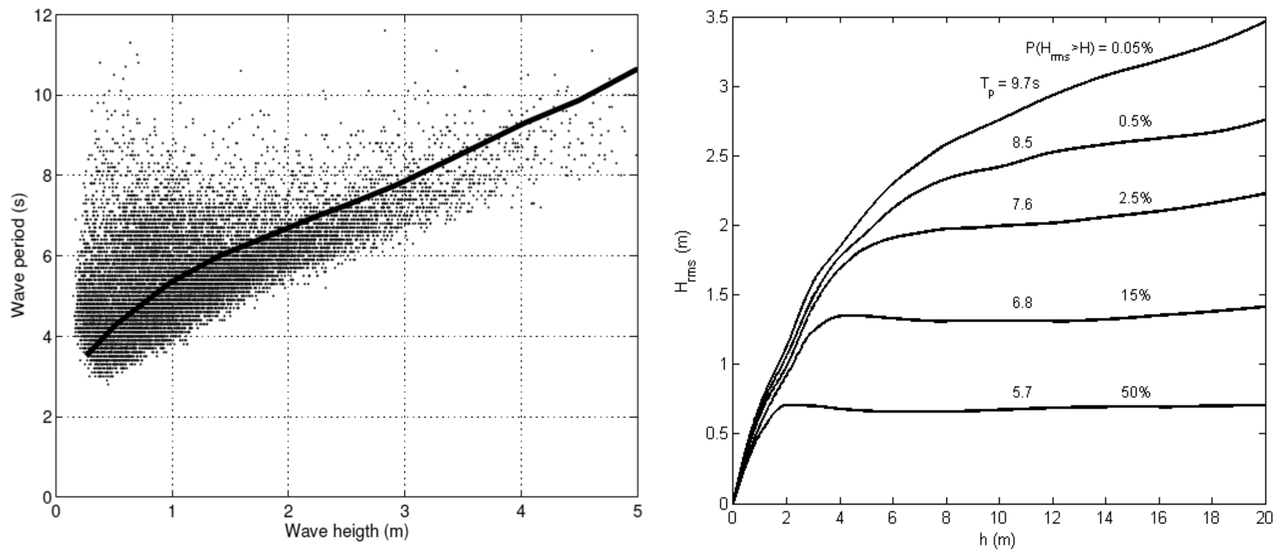

Figure 5-1: (a) Correlation between Hrms and Tp between 1997 and 2001 (De Leeuw, 2005). (b) Wave height evolution and probability of occurrence at different depths (Al-Salem, 1993)

sensitivity analysis in this chapter it is chosen to select a certain depth (h_d = 4m), assuming wave propagation towards the coast, a horizontal bed and no tidal velocity. The influence of wave height, peak period and sediment grain size is analyzed by varying each variable while keeping others constant.

The ranges that are considered for the wave height and the peak period are based on field data. Figure 5-1 shows the correlation between wave height and wave period measured at a buoy offshore of IJmuiden, where the water depth was 21 m (*De Leeuw, 2005*). It shows that the peak wave periods are between 4 and 10 s and small wave heights in general related to small wave periods and high waves to large wave periods. In the case of swell conditions wave height is small and wave periods can become large. Further, the wave height evolution and probability of occurrence is examined by Al-Salem (*1993*), which resulted in the representative wave height ranges for different depths.

Table 5-1 shows the settings and ranges that are used for the sensitivity analysis. The modified theory of Ruessink & Van Rijn (*in preparation*) with the orbital velocity amplitude modification defined by Grasmeijer & Ruessink (*2003*) is used, because this should in theory make a good representation of skewness, asymmetry and orbital velocity amplitudes. As standard a median sediment size of 0.2 mm is used, which is for analysis varied from 0.1 to 0.5 mm (D_{90} = 1.5*D_{50}, D_{10} = 2/3*D_{50}). For settings that are not mentioned, default values are used. For the transport formulations all the processes are included in the default runs: skewness, asymmetry, phase lag effects and surface wave effects.

5.3. Model behaviour

Before examining the sensitivity of transport loads, first an overview given on the hydrodynamic behaviour. This focuses on orbital velocities and wave forms, together with undertow velocities induced by breaking waves, which are used as input to the transport models. Next, the variation of respectively grain size, wave period and wave height is examined. For each variation of a variable the effect on the current and concentration profile is shown and the resulting transport loads. The influence of phase lag effects, wave asymmetry, surface wave effects and of the generated undertow due to breaking waves is examined by excluding them.

Table 5-1: Input for the intercomparison of the sand transport models

Symbol	Default	Range	Description
D_{50}	0.2 mm	0.1 – 0.5 mm	Sediment size
h_d	4 m		Depth
$H_{rms,0}$	1 m	0 – 1.6 m	Wave height
T_p	7 s	4 - 10 s	Peak wave period
θ_{wave}	0°		Shore normal waves
V_{tide}	0 m/s		No tidal velocity
V_{wind}	0 m/s		No wind
SWASYM: orbital velocity theory	6		Ruessink & Van Rijn (in preparation, amplitude based on Grasmeijer & Ruessink, 2003)
SWLONG: wave group effects	3		No wave group effects: orbital velocity translated from significant wave height.
VARGAMM: breaking coefficient setting	1		Breaking coefficient γ based on Ruessink et al. (2003)

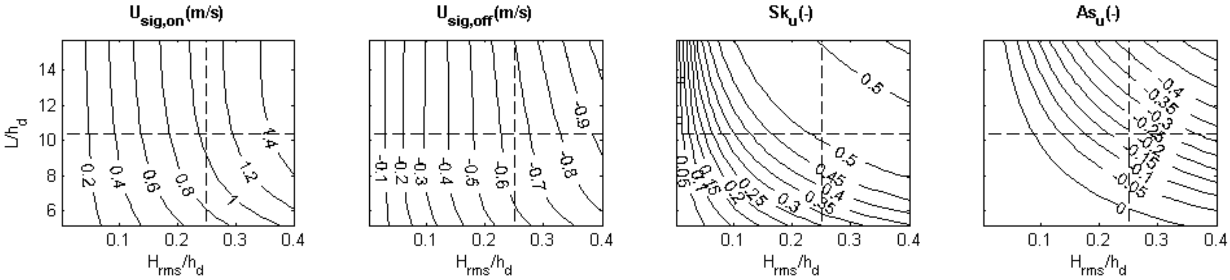

Figure 5-2: Orbital velocity characteristics: SWASYM = 6: RvR2: Ruessink & Van Rijn (in prep.), amplitude based on Grasmeijer & Ruessink (2003). Depth h_d = 4 m.

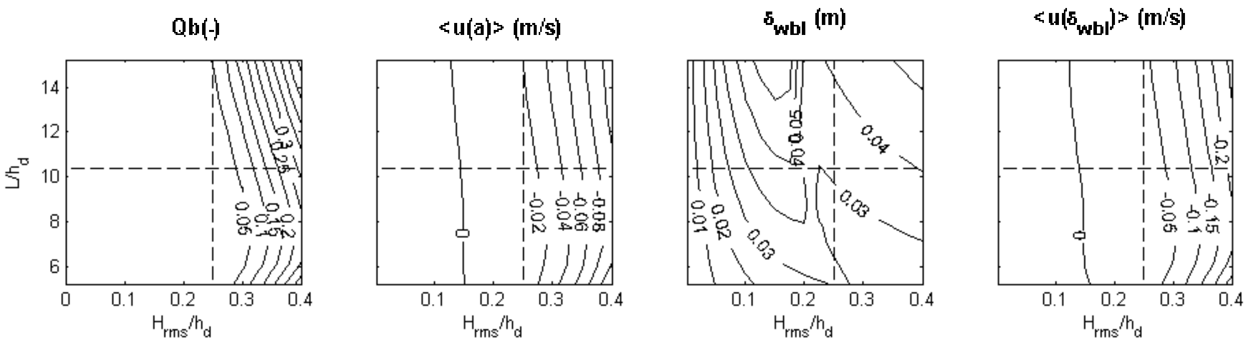

Figure 5-3: Current velocity aspects under breaking waves: (a) Part of breaking waves, (b) near bed mean velocity, (c) thickness wave boundary layer according to Sleath (1989) and (d) mean velocity at the edge of the wave boundary layer. h_d = 4 m, SWASYM = 6 and D_{50} = 0.2 mm

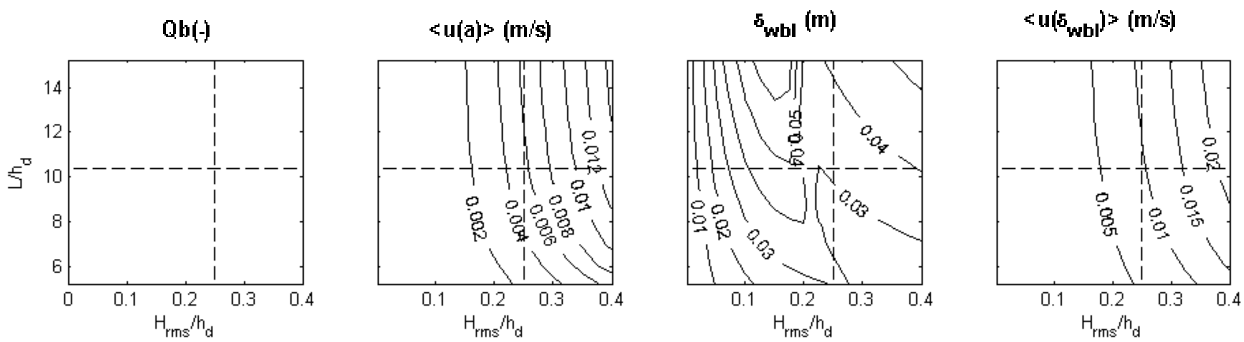

Figure 5-4: Current velocity aspects under non-breaking waves: (a) Part of breaking waves (breaking waves are excluded), (b) near bed mean velocity, (c) thickness wave boundary layer according to Sleath (1989) for D50 = 0.2 mm and (d) mean velocity at the edge of the wave boundary layer. h_d = 4, SWASYM = 6 and D_{50} = 0.2 mm.

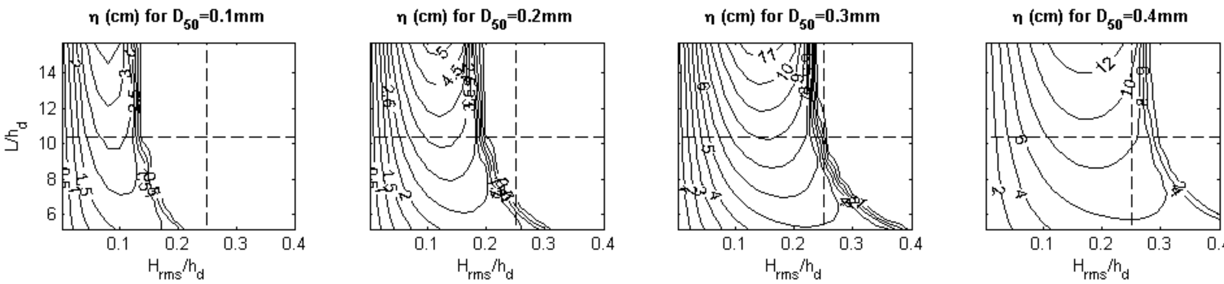

Figure 5-5: Ripple height according to the SANTOSS formulations for different sediment grain sizes. Depth h_d = 4 meters. SWASYM = 6.

5.3.1. Hydrodynamic exploration

Figure 5-2 shows how the maximum orbital velocities and the wave form depend on wave period and wave height. The chosen standard settings (shown with dashed lines) lead in this case to almost maximum skewness and the significant onshore velocity is about 1 m/s.

Due to the Rayleigh distribution of the wave heights always a part of the waves breaks. Figure 5-3 shows the amount of breaking waves, the mean velocity just above the bed <u(a)> (used as input for the bed load transport in the TR2004 model), the wave boundary layer thickness according to Sleath (*1987*) and the mean velocity at the edge of this proposed wave boundary layer (is used as input for the SANTOSS model). The amount of breaking waves depends mainly on the relative wave height although longer waves have the intention to break at smaller wave heights. The mean velocities at the bottom show that streaming is present for $H_{rms}/h_d < 0.15$. For higher waves the undertow overrules the streaming, which leads to negative velocities at the bed. Under breaking waves the mean velocities in the lowest computational layer (z=a) which are used by the TR2004 model are 2-3 times smaller than the velocities used by SANTOSS (velocities at the edge of the wave boundary layer). Figure 5-4 shows the same data only now the amount of breaking waves is set to zero. The breaking of waves has a large influence on the near bed mean velocity.

In Figure 5-5 the ripple heights are shown for different sediment grains sizes, from which can be concluded that under the proposed standard wave conditions ripples are predicted by the SANTOSS model for D_{50} > 0.3 mm. In the ripple regime the height of the ripples is clearly related to the orbital excursion amplitude, which increases with increasing wave period. Important is the small transition zone between high ripples and sheet-flow regime, which can lead to large changes in sediment transport.

5.3.2. Grain size variation

Variation of the sediment grains size can lead to changes in bed roughness and can affect the hydrodynamics in this way. In Figure 5-5 it was already shown that for D_{50} > 0.3mm ripples are predicted by the SANTOSS model and that ripple heights increase with sediment grain size. Figure 5-6 shows the wave-averaged current profile for the standard conditions for grain sizes varying from 0.1 to 0.4 mm. The roughness predicted by the TR2004 bed roughness predictor depends partly on the sediment grain size. The interaction between mean current and bed roughness (equilibrium defined using several iterations) leads to only a marginal difference between the current profiles. On the other hand, the concentration profile is strongly affected by changes in sediment grain size. With increasing sediment size, the reference concentration first decreases due to mainly increasing critical shear stress and thus decreasing effective stress. Later, the reference concentration increases again due to the large increase in bed roughness (due to ripples and mega-ripples) and thus effective shear stress. The steepness of the concentration profile depends on the sediment mixing coefficient and the fall velocity. The fall velocity increases with grain size which explains the rapid decrease of concentration over the depth for the larger grain sizes. The offshore-directed current-related suspended load is therefore only high for fine sediment.

Figure 5-7 (a) shows that the bed load transport computed by TR2004 increases slightly with D_{50} due to the increasing grain friction coefficient (=1D_{90}). In contrary, the wave-related suspended load transport (b) decreases with D_{50}, due to the rapidly decreasing sediment concentration. In the figure the influence of the phase lag effects is clearly visible and induces wave-related transport to change direction for the cases where the roughness height is high (where ripples are present). For fine sediment the wave related suspended load increases due to the higher concentration of suspended

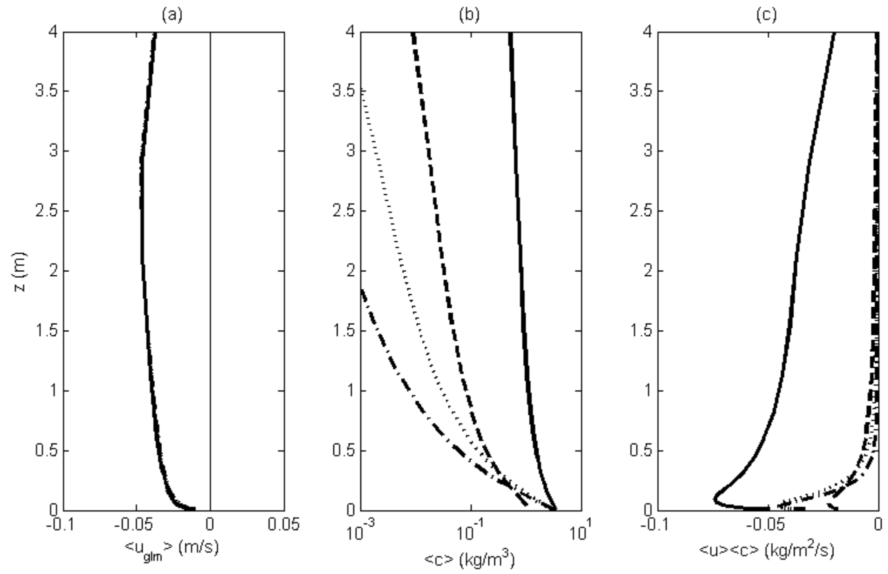

Figure 5-6: Vertical profiles of the wave-averaged cross-shore current (a), wave-averaged suspended sand concentration (b) and current-related suspended sediment transport (c) in cross-shore direction for D_{50}=0.1mm (solid), D_{50}=0.2mm (dashed), D_{50}=0.3mm (dotted) and D_{50}=0.4mm (dashed-dotted lines).

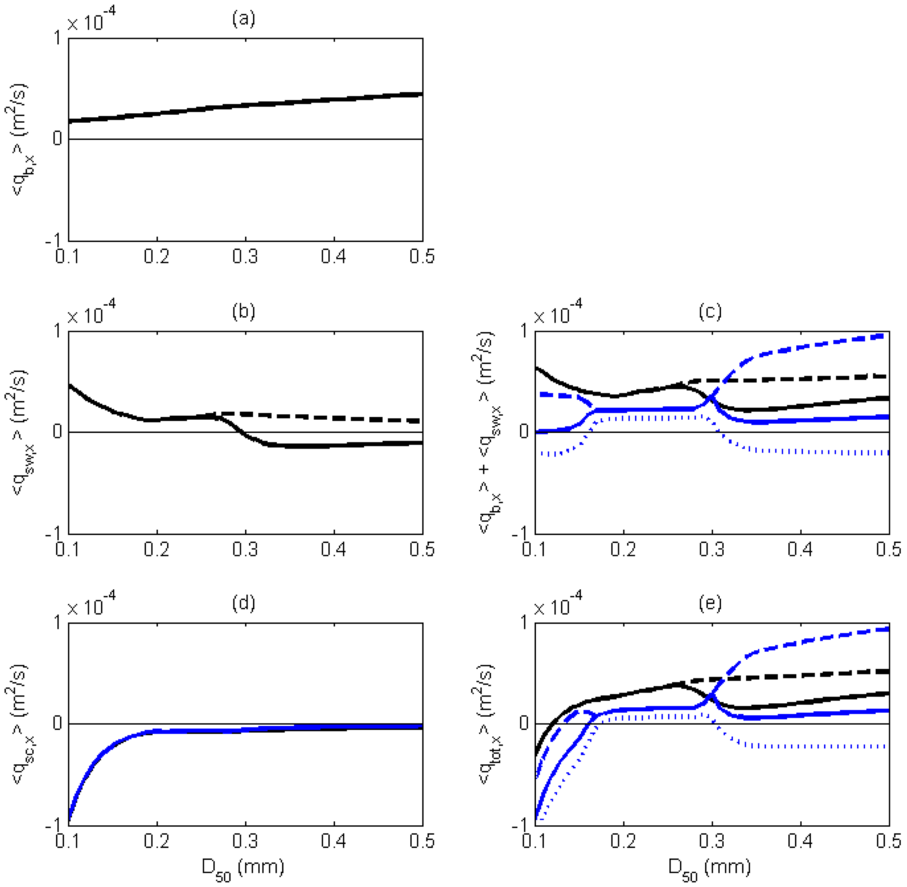

Figure 5-7: Predicted transport rates in cross-shore direction for changing sediment grain sizes: the bed load (a), the wave-related suspended load (b), the bed load + wave-related suspended load (c), current-related suspended load (d) and total load transport rates (e) by TR2004 (solid black line) and SANTOSS (solid blue line). Option added in figure: excluding phase lag effects (dashed lines) and excluding surface wave effects (dotted lines).

sediment. Despite the decreasing fall velocity there are no phase lag effect noticed, which can be explained by the small wave-related roughness height. The wave-related suspended load and bed load transport together give a positive transport rate for all grain sizes (c).

The SANTOSS transport predictions within the wave boundary layer shows partly the same behaviour as the bed load + wave-related suspended load transport predicted by TR2004 together (c). For D_{50} larger than 0.3 mm, ripples are present, which induce large phase lag effects: the phase lag effects reduce the transport rates to almost zero. Without the influence of the phase lag effects the transport rates over ripples is much higher in the ripple regime due to the higher roughness height. Also for fine sediment phase lag effects are predicted by the SANTOSS model which is caused by the low fall velocity. The small peak in transport for D_{50} = 0.3 mm (at the transition zone from flat bed to rippled bed) is caused by the development of small ripples (thus higher bed roughness), where the critical phase lag parameter is not yet exceeded.

The net total transport rates (e) predicted by TR2004 and SANTOSS are different for all sediment sizes, where the predictions by the SANTOSS model are always a bit lower. On the other hand show the two models the same behaviour: negative transport for fine sediment (for D_{50}<0.15mm the current-related suspended load becomes dominant), with increasing D_{50} sediment transport predictions stay constant until the ripple regime is reached, where the phase lag effect reduces the transport rates significantly.

Finally, transport predictions of the SANTOSS model without the recognized surface wave effects are shown in Figure 5-7 (c) and (e) with the dotted lines. The effect on the transport rates is relatively large especially under phase lag dominated conditions. When ripples are present (for large D_{50}) mainly vertical orbital velocities present under real waves induce transport rates to become positive again. For small D_{50} the influence of vertical orbital velocities in the sheet flow layer is marginal, because of the much lower reference level. Here, changes in half-cycle periods and the added streaming stress induce the net transport rates to become more positive.

5.3.3. Wave period variation

In the hydrodynamic analysis in Figure 5-2 and Figure 5-3 it was shown that variation of the wave period has a large effect on the wave form and only a small influence on the maximum orbital velocities. An increasing wave period until about 8 s leads for the standard conditions to an increase in skewness, but for higher wave periods the skewness stays the same or even become less. The asymmetry not present under short waves keeps increasing for increasing wave period. Orbital peak velocities are constant for large periods, but slightly smaller for lower wave periods. Next to these aspects ripples are predicted by the SANTOSS model for T_p < 5 s (which is L/h_d < 8, see Figure 5-5).

The vertical profiles of the mean current and the concentration and the suspended load flux are shown in Figure 5-8. In general, the undertow near the bed increases with wave period due to a higher mass flux in the upper layer and a small but increasing amount of breaking waves. Only for small wave period (T_p < 6) the amount of breaking waves increases with decreasing wave period (see Figure 5-3). The reference concentration is highest for T_p = 4 s due to the higher bed roughness (ripples). On the other hand, the concentration decreases rapidly with small wave period due to the small wave boundary layer.

The bed load computed by TR2004 increases with increasing wave period, mainly due to the increasing orbital velocities (especially increase when periods are low), skewness and asymmetry (see Figure 5-9 (a)). Excluding the effect of asymmetry has a large

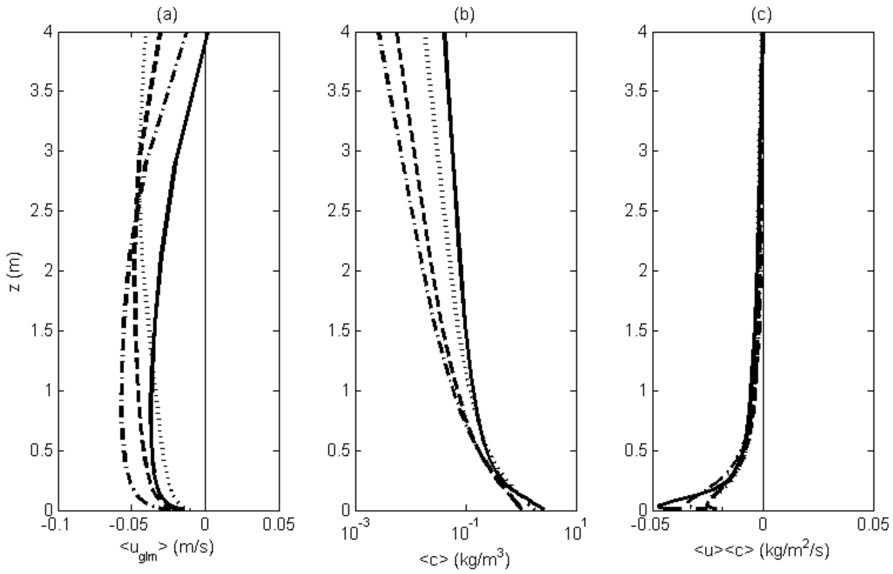

Figure 5-8: Vertical profiles of the wave-averaged cross-shore current (a), wave-averaged suspended sand concentration and current-related suspended sediment transport (c) in cross-shore direction for T_p = 4 s (solid lines), T_p = 6 s (dashed lines), T_p = 8 s (dotted lines) and T_p = 10 s (dashed-dotted lines).

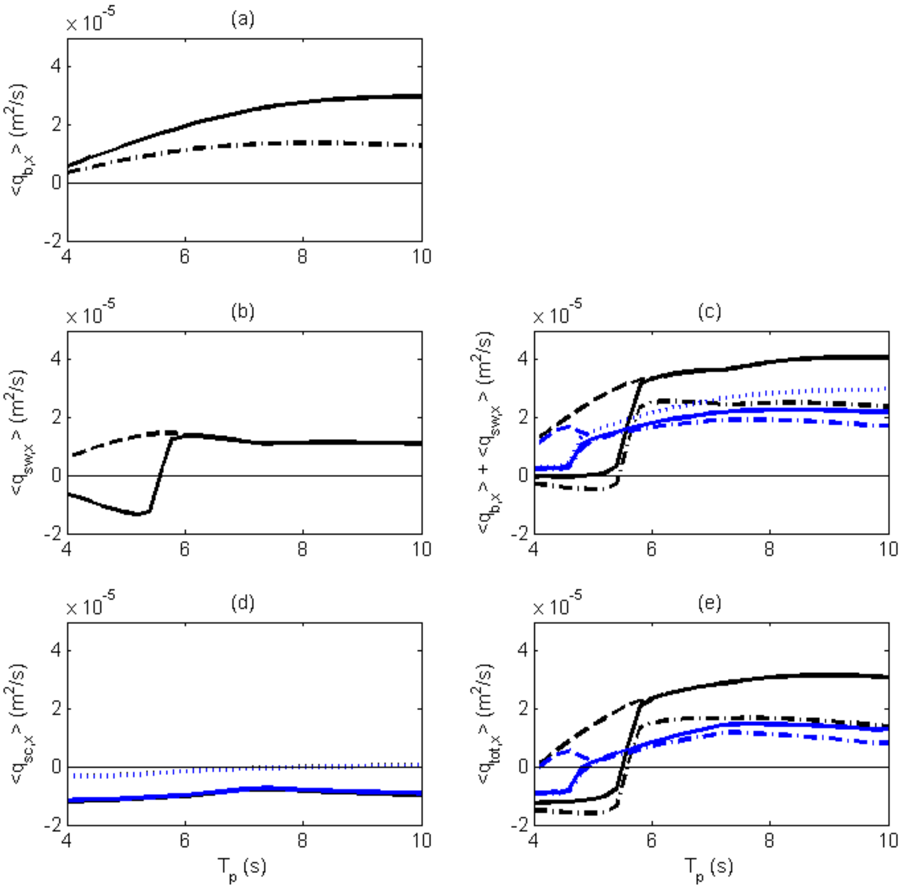

Figure 5-9: Predicted transport rates in cross-shore direction for changing wave period: the bed load (a), the wave-related suspended load (b), the bed load + wave-related suspended load (c), current-related suspended load (d) and total load transport rates (e) by TR2004 (solid black line) and SANTOSS (solid blue line). Options added in figure: excluding asymmetry effects (dash-dotted lines); excluding phase lag effects (dashed lines); and excluding breaking of waves (dotted lines, effect only shown for current-related suspended load transport: goes to zero).

influence on the bed load transport; it leads to a decrease of transport rates when skewness drops and waves become mainly asymmetric.

Despite the increasing skewness, the wave-related suspended load (b) stays about the same for all wave periods, which is caused by the slight decrease in concentration near the bed. Only for conditions where ripples are predicted (T_p<5.5 s) and phase lag effects become dominant, the wave-related suspended load becomes negative (induced by combination of the high wave-related roughness height and the small wave period).

The wave-related suspended load and bed load together predicted by TR2004 is higher than the SANTOSS predictions (about factor 2 higher, see (c)). Where ripples are present according to TR2004 the transport rate is reduced to zero. The same results are shown for the SANTOSS predictions in the ripple-regime, although the transition between ripples-regime and sheet-flow regime take place under different conditions. The effect of asymmetry on SANTOSS predictions for these conditions is rather small especially compared to the effect of the asymmetry on the TR2004 predictions. Due to the small amount of breaking waves for H_{rms} = 1 (only 2-5% of the waves), the influence of the breaking waves is small. Excluding leads to a bit more onshore net transport for the SANTOSS predictions and has no influence on the predicted bed load and wave-related suspended load by TR2004.

The current-related suspended load (d) is almost constant for changing wave period, which is primarily caused by the relatively constant amount of breaking waves. The total amount of current-related suspended load can be linked to breaking waves. The total load for non-breaking waves is therefore the same as in (c), while for breaking waves the total load reduces and becomes negative above ripples.

The surface wave effects (transports without surface wave effects are not shown in Figure 5-9) induce more onshore directed transport over the whole range of about $1.0 \cdot 10^{-5}$ m^2/s.

5.3.4. Wave height variation

An increasing wave height not only increases the amplitude of the orbital velocity but also changes the wave form. According to Figure 5-2 the skewness increases directly and until its maximum at about H_{rms} = 1.1m, after which the skewness stays about constant. The asymmetry increases much slower but keeps increasing over the whole range. Furthermore, an increasing wave height leads to an increase of the undertow due to the higher mass flux in the upper layer and the higher amount of breaking waves. The energy dissipation due to breaking induces an undertow which is already noticeable at relatively small wave heights. Figure 5-10 shows the current, suspended sediment concentration and sediment flux profiles over the whole depth for different wave heights. For wave heights lower than 0.6 m the streaming is noticeable, for higher wave heights the undertow becomes dominant.

The effect of the bed roughness predictor of TR2004 is visible in the reference concentrations near the bed. The predicted ripples for small waves (H_{rms} ≤ 0.8 m) induce high bed shear stresses and relatively high reference concentrations (the same reference concentration are noticeable for H_{rms} = 0.8 and 1.2 m). The suspended sediment fluxes are especially dominant under high waves (combination of high concentration and high undertow velocities).

Figure 5-11(a) shows that the bed load transport predicted by TR2004 increases with increasing wave height, due to skewness and asymmetry and despite the influence of the increasing undertow velocity. The large undertow under high and breaking waves has little influence on the bed load transport rates because the mean velocity in the

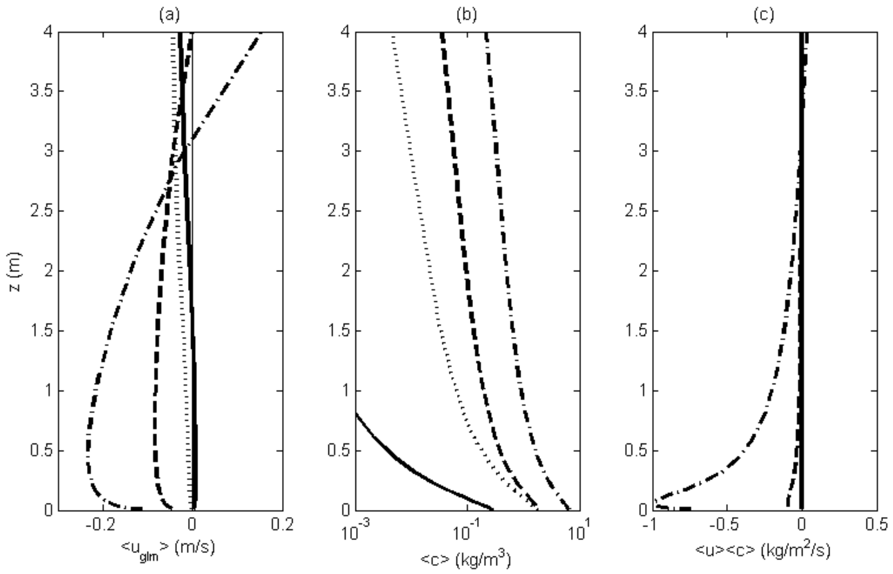

Figure 5-10: Vertical profiles of the wave-averaged cross-shore current (a), wave-averaged suspended sand concentration and current-related suspended sediment transport (c) in cross-shore direction for H_{rms} =0.4 m (solid lines), H_{rms}=0.8 m (dashed lines), H_{rms}=1.2 m (dotted lines) and H_{rms}=1.6 m (dashed-dotted lines).

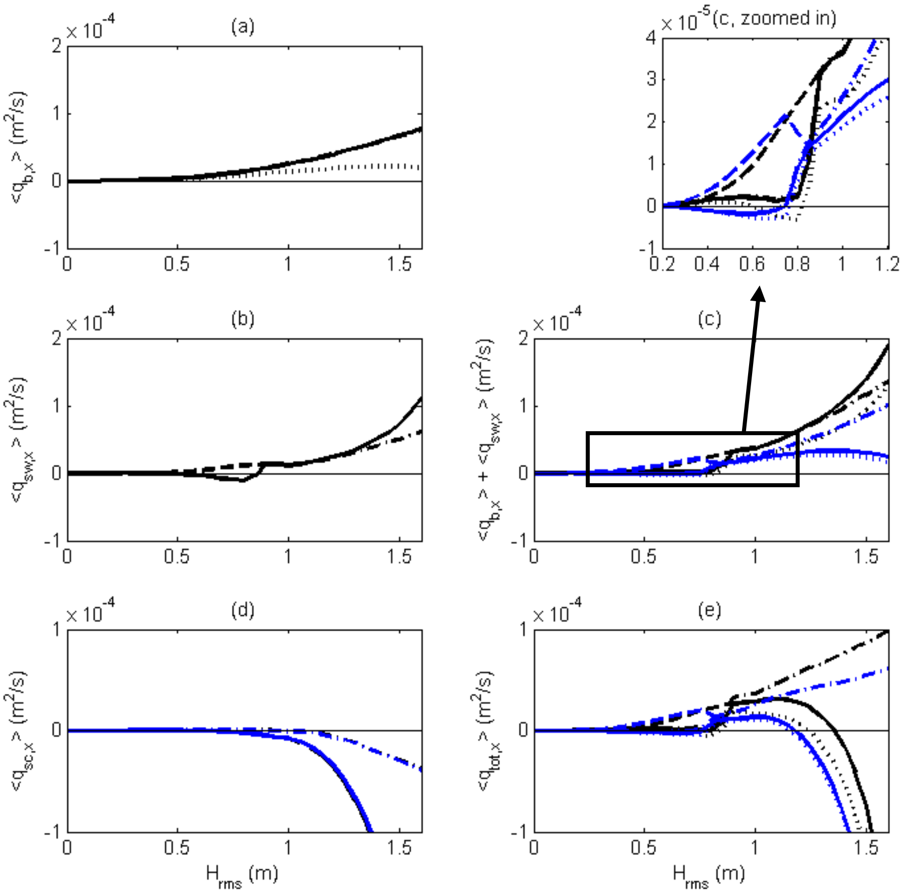

Figure 5-11: Predicted transport rates in cross-shore direction for changing wave heights: the bed load (a), the wave-related suspended load (b), the bed load + wave-related suspended load (c), current-related suspended load (d) and total load transport rates (e) by TR2004 (solid black line) and SANTOSS (solid blue line). Options added in figure: excluding asymmetry effects (dotted lines), excluding phase lag effects (dashed lines) and excluding breaking of waves (dash-dotted lines).

lowest computational point is used as input. Excluding the influence of asymmetry leads to lower predicted bed load transport rates for TR2004.

The wave-related suspended transport rates (b) are of the same size as the bed load transport rates for the whole range of wave heights and increase in general with increasing wave heights. For $0.4<H_{rms}<0.8$m the wave-related suspended load is a little bit higher due to the high roughness height (ripple regime) and thus higher concentrations above the bed. In case of taking into account the phase lag effects, it will lead to slightly negative transport rates above the predicted ripples. For H_{rms} > 1.2 m the increase of concentration due to breaking waves (which induces a higher reference concentration and a higher mixing coefficient) enhances wave-related transport in the onshore direction.

Figure 5-11(c) shows that predictions by the SANTOSS model in the ripple regime are negative, but close to zero. In the sheet flow regime first an increase is noticed due to higher skewness and asymmetry, but the undertow velocity induced by breaking waves negatively affects the transport rates more and more for higher wave heights. The combination of bed load and wave-related suspended load transport rates predicted by TR2004 results in higher transport rates which keeps increasing for higher waves. Here the increase of net transport due to higher orbital amplitude and asymmetry is not overcome by the undertow. The influence of a superimposed current is much higher for the SANTOSS model especially due to the higher level from which the velocity is taken.

The influence of asymmetry on the SANTOSS predictions is much lower than compared to the influence on the TR2004 predictions, which is caused by the different methods used by the two models to take into account the wave asymmetry / acceleration effects. The time-domain-filter method of Nielsen and Callaghan *(Nielsen & Callaghan, 2003)*used in the TR2004 formulations increases shear stresses due to acceleration, which mean that it actually also increases wave skewness.

The current-related suspended transport is highly influence by the breaking of waves. Not only the increasing concentration, but also the increasing undertow enhances offshore transport. The offshore directed current-related suspended transport begins to increase for H_{rms} = 1.0 meter and is dominating for H_{rms} > 1.2 m. The current-related suspended transport rates are in the TR2004 formulations slightly compensated by the slower increasing wave-related suspended load and bed load transport.

5.4. Comparison between orbital velocity theories

In this paragraph the resulting transport rates of the different orbital velocity theories are compared. Because transport rates are mainly affected by wave height, this is the variable that is varied for comparison. The next four theories are compared:

- Elfrink: Elfrink et al. (*2006*)
- vTdV: Van Thiel de Vries (*2009*)
- R&vR1: Ruessink & Van Rijn (*in preparation*), amplitude based on linear wave theory.
- R&vR2: Ruessink & Van Rijn (*in preparation*), amplitude modified with factor r from equation (4.4.17).

The first and latter two theory are adjusted (improved) with the formula of Abreu et al. (*2010*), see paragraph 4.4 for more details. In Figure 5-12 the orbital velocity characteristics of these theories are shown. Important observations are:

- Orbital velocity amplitude: amplitude especially depends on the wave height. vTdV show smallest amplitudes, R&vR1 show largest amplitudes, while Elfrink and R&vR2 are comparable. Differences in amplitudes become clearer for higher waves.

- Skewness: Increases with both wave height as wave period within the considered ranges for all theories at this depth. For R&vR1 and R&vR2 skewness is limited to Sk = 0.5, while vTdV and Elfrink keep increasing.
- Asymmetry: according to Elfrink asymmetry increases with increasing wave period and decreasing wave height. The other theories show the same asymmetry, which is zero for low wave height or low periods, but increases with increasing wave period and wave height.

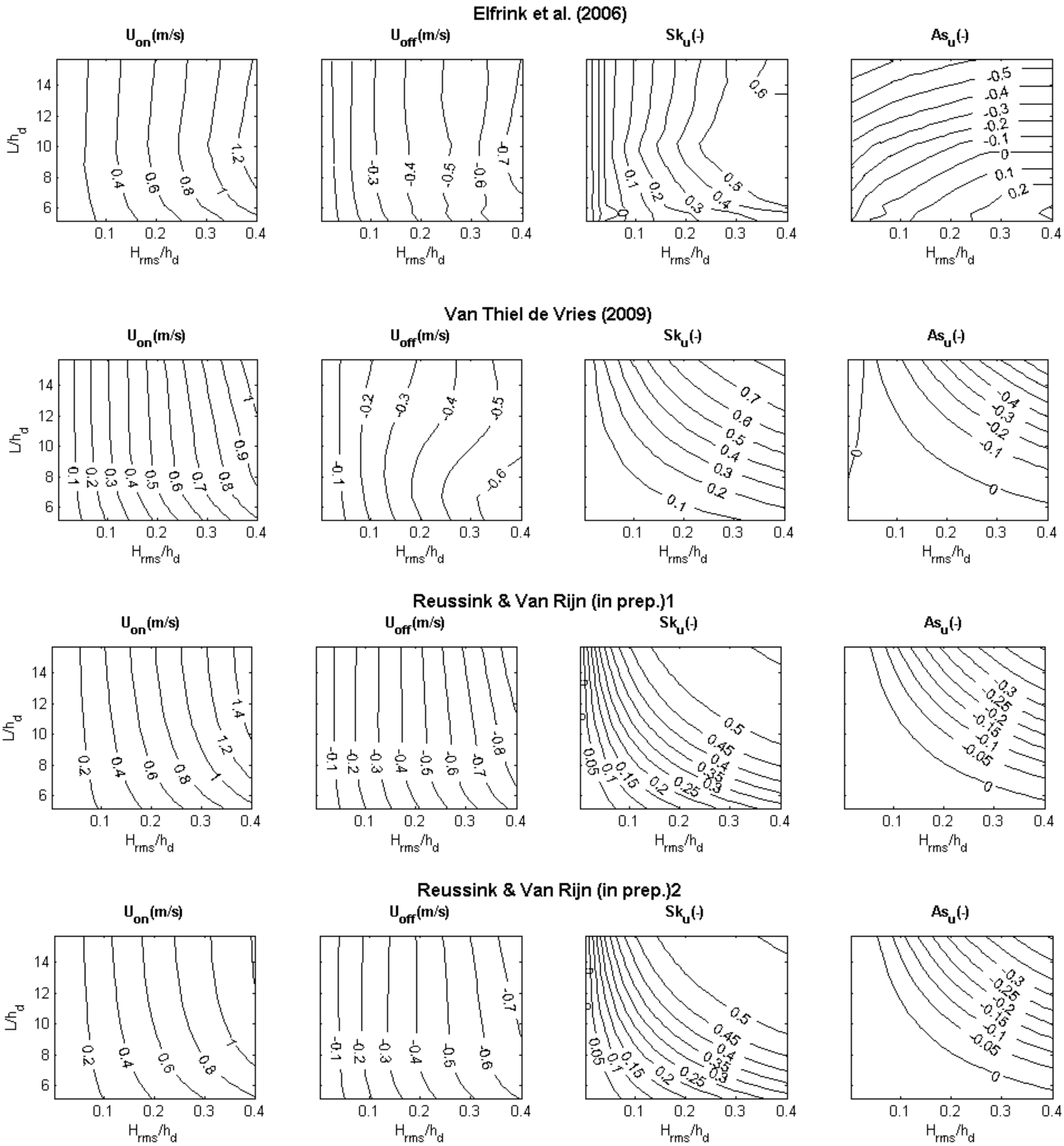

Figure 5-12: Orbital velocity characteristics based on the different orbital velocity theories for h_d = 4m. R&vR1: amplitude based on linear wave theory, R&vR2: amplitude modified based on Grasmeijer and Ruessink (2003)

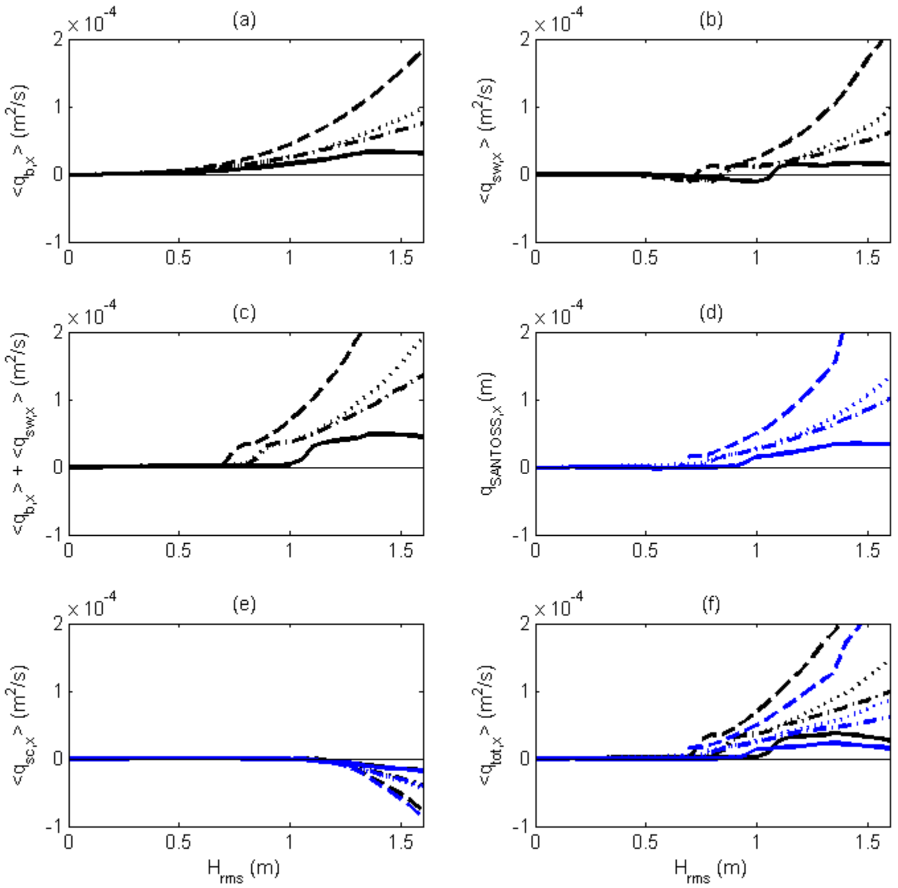

Figure 5-13: Predicted transport rates in cross-shore direction for changing wave heights under non-breaking waves: the bed load (a), the wave-related suspended load (b), the bed load + wave-related suspended load (c), the transport within the wave boundary layer predicted by the SANTOSS model (d), current-related suspended load (e) and total load transport rates (e) by TR2004 (black lines) and SANTOSS (blue line). In each figure the results are shown using different orbital velocity theories: Elfrink (dotted lines), vTdV (solid lines) , R&vR1 (dashed lines) and R&vR2 (dash-dotted lines).

The influence of the different orbital velocity theories on the transport rates for varying wave height (using standard conditions from Table 5-1) are illustrated in Figure 5-13 and Figure 5-14 for respectively non-breaking and breaking waves.

A general examination shows already that especially the orbital velocity amplitudes have an effect on the transport rates. Differences in amplitudes lead to differences in prediction of ripple regime (transition ripple-sheet flow clearly visible in figures between0.7 < H_{rms} < 1.1m). In the ripple regime net transport rates become for all orbital velocity theories almost zero, where those of TR2004 are slightly positive and those of SANTOSS negative.

In the sheet-flow regime under non-breaking waves (Figure 5-13) the theory of R&vR1 shows the highest transport loads (bed load and wave-related and current-related suspended load), the use of vTdV results in lowest transport loads and the theory of Elfrink and R&vR2 results in almost the same transport loads. The magnitude of the transport rates increase here with orbital velocity amplitude when skewness stays constant (predicted skewness by the different theories is the same). The two transport models show the same behaviour under non-breaking waves for each orbital velocity

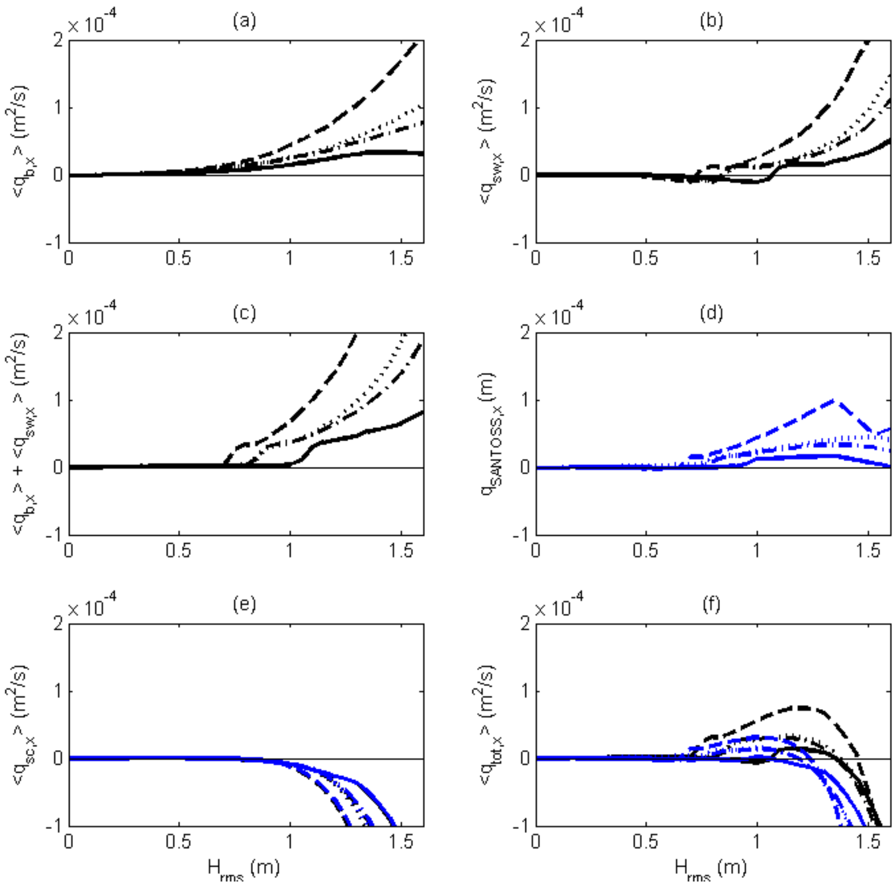

Figure 5-14: Same as Figure 5-13 but for breaking waves

theory; only the predicted net transport rates by the TR2004 model are slightly higher than the predictions by SANTOSS (up to 50% higher for the sheet flow regime).

Under breaking waves (Figure 5-14) the high current-related suspended load becomes dominant for almost the whole sheet flow regime. The undertow has again a large effect on the transport in the wave boundary layer predicted by SANTOSS. This is why the net transport rates predicted by SANTOSS are much lower under breaking waves and current-related transport becomes dominant at lower wave height.

A remarkable feature is the change in net transport rate for the theory with the largest orbital velocity amplitude (R&vR1) at about H_{rms} = 1.2m. This shows the effect of extra roughness induced by the mobile bed effects. This aspect is not implemented in the TR2004 formulations, but it is in the SANTOSS model. In this case the average Shields parameter is higher than 1, at which the mobile bed effects induce higher roughness, higher shear stresses, more entrained loads, higher sheet flow thicknesses and higher phase lag parameters. Under these conditions phase lag effects are noticed again. In case of non-breaking waves net transport rates predicted by SANTOSS increase despite the phase lag effects. Under breaking waves the combination of phase lag effects with a high undertow velocity leads to lower net transport rates.

5.5. Conclusions

In this chapter the predicted transport rates by the SANTOSS model are compared to those of the TR2004 model under varying conditions, focusing on wave-induced transport. The transport predictions are compared systematically for varying median grain size, wave period and wave height for a water depth of 4m.

The bed load and the wave-related suspended load are in all cases of the same order, although the wave-related suspended load becomes negative in the ripple regime due to phase lags. Due to this the net transport rate predicted by TR2004 is almost zero. From a certain wave height the part of breaking waves increases rapidly which induces an undertow that is directly measurable at the bed. Due to the undertow the current-related suspended load can rapidly increase and dominate the net transport.

The transport predictions by the SANTOSS model in the ripple regime are also close to zero, but are slightly negative. Under sheet flow conditions the SANTOSS predictions within the wave boundary layer are much more affected by the undertow induced by breaking waves compared to the bed load and wave-related suspended load of TR2004, due to the fact that the SANTOSS model uses the current velocity from a higher level as input. The current-related suspended load used by the SANTOSS model, also dominates here for high waves.

The influence of several processes is analyzed by switching the processes off:

- The influence of wave breaking on the net transport rate is significant considering the large current-related suspended load. For non-breaking waves the SANTOSS model predictions are comparable with the combined bed load and wave-related suspended load of TR2004, only a bit lower.
- The way wave asymmetry (acceleration effects) is taken into account by the two models is different, which leads to a large influence of the wave asymmetry on the bed load prediction of TR2004 but only a small influence on the transport in the wave boundary layer predicted by SANTOSS.
- The phase lag effects are noticeable in the ripple regime, where it will mainly reduce the transport rates. Without the phase lag effects, the increased roughness due to ripples increases the onshore net transport rates. The phase lag effects in the sheet flow regime (only predicted by the SANTOSS model) are only noticed at high waves or at fine sediment where the current-related suspended load is dominating.
- The surface wave effects (streaming, vertical orbital velocities and Lagrangian effects) are only shown for the SANTOSS predictions on which they have a small positive (onshore directed) effect under sheet flow conditions and a significant positive influence in the ripple regime due to the effect of the vertical velocities on the phase lags effects.

Finally, the importance of a good representation of the orbital velocities is shown using different available orbital velocity theories as input for the transport models. Large differences are found for the different theories, which can be explained by the difference in predicted orbital amplitudes and the comparable skewness. The two transport models respond about the same on the change of orbital velocity theory.

6. Application of SANTOSS model to test cases

6.1. Introduction

Two test cases are used to explore the differences in transport predictions in practice and the performance of morphological evolution of the two models. It was chosen to use two of the LIP11D flume experiments: test 1B and 1C. A big advantage of these experiments is that many measurements are available of hydrodynamics, suspended sediment concentration and morphological evolution. The two test cases are interesting cases, because it is an erosive case (test 1B) where a sand bar is developed and an accretive case (test 1C) with onshore bar movement. Test 1C interesting, because due to the calm conditions the predicted current-related suspended sediment is low and the SANTOSS model covers than a relative large part of the total sediment transport. This makes this test case more interesting, especially when focusing on the influence of acceleration effects, phase lags and surface waves. First a short description of the test cases is given, followed by the calibration of the hydrodynamics based on measurements and the resulting transport rates. Also the morphological evolution is described together with the effects of several transport processes. At the end of each paragraph the results are discussed.

6.2. Description LIP IID experiments

Within the framework of the European Large Installation Plan (LIP) a programme of detailed measurements of hydrodynamics and sediment transport in the surf zone has been carried out in Delft Hydraulics Delta Flume. The objective was the generation of high quality and high resolution data on hydrodynamics and sediment transport dynamics on a natural equilibrium beach (Dean type beach with constant slope near and above the water line as a start), under erosive and accretive conditions. Special attention was paid to long-wave effects and near-bottom resolution *(Roelvink & Reniers, 1995; Sanchez-Arcilla, et al., 1995)*.

The LIP11D flume experiments were large-scale, purely 2D laboratory experiments, which offer ideal test cases for UNIBEST-TC. The flume experiments were conducted in the 240 m long Delta flume of Delft Hydraulics (now Deltares). During the experiments, wave heights, water levels, flow velocity profiles, orbital velocities, concentration profiles and bottom changes were measured.

The bed material consisted of sand with D_{50} = 0.22. The maximum offshore water depth to still water level was 4.1 m in all tests. During the experiments narrow-banded random waves were generated such that the wave steepness at the peak frequency in combination with the water level was expected to result in a stable, erosive and accretive beach. Test 1B is the erosive case with a peak period of T_p=5s and a high wave height of H_{rms} = 0.86m. Test 1C is the accretive case with a peak period of T_p=8s and a small wave height of H_{rms} = 0.41m.

6.3. Hydrodynamic calibration

The hydrodynamics are step by step calibrated on measurements of wave height, mean water level, current profiles and finally the orbital flow velocities. It is tried to use the default values if possible and use the same values for the two test cases. This calibration is purely done by hand (qualitative analysis) and no statistical analysis is used to minimize errors. The recommendations of the UNIBEST-TC User Guide (*Walstra, 2000*) are followed as far as possible (see
Table 6-1 for final settings). The Figures can be found a couple of pages further where first the results of Test 1B are shown, followed by those of Test 1C.For the calibration of the wave heights (1B: Figure 6-2, 1C: Figure 6-14) the breaker parameter γ defined by

the theory of Battjes & Stive *(1985)* is used. The locally variable parameter defined by Ruessink, et al. (*2003*) did not result into better agreement with the measured wave height. Some small modifications on the dissipation coefficient α and wave friction factor are made to get even better agreement. For test 1C a breaker delay (spatial lag between break point, described by depth and wave height, and the actual breaking) was necessary, which was set on F_LAM = 0.7.

The mean water level is calibrated together with the mean undertow velocity (estimated from the current profiles) using the slope of the wave front (BETD). The roller model is in this way influenced which determines the lag of energy transfer from waves to the underlying water. A low value of BETD led to the best result of mean water level (Figure 6-3 and Figure 6-15) and also gave the best results for the mean undertow velocities. In both cases the undertow in the through behind the bar is slightly underestimated (1B: Figure 6-10, 1C: Figure 6-22).

The shape of the undertow velocities is calibrated using the viscosity parameter f_v (FCVISC), which is a multiplication parameter to scale the viscosity distribution. By decreasing f_v the wave-induced turbulence decreases, which leads to a decrease of the total amount of eddy viscosity. As a result, less momentum is transported in the vertical direction, which results in a less uniform profile (a value of FCVISC = 0.05 was sufficient). For the thickness of the wave boundary layer the default multiplication value is used (FACDEL = 20).

For the orbital velocities the four analyzed theories (see 4.4 for more details about the theories) are applied to both cases. The significant orbital velocities are computed using the significant wave height $H_s = \sqrt{2}*H_{rms}$ as input. Figure 6-6 to 6-9 (1B) and Figure 6-18 to 6-20 show the resulting significant orbital velocities compared to the measurements and also show the computed skewness and asymmetry of the waves (for sinusoidal waves counts: Sk = 0 and As = 0).

For test 1B the combined of theory RvR2 (Ruessink & Van Rijn (*in preparation*), Abreu et al. (*2010*) and Grasmeijer & Ruessink (*2003*)), is in good agreement with the measurements. Elfrink shows a slightly overestimation of the orbital velocity amplitude, RvR1 strongly overestimates and vTdV strongly underestimates the orbital velocities amplitudes. For test 1C none of the theories agrees well with the measurements. R&vR2 and Elfrink show about the right characteristic orbital amplitude ($0.5*U_{w,on}+0.5*U_{w,off}$), but strongly underestimates skewness. The other two theories also underestimate the skewness of the wave and show again a strong over- or underestimation of the orbital velocities. Because RvR2 works the best in Test 1B and is one of the two best in Test 1C, it is chosen to use this theory for both test cases.

A short review of the calibrated hydrodynamics:

- LIP IID 1B:
  - The modelled wave heights, mean water level and undertow profiles do agree very well with the measurements. Only the undertow velocities near the shoreline are overestimated.
  - Orbital velocities can be represented accurately when using RvR2. The theory of Elrink et al. *(2006)* overestimates the velocities slightly.
  - The portion of breaking waves Q_b can be used as indication for locations where breaking of waves is concentrated. Here, it is underestimated on the offshore side of the bar crest, but no strange peaks are here visible.
- LIP IID 1C:
  - The modelled wave heights, mean water level and undertow profiles do agree very well with the measurements.

- Only the undertow velocities just offshore of the bar crest (x=145) is underestimated. It can be expected that this will have an influence on the predictions of the growth of the sand bar.
- The orbital velocities cannot be represented well. Again RvR2 is chosen, but here velocity skewness is clearly underestimated.
- The measured portion of breaking waves Q_b shows a peak in the trough on the onshore side of the bar crest, while this was not modelled. This might be an indication that the breaking of waves is not simulated well and that maybe a larger breaker delay is necessary or a different definition of the breaker parameter. This has been tried, but with the available theories in UNIBEST-TC it was not possible.

Table 6-1: Input for the morphological runs

Symbol	**1B**	**1C**	**Description**
D_{50}	0.22 mm	0.22 mm	Sediment grain size
H_0	4.1 m	4.1 m	Mean water level
$H_{rms,0}$	0.86 m	0.41 m	Root-mean-square wave height at wave maker
T_p	5 s	8 s	Peak wave period
V_{tide}	0 m/s	0 m/s	Tidal flow velocity
V_{wind}	0 m/s	0 m/s	Wind velocity
Θ	0°	0°	Angle with normal of the shore
GAMMA	0.00	0.00	Breaking coefficient γ (0 = based on Battjes & Janssen *(1978)*)
ALFAC	0.80	0.80	Dissipation coefficient for wave breaking
BETD	0.03	0.03	Slope of the wave front in the expression for the wave roller energy
FWEE	0.03	0.03	Friction factor in the expression for the wave energy dissipation due to
K_IJL	0	1	Breaker delay switch (0 = off, 1 = on)
F_LAM	0	0.7	Number of wave lengths used for breaker delay
FACDEL	20	20	Factor for wave boundary layer thickness (20 = irregular waves).
SWGLM	2	2	Generalized Lagrangian Method (2 = on)
SWASYM	6	6	Ruessink & Van Rijn (in preparation, amplitude based on Grasmeijer & Ruessink, 2003)
SWLONG	3	3	Wave group effects (0 = no wave group effects regular orbital velocity translated from local H_{rms})
AS_EFF	1	1	Effects acceleration skewness (assymetry) on the transport (0 = off, 1 = on)
PL_EFF	1	1	Effects phase lags on the transport (0 = off, 1 = on)
TANPHI	0.6	0.6	Angle of repose (for slope effects)
ZDRY	3	3	Extrapolate transport over dry part of the profile (vertical + run-up)
TDRY	18	30	Minimum water depth at the upwave boundary $h_{min} = g(Tp/Tdry)^2$

6.4. Transport predictions and morphology

For the transport predictions by the two models, the default values for the transport formulations are used, which means that no calibration took place on the bed roughness predictor and for the angle of repose the normal value of $\tan(\varphi_r) = 0.6$ is used (this is the natural value).

Because UNIBEST-TC is not good in predicting the transport rates at really shallow water near the coast line (it computes a large suspended load) the transport rates must be extrapolated (ZDRY = 3 extrapolates towards the run-up point) from a certain depth. The point from which the transport rates need to be extrapolated is at x = 160 m. Therefore, for minimum depth is defined by TDRY (18 for 1B and 30 for 1C).

For analysis of the transport rates the inferred transport rates are calculated. These transport rates are determined using the bed level changes and starting from both ends of the wave flume. The final inferred transport rates are determined using linear interpolation.

Test case 1B was simulated one time with both the transport models (using the standard settings). The concentration profiles in Figure 6-10 show that concentration are strongly overestimated on the foreshore, do agree pretty well around the bar and overestimate again near the shoreline. Figure 6-11 and Figure 6-12 show the resulting morphological change around the bar and the time-average transport loads (time-averaged over the whole simulation time) and net transport rates compared to the inferred transport rates over the whole wave flume.

The morphological evolution shows that according to both models the sand bar migrates too much offshore and the sand bar diffuses slowly. Comparison of the transport rates shows that the transport rates predicted by the SANTOSS model are much more offshore directed over the whole wave flume, compared to TR2004. According to TR2004 the positive bed load and wave-related suspended load can compensate the current-related suspended load. The SANTOSS component on the other hand, is much more affected by the undertow velocity and becomes negative just offshore of the bar. Onshore of the sand bar ripples are predicted and the undertow becomes smaller which induces the transport rates to become positive again. Also in comparison with the inferred transport rates the transport rates are over the whole profile too much offshore directed.

Test case 1C is analyzed in more detail, because in this case the current-related suspended load plays a smaller role and thus the transport in the wave boundary layer a much larger role. First of all, SANTOSS predicts over the whole profile ripples. In Figure 6-22 the concentration profiles over the profile can be found. It shows that the suspended sediment concentrations are only predicted well on the bank and are overestimated on other locations. Both the SANTOSS as well as the TR2004 model do not predict onshore bar movement. Over most of the profile no undertow is present due to the calm conditions. This leads to a good agreement between the predicted transport rates of TR2004 and SANTOSS.

For test 1C the runs are also executed without the influence of several processes and with the different orbital velocity theories. For the predicted transport rates on the foreshore no new conclusions can be drawn compared to those from the sensitivity analysis. The TR2004 model predicts on the fore shore some higher positive transport than the SANTOSS model. Further, acceleration effects enhance onshore transport (more for TR2004 than for SANTOSS) and phase lag effects reduce the transport rates (become more offshore directed). At the undertow peak (at the bar crest) the gradients in transport are still smaller than those of the inferred transport rates and are located too much offshore.

Also the application of the other orbital velocity models leads to the same effects on the transports as was discussed in Chapter 5. The changes in transport rates, do not lead to significant changes in morphological evolution, which is mainly due to the small changes in gradients in sediment transport and the location of the gradients which does not change.

6.5. Conclusions

In this chapter the two transport models which are implemented in the UNIBEST-TC model are tested on two test cases. Both versions of UNIBEST-TC show too much erosion (or too less accretion), which can be primarily linked to the hydrodynamics. Strikingly is the wrong prediction of the orbital velocities for Test 1C (by all theories), while the predictions for Test 1B can be represented almost perfect. This implies that the parameterization of Ruessink & Van Rijn (*in preparation*) does not predict the non-linearity accurately for this case, but maybe also for other swell conditions.

The modelled hydrodynamics of test 1B do agree with the measurements. The erosion (offshore bar migration) predicted by SANTOSS is slightly larger than that predicted by TR2004. Also this can be linked to the large undertow (over the whole profile) and the higher reaction of the SANTOSS predictions on an undertow velocity.

For test 1C the two transport models show much more agreement in predicted transport rates and morphological evolution, although both models predict a slight offshore bar migration, while onshore migration is measured. Next to the underestimation of the velocity skewness, the undertow velocities are underestimated. These two processes can explain the low gradient in transport rates and the wrong location compared to the inferred transport rates. Also the wave breaking and the delay between breaking and undertow can be the reason of the wrong location of the gradient in transport rates.

The sensitivity to different processes is tested by excluding the processes or choosing a different orbital velocity theory. This does result in changes in transport rates as expected from the sensitivity analysis, but the changes do take place over the whole profile which leads to only minor changes in morphological evolution (are also small because the morphological evolution is small in this case).

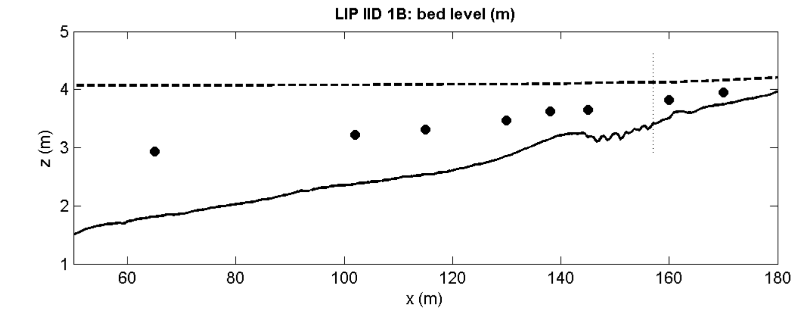

Figure 6-1: Test 1B: Bed profile + measurement locations

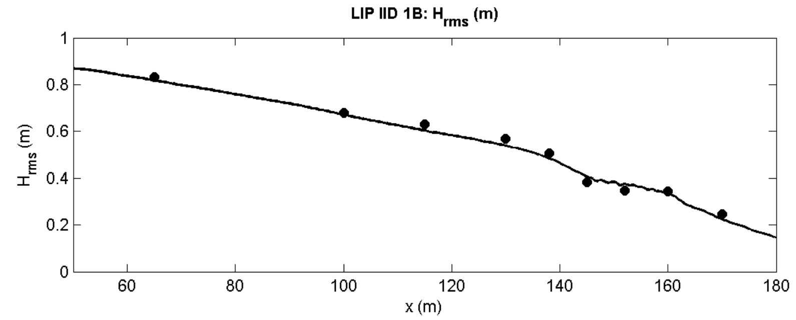

Figure 6-2: Test 1B: wave height evolution + measurements

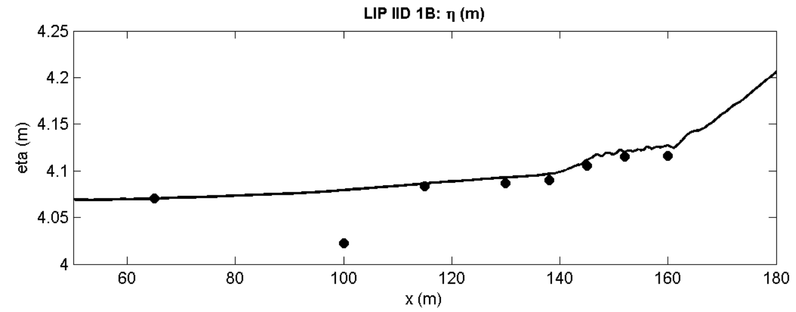

Figure 6-3: Test 1B: mean water level η

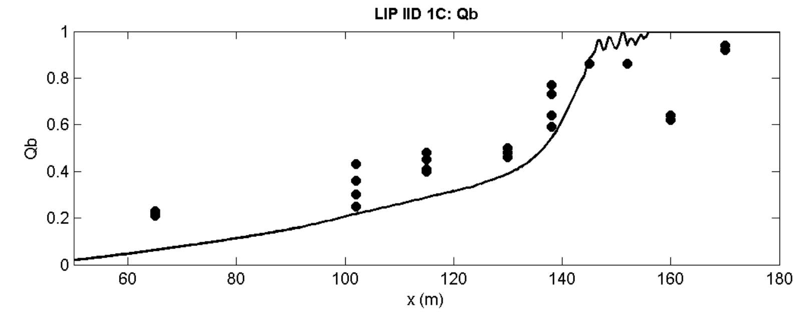

Figure 6-4: Test 1B: Part of wave breaking Qb

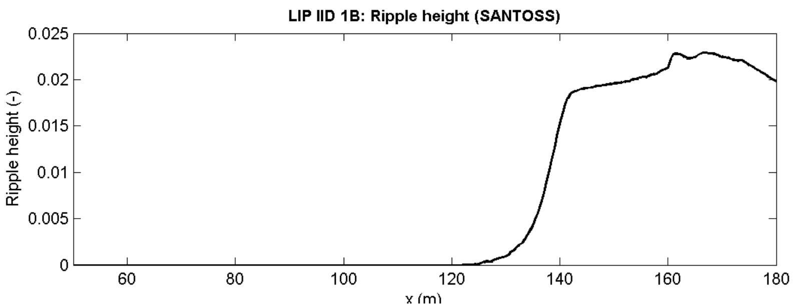

Figure 6-5: Test 1B: Ripple height predicted by SANTOSS

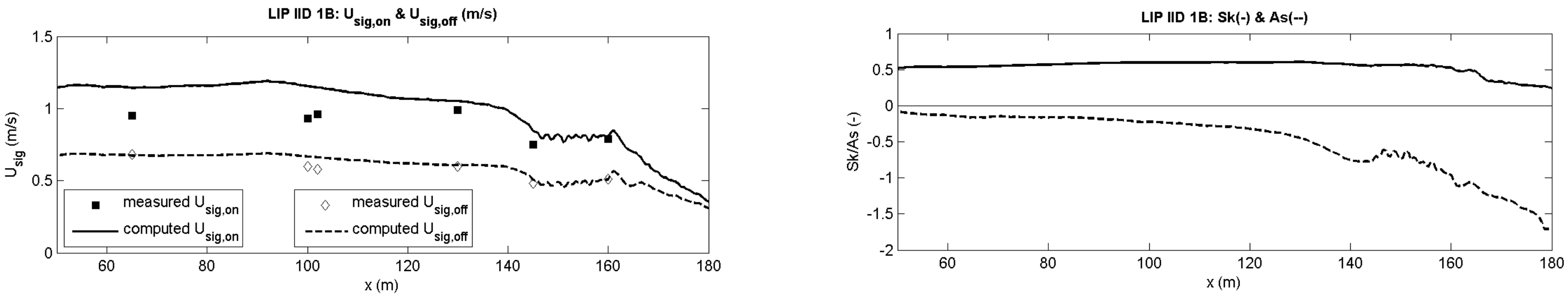

Figure 6-6: Test 1B: Elfrink, significant on- and offshore orbital velocities and Skewness vs Asymmetry

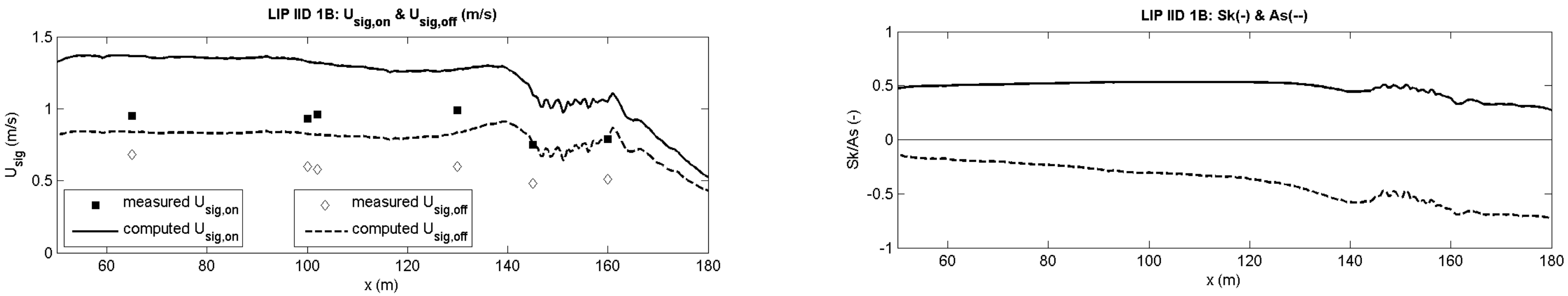

Figure 6-7: Test 1B: R&vR1, significant on- and offshore orbital velocities and Skewness vs Asymmetry

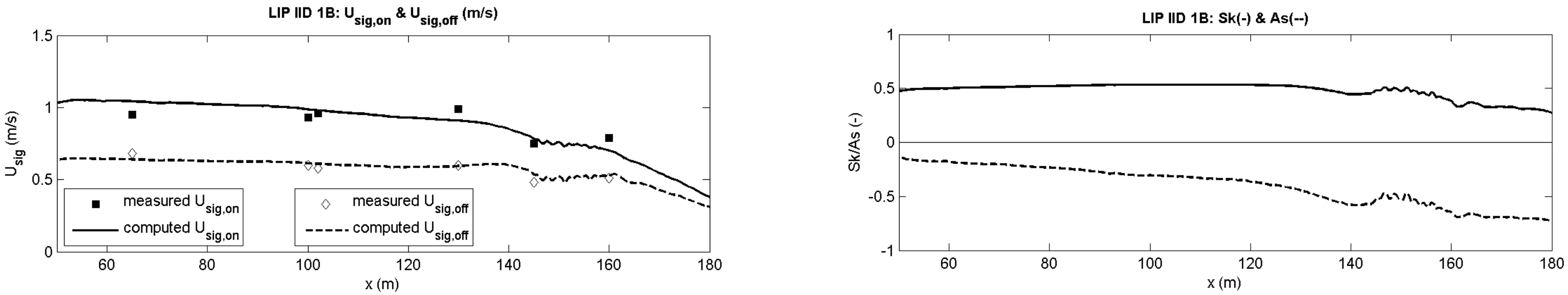

Figure 6-8: Test 1B: R&vR2, significant on- and offshore orbital velocities and Skewness vs Asymmetry

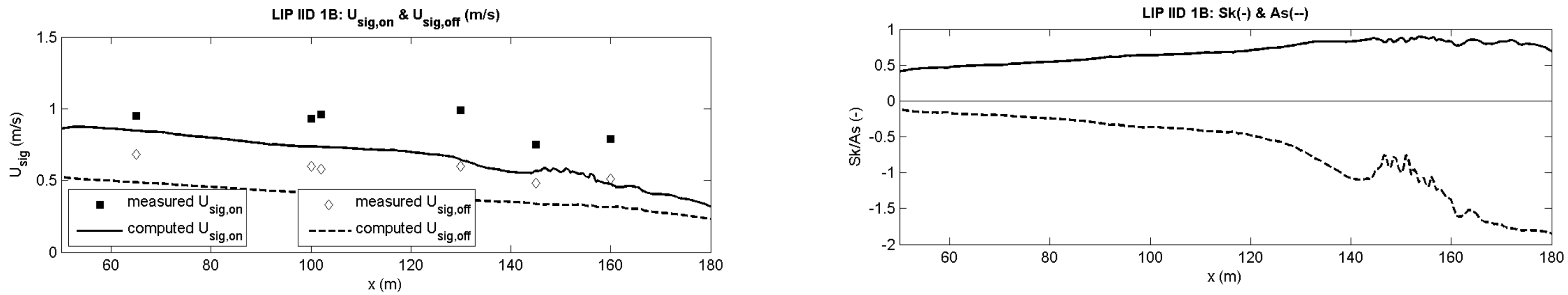

Figure 6-9: Test 1B: vTdV, significant on- and offshore orbital velocities and Skewness vs Asymmetry

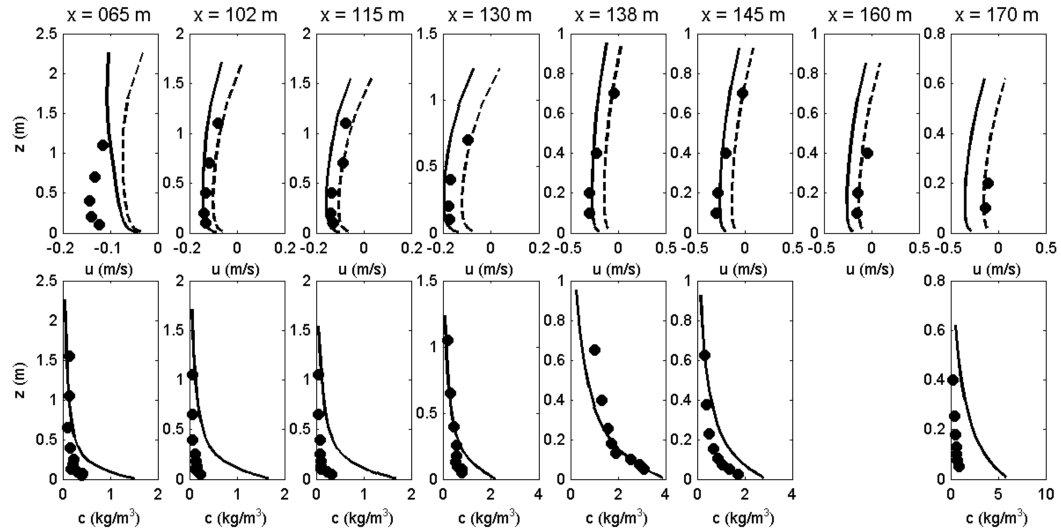

Figure 6-10: Test 1B: Velocity (upper plots, lines = Eulerian velocities, dashed = Lagrangian velocities) and concentration profiles (lower plots)

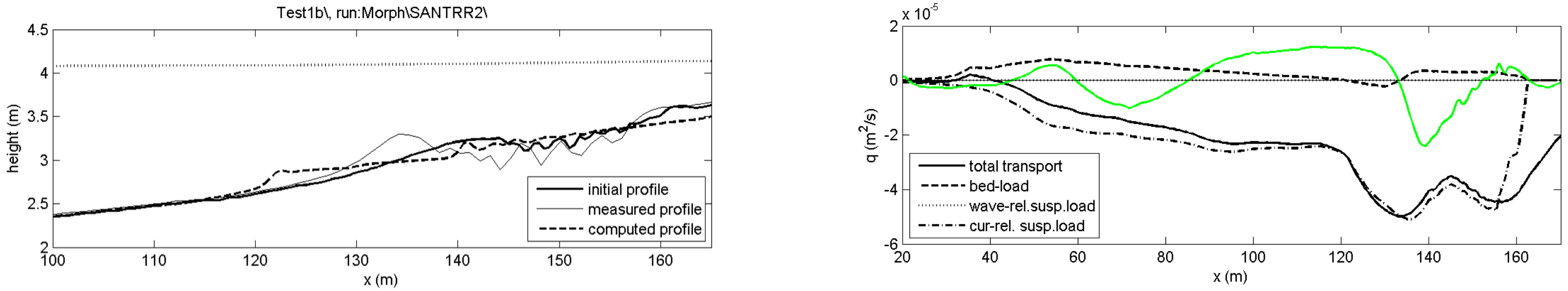

Figure 6-11: Test 1B SANTOSS: Rv&R2, asymmetry effects on, phase lag effects on (x-axes are scaled different and the green line shows inferred transport rate)

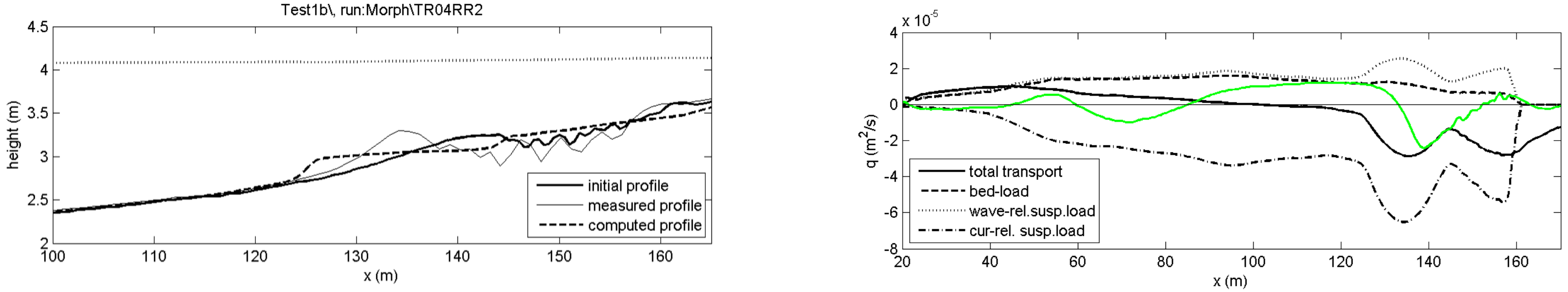

Figure 6-12: Test 1B TR2004: Rv&R2, asymmetry effects on, phase lag effects off

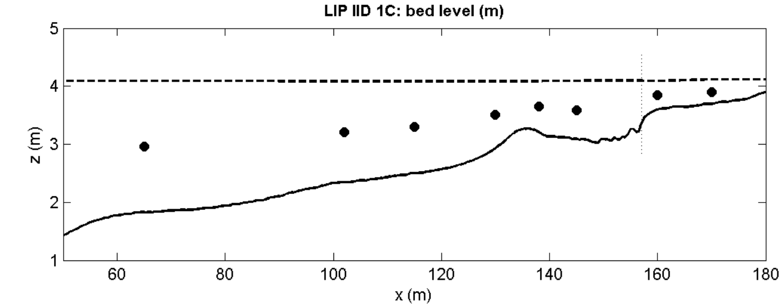

Figure 6-13: Test 1C: Bed profile + measurement locations

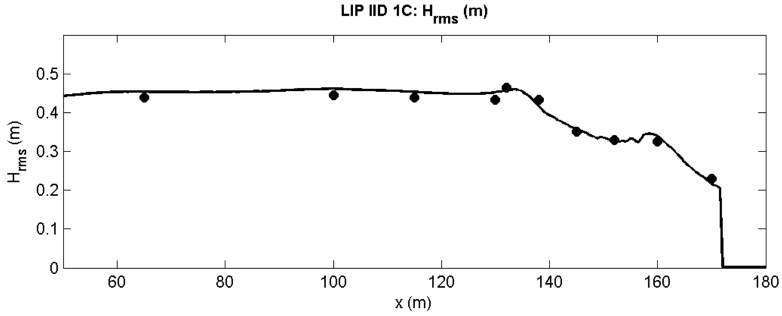

Figure 6-14: Test 1C: Elfrink, wave height evolution + measurements

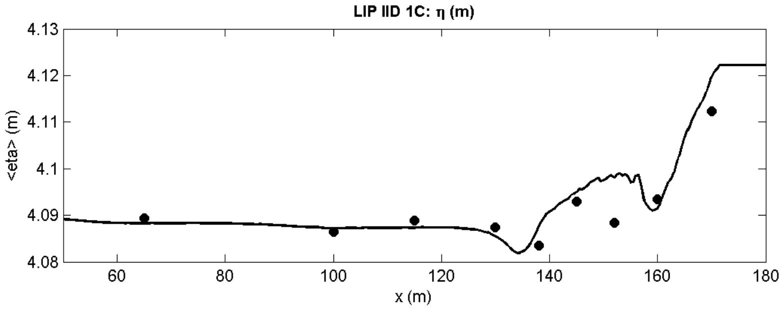

Figure 6-15: Test 1C: set-up η

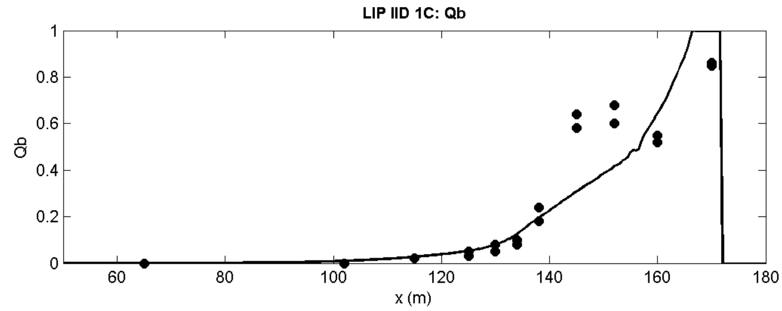

Figure 6-16: Test 1C: Breaking waves Qb

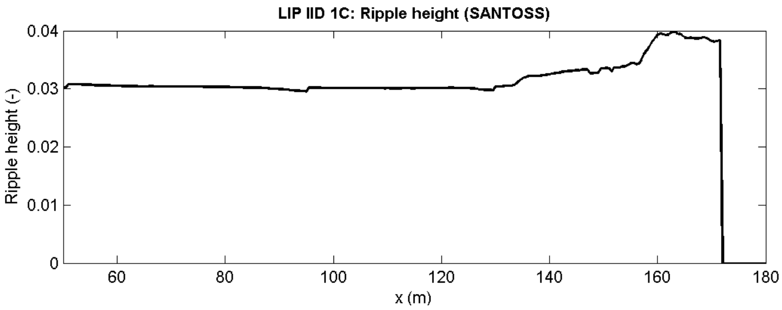

Figure 6-17: Test 1C: Ripple height predicted by SANTOSS

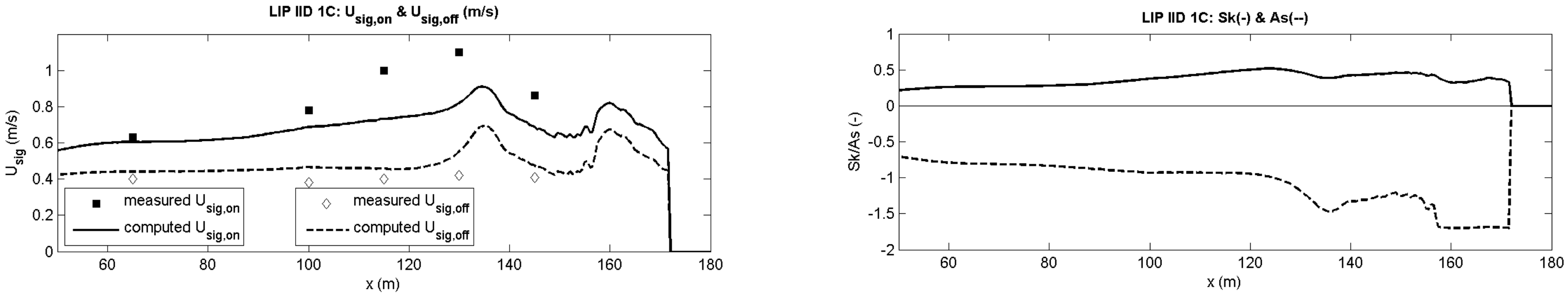

Figure 6-18: Test 1C: Elfrink, significant on- and offshore orbital velocities and Skewness vs Asymmetry

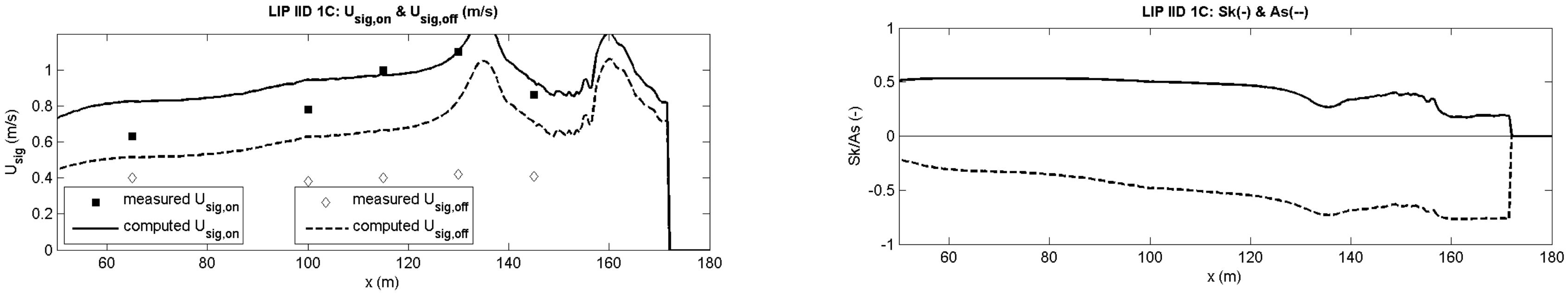

Figure 6-19: Test 1C: R&vR1, significant on- and offshore orbital velocities and Skewness vs Asymmetry

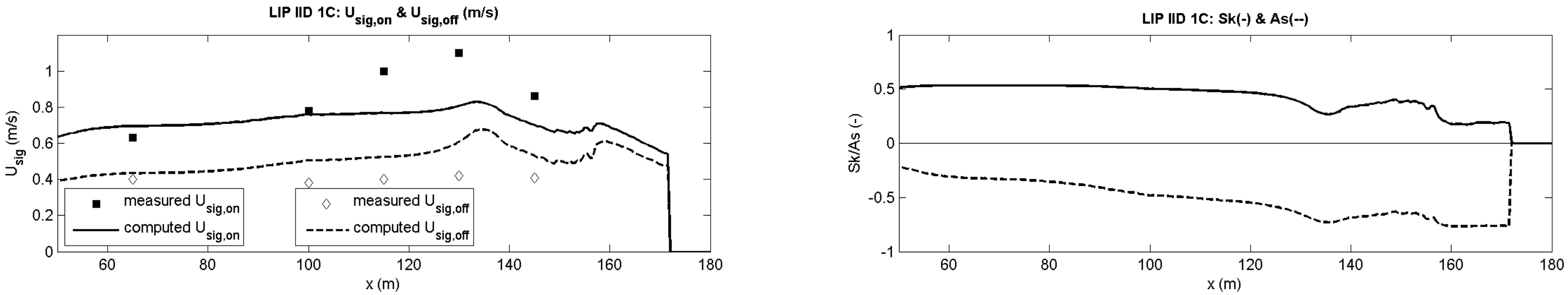

Figure 6-20: Test 1C: R&vR2, significant on- and offshore orbital velocities and Skewness vs Asymmetry

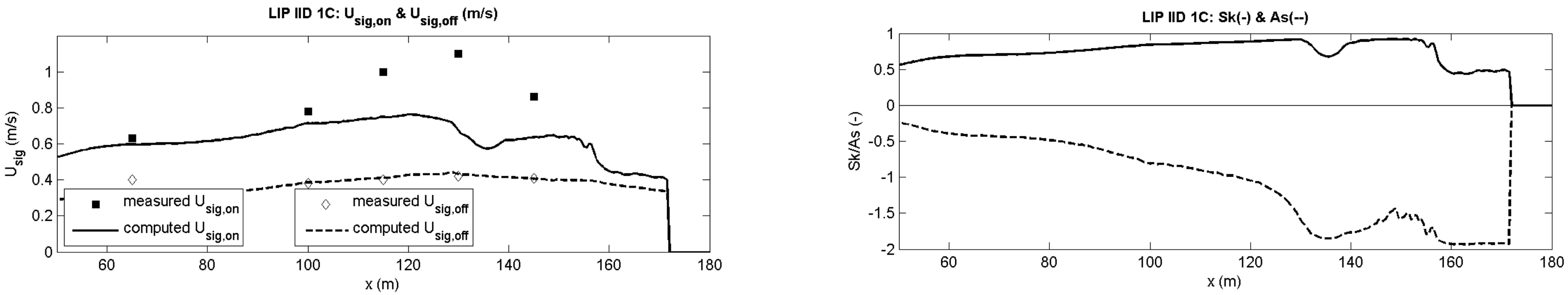

Figure 6-21: Test 1C: vTdV, significant on- and offshore orbital velocities and Skewness vs Asymmetry

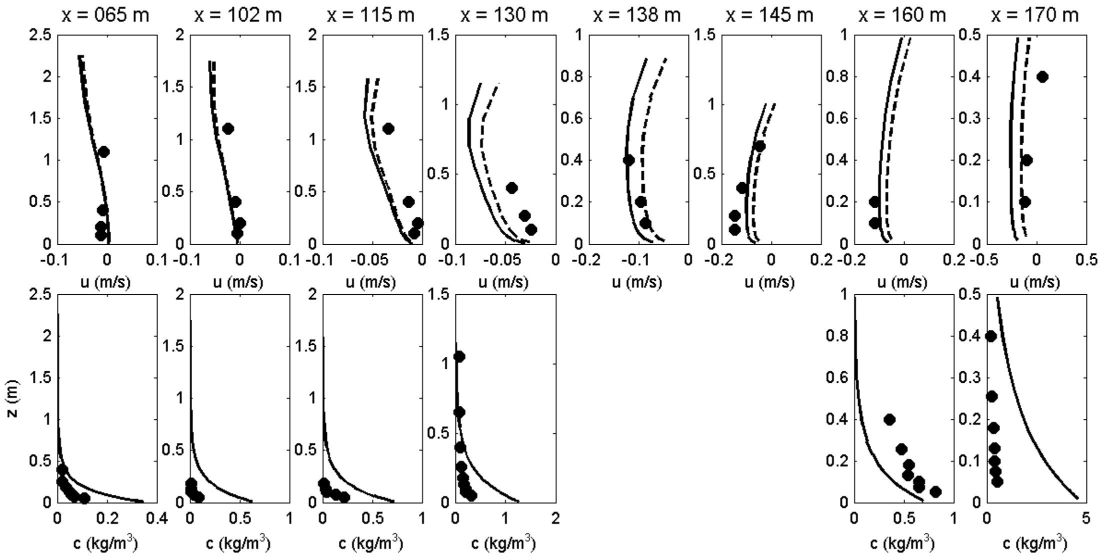

Figure 6-22: Test 1C: Velocity (upper plots, lines = Eulerian velocities, dashed = Lagrangian velocities) and concentration profiles (lower plots)

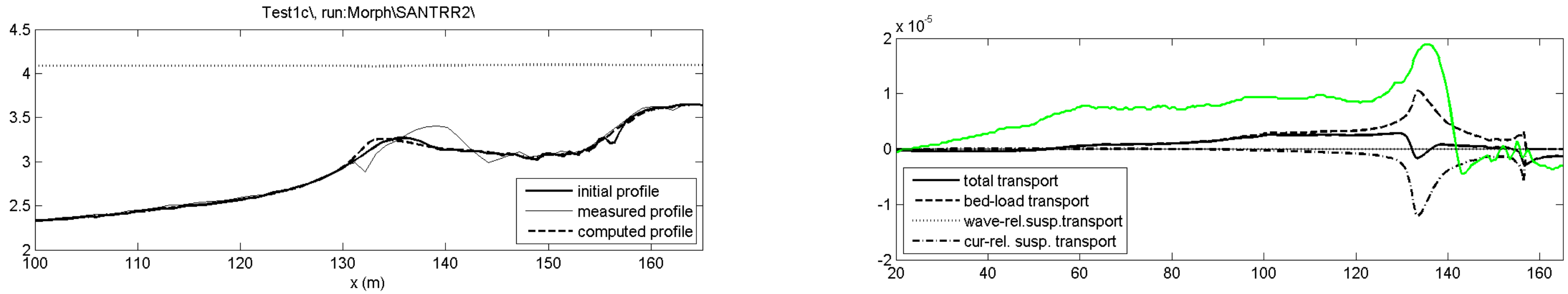

Figure 6-23: Test 1C SANTOSS: Rv&R2, asymmetry effects on, phase lag effects on

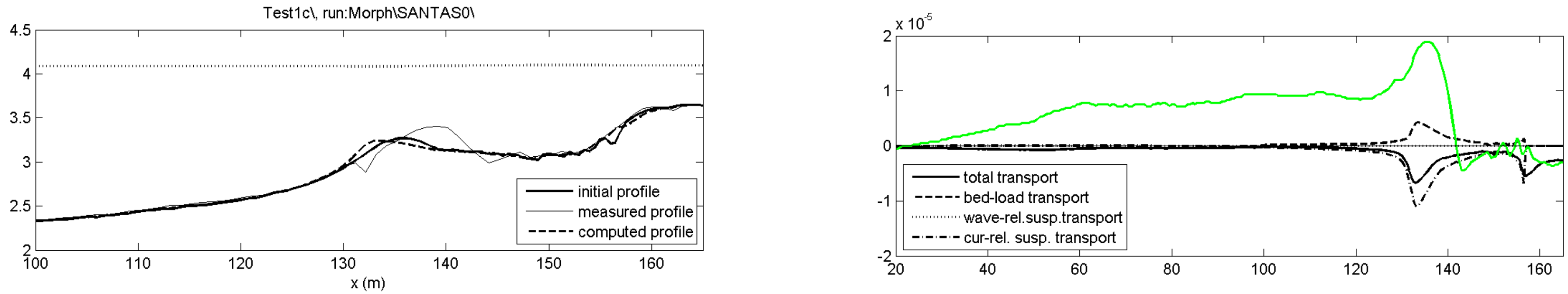

Figure 6-24: Test 1C SANTOSS: Rv&R2, asymmetry effects off, phase lag effects on

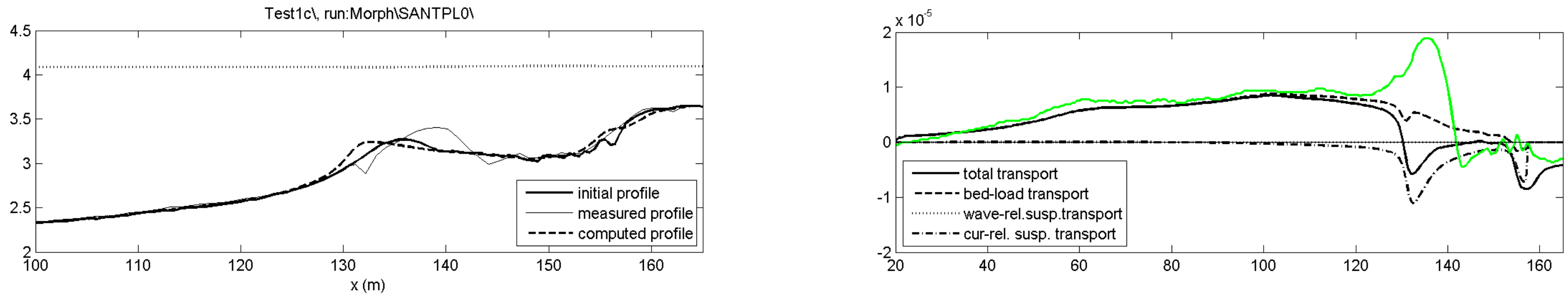

Figure 6-25: Test 1C SANTOSS: Rv&R2, asymmetry effects on, phase lag effects off

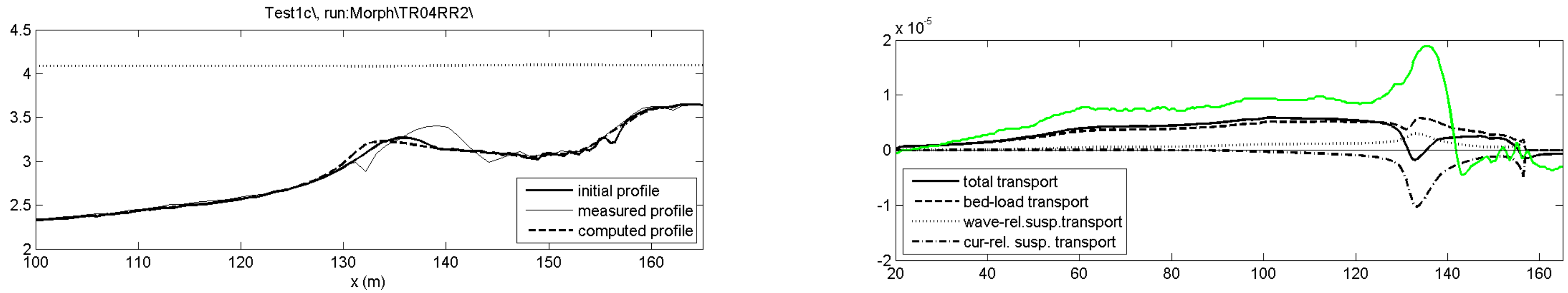

Figure 6-26: Test 1C TR2004: Rv&R2, asymmetry effects on, phase lag effects off

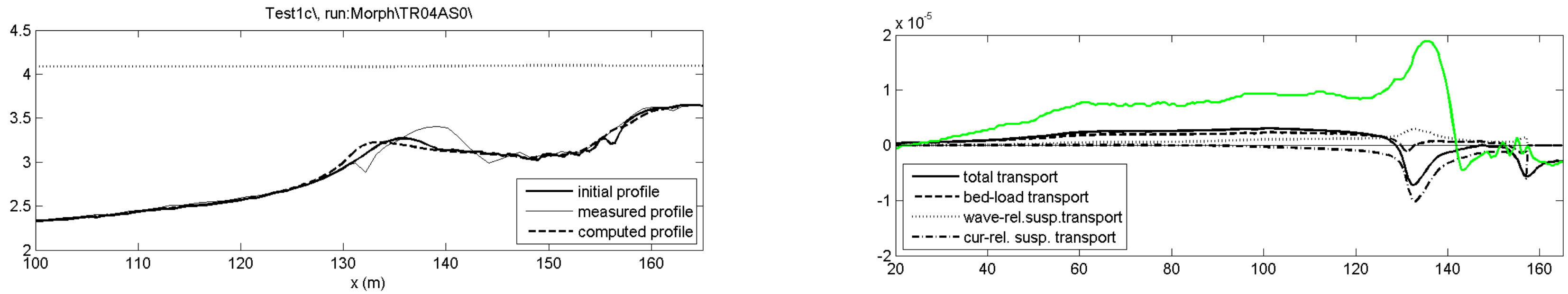

Figure 6-27: Test 1C TR2004: Rv&R2, asymmetry effects off, phase lag effects off

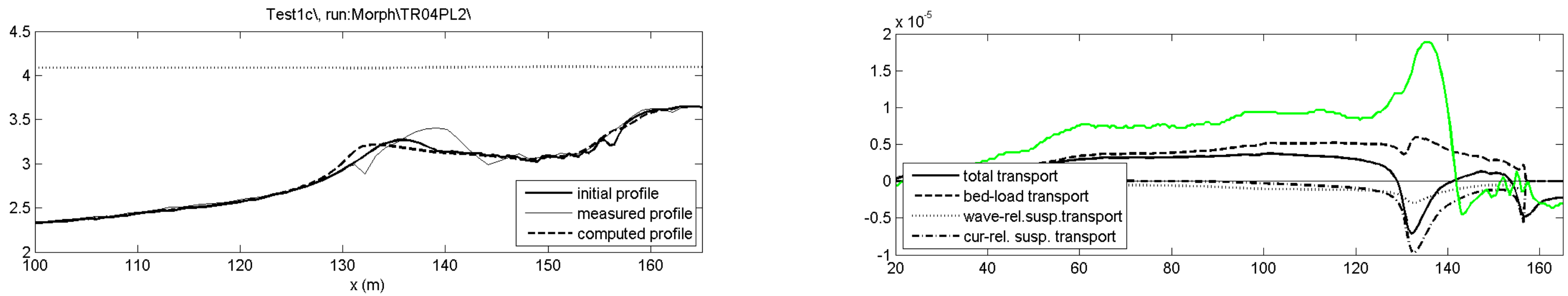

Figure 6-28: Test 1C TR2004: Rv&R2, asymmetry effects on, phase lag effects on

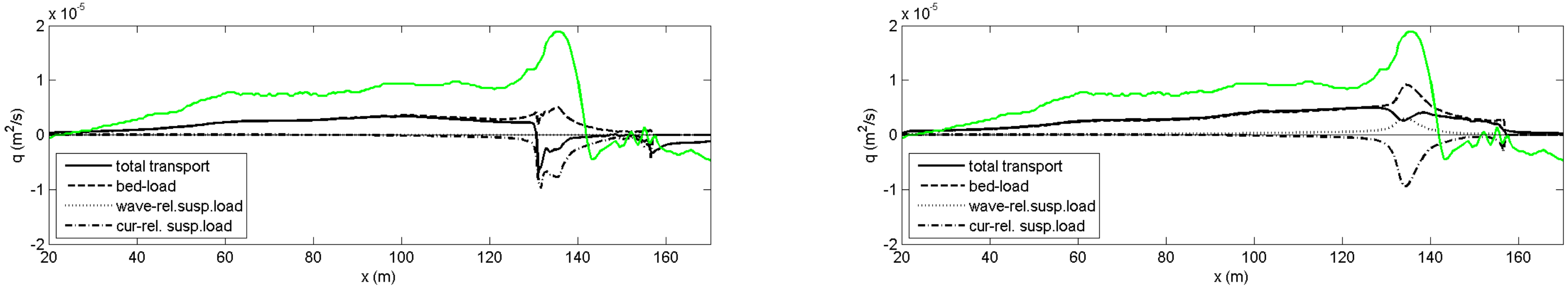

Figure 6-29: Test 1C Elfrink: left = SANTOSS (asymmetry on, phase lags on), right = TR2004 (asymmetry on, phase lags off)

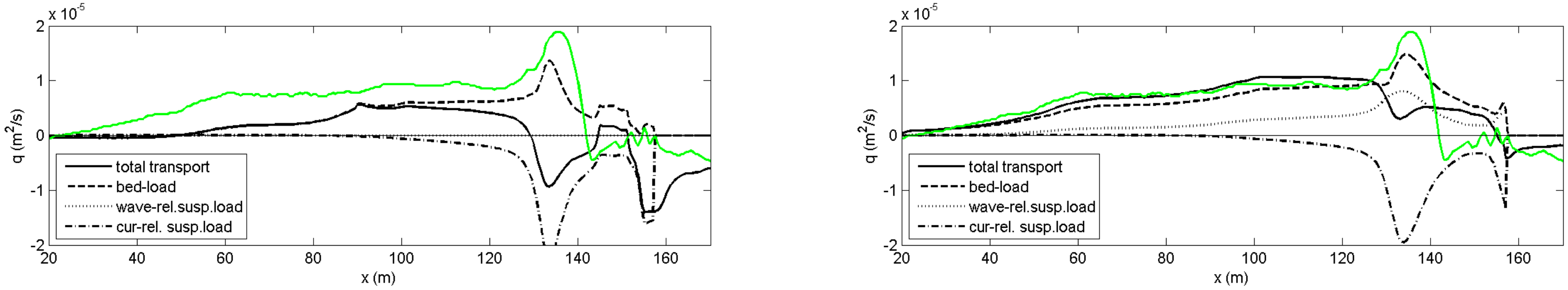

Figure 6-30: Test 1C R&vR1: left = SANTOSS (asymmetry on, phase lags on), right = TR2004 (asymmetry on, phase lags off)

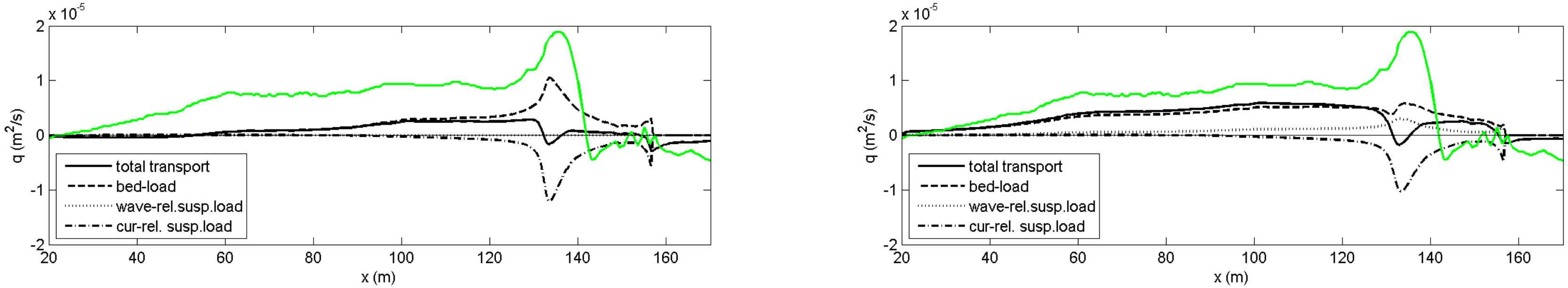

Figure 6-31: Test 1C vTdV: left = SANTOSS (asymmetry on, phase lags on), right = TR2004 (asymmetry on, phase lags off)

7. Conclusions, discussion and recommendations

7.1. Introduction

In this chapter first the conclusions from this study are described by answering the research questions. Next in the discussion some comments are made on this research are reviewed in the discussion paragraph. This chapter finishes with some recommendations for the transport model and further research.

7.2. Conclusions

The objective of this research was to explore the applicability and behaviour of the SANTOSS sand transport model in comparison with TRANSPOR2004 within the cross-shore profile model UNIBEST-TC. The SANTOSS transport model is successfully implemented in UNIBEST-TC and predicted transport rates are analyzed by comparing the transport predictions for a large range of conditions with those of TR2004. Finally, two test cases are used to assess the performance of predicting morphological evolution.

Below the five research questions are answered:

1. *What are the main characteristics of the morphological model UNIBEST-TC and the two sand transport models and what are necessary changes for the implementation of the SANTOSS model?*

The morphological model UNIBEST-TC consists of various modules: The morphological evolution is driven by gradients in the transport rates. The transport predictions are based on input from a computed mean current profile and orbital velocity characteristics, which are driven by the computed wave heights over the whole cross-shore profile.

The TR2004 model is based on experiments but also verified on field data (from river, tidal and coastal flow). It uses an intra-wave quasi-steady approach for bed load transport and a time-averaged approach for the wave-related and current-related suspended load. Some recommended modifications to the TR2004 model are implemented to also take into account acceleration effects (applied to the bed load) and phase lag effects (applied to the wave-related suspended load).

SANTOSS uses a quasi-unsteady half-cycle approach to describe the total transport in the wave boundary layer including phase lag, acceleration and surface wave effects and is based on detailed experimental data in oscillatory flow tunnels or wave flumes. The formulations are slightly modified to also include slope effects and the current related suspended load above the wave boundary layer predicted by TR2004 is also added to include also the transport by high currents and under breaking waves.

For this research it was necessary to use an orbital velocity theory, which represents both velocity and acceleration skewness and shows no unrealistic wobbles and discontinuities in velocity and acceleration. This was necessary for application of the two transport models and to extract different wave form characteristics. Several orbital velocity theories were implemented or improved, analyzed and tested.

2. *What are the differences in total sand transport rates predicted by the two sand transport models under a large range of conditions (e.g. grain size, wave height, wave period, wave shape)?*

The sensitivity analysis in which the SANTOSS model was compared with the TR2004 model over a large range of conditions for a depth of h_d = 4 m showed that the SANTOSS model reacts almost in the same way as the bed load and wave-related suspended load of TR2004 together. Only the transport rates predicted by the SANTOSS model are lower over the whole range. The SANTOSS model uses also the current-related suspended load component above the wave boundary layer, but it was found that this component is almost equal to the total current-related suspended load predicted by TR2004.

Large transitions in transport rates are visible between the different regimes. In the ripple regime the transport rates predicted by SANTOSS are reduced to zero or become even slightly negative due to phase lag effects. Results of the TR2004 model are also reduced to almost zero, when a phase lag factor is applied to the wave-related suspended load.

In the sheet flow regime the large undertow velocity and the enhanced suspended sediment generate a high offshore directed current-related suspended load, which is used for both transport models and becomes dominant (the excluding of the current-related suspended load in the wave boundary layer by the SANTOSS model, has only a really small effect. Important difference between the two transport models is that the SANTOSS predictions for the transport in the wave boundary layer is more affected by an undertow than the TR2004 bed load and wave-related suspended load. This is because the SANTOSS model extracts the current velocity that is used as input from a higher level above the bed compared to the TR2004 model.

3. *What is the relative influence of the specific transport aspects (e.g. bed form and phase lag, surface wave and acceleration effects) on the sediment transport rates?*

The effects on the transport rates are analyzed by excluding these effects from the transport formulations:

- Acceleration effects are taken into account by the two transport models, but in a different way. Both methods lead to an increase (onshore directed) of the predicted transport rates in the considered range of conditions, but for TR2004 the effect is higher and over the whole range. SANTOSS only corrects the transport rates when waves become asymmetric (acceleration skewed), while TR2004 also takes this effect for velocity skewed waves.
- The phase lag effects can have a significant effect on the transport rates, especially in the ripple regime. Here, the predicted transport rates are reduced to zero or can even become slightly negative. Excluding the phase lag effects show that the SANTOSS model predicts much higher transport rates also compared to the TR2004 model, which can be explained by a high roughness height.
- The surface wave effects (near-bed streaming, Lagrangian movement and vertical orbital velocities) are only tested for the SANTOSS model and have a slight positive effect on the transport rates in the sheet flow regime but become important when phase lag effects are high (ripple regime and also in the higher sheet flow regime).

Also the effect of breaking wave is analyzed by setting the amount of breaking waves to zero. For non-breaking waves the current-related suspended load becomes almost zero, while the wave-related suspended load is only affected for high waves. The TR2004 model still predicts higher transport rates, but the behaviour is almost the same. The use of different orbital velocities resulted into other net transport rates, mainly affected by the in predicted orbital velocity amplitude (theories show about the same velocity skewness), but the two transport models react in the same way on the changes. The two theories that are based on extensive field measurements *(Elfrink et al, 2006; modified version of Ruessink & Van Rijn, in prep.)* show high agreement with each other, although the predicted acceleration skewness (asymmetry) is not the same.

4. *To what extent is it possible to predict morphological changes using the UNIBEST-TC version with the SANTOSS model in comparison to TR2004?*

The two UNIBEST-TC versions are applied to an erosive case, (LIP IID test 1B) and an accretive case (test 1C) to test the morphological predictions. Both versions of UNIBEST-TC show too much erosion (or too less accretion), which can be primarily linked to the wrong predictions of hydrodynamics and suspended sediment concentration.

The modelled hydrodynamics of test 1B do agree with the measurements (undertow and orbital velocities). The erosion (offshore bar migration) predicted by SANTOSS is slightly larger than that predicted by TR2004. This can be linked to the large undertow (over the whole profile) and the higher reaction of the SANTOSS predictions on this undertow velocity.

For test 1C the two transport models show much more agreement in predicted transport rates and morphological evolution, although both models predict a slight offshore bar migration, while onshore migration is measured. Next to the underestimation of the velocity skewness, the undertow velocities are underestimated. These two processes can explain the low gradient in transport rates and the wrong location compared to the inferred transport rates. Also the wave breaking and the delay between breaking and undertow can be the reason of the wrong location of the gradient in transport rates.

5. *What is the relative influence of specific hydrodynamic and transport aspects (e.g. bed forms, wave asymmetry, surface wave effects and phase lag effects) on the morphological behaviour?*

The sensitivity to different processes is tested by excluding the processes or choosing a different orbital velocity theory. This does result in the same changes in transport rates as expected from the sensitivity analysis. Because the changes do take place over the whole profile, this leads to only minor changes in morphological evolution (are also small because the morphological evolution is small in this case).

7.3. Discussion

Some discussion points can be made about the transport models and the application in the UNIBEST-TC model.

The SANTOSS model covers in principal all the sediment transport in the wave boundary layer. It has been chosen to let the SANTOSS model predictions replace the bed load, the total wave-related suspended load and the current-related suspended load within the wave boundary layer. Thus, only the current-related suspended load above the wave boundary layer was not covered by the SANTOSS model. This choice is mainly based on the experience under non-breaking waves, but it is possible that especially under breaking waves, suspended sediment above the wave boundary layer is not only transported by the current velocity but also by the waves.

Another note has to be made on the SANTOSS model concept: the half-cycle approach. It is possible to implement the SANTOSS model concept in UNIBEST-TC or any other cross-shore profile model, but application in a more advanced coastal model (2DH or 3D) will lead to problems. The transition zone between wave+current to current-alone or current-dominated (current velocity near the bed stronger than the orbital flow velocities) is hard to cover with this concept, because then half-cycles are not possible to recognize. Problems can arise at locations, where currents are concentrated (e.g. rip currents or a return flow between two adjacent sand bars) or at deeper water where the orbital velocity can become really low.

Another discussion point is the high dependency of the transport predictions on the hydrodynamic input and the uncertainty in the representation of the hydrodynamics. The two transport models considered in this study and especially the SANTOSS model link their transport predictions to detailed characteristics of the near bed velocities. It is assumed that the near-bed velocities can be represented by a time-averaged current profile and an orbital velocity theory which predicts the velocity time series including wave form based on a local wave height and period. Wave irregularity and bound long waves are not taken into account and the differences between the orbital velocity theories give also an indication of the uncertainty.

Next to the orbital velocities, the wave-current-sediment interaction is important, especially when waves start to break. The influence of the superimposed current on the transport predictions depends largely on the level from which the velocity is taken for use in the transport formulations. Physically it might be more correct to use the velocity at the edge of the wave boundary layer (as proposed by Ribberink et al. (*2010*)). On the other hand, there is any debate on the definition of the wave boundary layer thickness and the wave boundary layer thickness changes over the whole wave period. The use of the lowest computational points seems easier in use and also the streaming component (if present) is this way included (is already taken into account in the Quasi-3D current profile). The TR2004 model in the UNIBEST-TC version uses also this velocity, although this is not the way as it was proposed by Van Rijn *(2007a, 2007b)*. Another aspect of the wave-current interaction which is not yet included in the SANTOSS model is the influence of a superimposed current on ripple dimensions and sheet flow layer thicknesses.

7.4. Recommendations

Implementing and testing the SANTOSS transport model in a coastal morphologic model gave a lot of insight in how the hydrodynamics are/should be coupled to the sand transport processes described in the transport model. Especially comparison with the TRANSPOR2004 model and the way this model is implemented or takes into account the different processes led to a list of topics on which improvements can be made.

Extension of this research:

- *Extension sensitivity analysis:* the sensitivity analysis in this report gives good insight in the differences in transport predictions and the influence of specific processes. It is recommended to extend the analysis to different depths (still with realistic conditions) to get more insight in how for example bed form regimes, wave forms, breaking waves and different transport loads relate to each other along a profile. These insights show also on which conditions the focus should lay and on which conditions improvements can be expected or generated. The effect of longshore velocities (tide) on the transport rates is not included in this research, because this will have a large influence on the longshore and cross-shore transport rates.
- *Application on more test cases:* In this research the SANTOSS version of UNIBEST-TC has been applied to two test cases and the predicted transport rates are extensively analyzed. It is recommended to apply the model to more cases (for example all the cases in the benchmarking database, see for example Roelvink, et al. (*2000*)). Runs of only one time step are enough to show whether transport predictions meet the transport rates computed from the measured profiles. It can also be interesting to implement the formulations in another profile model CROSMOR and use this model, because this model is more extensively tested on these two test

cases and uses slightly different formulations for wave breaking, current profiles.

Proposed improvements of the SANTOSS model:

- *Validation of ripple regime under field conditions*: The sensitivity analysis showed that the phase lag effects in the ripple regime are relevant for the net transport rates, but are also highly influence by the surface wave effects (especially vertical orbital velocities). Validation of the model for ripple conditions under real waves is therefore recommended, especially because in this regime improvements are expected (in the sheet flow regime the current-related transport becomes dominant due to breaking). The model is not calibrated on transport measurements under real waves in the ripple regime, which is why the surface wave effects might not work correctly in this regime. Here, especially the vertical velocities (taken from z=3*ripple height) have a large influence on the phase lag effects and the resulting net transport rates.
- *Acceleration effects:* The method used by SANTOSS to apply acceleration effects only corrects the bed shear stresses when the wave shows acceleration skewness and not for velocity skewed waves. On the other hand, the method used by TR2004 ("sediment mobilising velocity" of Nielsen and Callaghan *(2003)* as input for the bed shear stress) takes always the acceleration into account (in Chapter 5 it was shown that this method has a significant effect on the net transport for skewed waves). An adjustment due to acceleration seems physically also more correct for velocity skewed waves, because the acceleration of crest and trough differ significantly and thus should a correction been made in the friction factor or in the used velocities. Off course the model should then be recalibrated (the TR2004 bed load model should actually also be recalibrated with inclusion of the acceleration effects).

Additional research:

- *Orbital velocities under waves:* The proposed combination of three orbital velocity theories seems to be promising, but showed some disagreements with the accretion test case LIP IID 1C. This implies that the formulations of the skewness and asymmetry by Ruessink & Van Rijn (*in preparation*) do not seem to fit for these conditions. It is recommended to test the theory on more measurements/test cases, whether this is a returning problem or this is case specific. The use of a calibration factor within the theory can also be recommended, which can change for example the ratio between skewness and asymmetry or the total amount of non-linearity. The orbital velocity theory of Isobe & Horikawa (*1982*) adjusted by Grasmeijer & Van Rijn (*1998*) and Grasmeijer & Ruessink (*2003*) is better able to predict the maximum orbital velocities but does only focus on skewness (which was the reason why it was not used).
- *Wave irregularity:* In this research the orbital velocities time series are based on a representative regular wave. Wave irregularity or in more detail wave groups and bound long waves play a vital role in new hydrodynamic models (XBeach, Delft3D-Surfbeat). The alternating wave height and the velocities induced by long waves can have a large influence on the net transport rates (long wave velocities decrease overall velocity skewness outside the surf zone and increase velocity skewness within the surf zone).
- *Breaking waves:* Short-term morphological changes are mainly induced by breaking waves, which induce a high undertow and suspended sediment is entrained to high levels. In this research these effects are included by including the current-related suspended load formulations of TR2004. A more detailed analysis on depth-depended sediment concentration, velocities and turbulence under breaking waves (intra-wave) can give more

insight in the transport rates and how these should be included in or added to the SANTOSS model.

- *Influence of bed slopes on the transport rates under waves:* Primarily, the effect of bed slopes on transport rates under steady flows is analysed in different studies. For the effect of bed slopes under coastal conditions some pragmatic simple formulations are implemented and the results are calibrated per case. More complicated/advanced because otherwise no stable morphological results are generated. More knowledge on slopes effects on different processes can lead to better predictions of the net transport rates.

8. References

Abreu, T., Silva, P. A., Sancho, F., & Temperville, A. (2010). Analytical approximate wave form for asymmetric waves. *Coastal Engineering, Vol. 57*(7), p. 656-667.

Al-Salem, A. A. (1993). *Sediment transport in oscillatory boundary layers under sheet flow conditions.*, Delft University of Technology.

Apsley, D. D., & Stansby, P. K. (2008). Bed-Load Sediment Transport on Large Slopes; Model Formulation and Implementation within a RANS Solver. *Journal of Hydraulic Engineering, 134*(10), 1440-1451.

Battjes, J. A., & Janssen, J. P. F. M. (1978). *Energy loss and set-up due to breaking in random waves.* Paper presented at the Proc. 16th Int. Conf. on Coastal Eng., ASCE.

Bosboom, J., Aarninkhof, S., Reniers, A., Roelvink, J., & Walstra, D. J. R. (2000). *Unibest-TC 2.0, overview of model formulations*. Delft: WL | Delft Hydraulics.

De Leeuw, C. J. (2005). *Model predictions of wave-induced sediment transport on the shoreface*. Enschede, The Netherlands: University of Twente.

Dean, R. G., & Dalrymple, R. A. (2002). *Coastal Processes with Engineering Applications.* Cambridge, UK: Cambridge University Press.

Dey, S. (2003). Threshold of sediment motion on combined transverse and longitudinal sloping beds. *Journal of Hydraulic Research, 41*(4), 405 - 415.

Dibajnia, M., & Watanabe, A. (1998). Transport Rate Under Irregular Sheet Flow Conditions. *Coastal Engineering, Vol. 35*(3), pp. 167-183.

Dohmen-Janssen, C. M. (1999). *Grain size influence on sediment transport in oscillatory sheet flow: phase lags and mobile-bed effects.* Doctoral thesis, Delft University of Technology.

Dohmen-Janssen, C. M., & Hanes, D. M. (2002). Sheet flow dynamics under monochromatic nonbreaking waves. *Journal of Geophysical Research*, 107 (C110); 3149.

Dohmen-Janssen, C. M., Kroekenstoel, D. F., Hassan, W. N., & Ribberink, J. S. (2002). Phase-lags in oscillatory sheet flow: experiments and bed load modelling. *Coastal Engineering, Vol 46*(1), 61-87.

Drake, T. G., & Calantoni, J. (2001). Discrete particle model for sheet flow sediment transport in the nearshore. *Journal of Geophysical Research, Vol. 106*(No. C9), pp. 19,859-819,868.

Elfrink, B., Hanes, D. M., & Ruessink, B. G. (2006). Parameterization and simulation of near bed orbital velocities under irregular waves in shallow water. *Coastal Engineering*, 915-927.

Grasmeijer, B. (2002). *Process-based cross-shore modelling of barred beaches.* University of Utrecht, Utrecht.

Grasmeijer, B., & Ruessink, B. G. (2003). Modelling of waves and currents in the nearshore parametric vs.

Grasmeijer, B., & Van Rijn, L. C. (1998). *Breaker bar formation and migration.* Paper presented at the Proceedings Coastal Engineering, Virginia, USA.

Isobe, M., & Horikawa, K. (1982). Study on water particle velocities of shoaling and breaking waves. *Coastal Engineering, Jpn. 25*, pp 109-125.

Longuet-Higgins, M. S. (1953). Mass transport in water waves. *Phil. Trans. R. Soc. Lond. A, vol. 245*(no. 903), pp. 535-581.

Longuet-Higgins, M. S. (2005). On wave set-up in shoaling water with a rough sea bed. *Journal of Fluid Mechanics, Vol. 527*, pp. 217-234.

Malarkey, J. (2008). *SANTOSS UWB Internal Report Number 2: A Review of Freestream Descriptions of Velocity and Acceleration Skewness*. Bangor: Bangor University.

Nairn, R. B., Roelvink, J. A., & Southgate, H. N. (1990). *Transition zone width and implications for modelling surfzone hydrodynamics.* Paper presented at the Proc. of the Int. Conf. Coastal Energineering Conference, Delft, The Netherlands.

Nielsen, P. (2006). Sheet flow sediment transport under waves with acceleration skewness and boundary layer streaming. *Coastal Engineering*, 749-758.

Nielsen, P., & Callaghan, D. P. (2003). Shear stress and sediment transport calculations for sheet flow under waves. [doi: DOI: 10.1016/S0378-3839(02)00141-2]. *Coastal Engineering, 47*(3), 347-354.

O'Donoghue, T., Doucette, J. S., van der Werf, J. J., & Ribberink, J. S. (2006). The dimensions of sand ripples in full-scale oscillatory flows. [doi: DOI: 10.1016/j.coastaleng.2006.06.008]. *Coastal Engineering, 53*(12), 997-1012.

O'Donoghue, T., & Ribberink, J. S. (2007). Laboratory Experiments and the Development of Wave-Driven Sand Transport Models. *Publs. Inst. Geophys. Pol. Acad. Sc., E-7*(401).

Reniers, A., Thornton, E. B., Stanton, T. P., & Roelvink, J. A. (2004). Vertical flow structure during Sandy Duck: observations and modelling. *Coastal Engineering, 51*, pp. 237-260.

Ribberink, J. S. (1998). Bed-load transport for steady flows and unsteady oscillatory flows. *Coastal Engineering, Vol 34*, 59-82.

Ribberink, J. S., Van der A, D. A., & Buijsrogge, R. H. (2010). *SANTOSS transport model; A new formula for sandtransport under waves and currents*. Enschede/Aberdeen: Universtity of Twente/University of Aberdeen.

Rienecker, M. M., & Fenton, J. D. (1981). A Fourier approximation method for steady water waves. *Journal of Fluid Mechanics, Vol. 104*, pp. 119-137.

Roelvink, J. A., Meijer, T. J. G. P., Houwman, K., Bakker, R., & Spanhoff, R. (1995). *Field validation and application of a coastal profile model.* Paper presented at the Int. Proc. Coastal Dynamics 1995.

Roelvink, J. A., & Reniers, A. J. H. M. (1995). *LIP 11D Delta Flume experiments, a profile dataset for profile model validation, Report H2130*. The Netherlands: Delft Hydraulics.

Roelvink, J. A., & Stive, M. J. F. (1989). Bar-generating cross-shore flow mechanisms on a beach. *Journal of Geophysical Research, Vol. 94*(no. C4), pp. 4785-4800.

Roelvink, J. A., Van Koningsveld, M., Ruessink, B. G., Walstra, D. J. R., & Aarninkhof, S. G. J. (2000). *Benchmarking database UNIBEST-TC*: WL Delft Hydraulics.

Ruessink, B. G., Kuriyama, Y., Reniers, A. J. H. M., Roelvink, J. A., & Walstra, D. J. R. (2007). Modelling cross-shore sandbar behavior on the timescale of weeks. *J. of Geoph. Res., Vol. 112*(F03010).

Ruessink, B. G., Van Der Berg, T. J. J., & Van Rijn, L. C. (2009). Modelling sediment transport beneath skewed asymmetric waves above a plane bed. *Journal of Geophysical Research, Vol. 114*(C11021), doi:10.1029/2009JC005416.

Ruessink, B. G., & Van Rijn, L. C. (in preparation). Observations and empirical modelling of near-bed wave skewness and asymmetry.

Ruessink, B. G., Walstra, D. J. R., & Southgate, H. N. (2003). Calibration and verification of a parametric wave model on barred beaches. *Coastal Engineering, Vol. 48*(No. 3), p. 139-149.

Sanchez-Arcilla, A., Roelvink, J. A., O'Connor, B. A., Reniers, A., & Jimenez, J. A. (1995). *The delta flume experiment.* Paper presented at the Proc., Coastal Dynamics, Barcelona, Spain.

Schretlen, J. L. M., Van der Werf, J. J., Ribberink, J. S., Uittenbogaard, R. E., & O'Donoghue, T. (2008). *Surface wave effects on sheet-flow sand transport.* Paper presented at the River, Coastal and Estuarine Morphodynamics: RCEM 2007, Enschede.

Sleath, J. F. A. (1987). Turbulent oscillatory flow over rough beds. *Journal of Fluid Mechanics, Vol. 182*, pp 369-409.

University of Twente. (2010). Project description SANTOSS research project. Retrieved 25 September, 2010, from http://www.utwente.nl/ctw/santoss

Van der A, D. A., O'Donoghue, T., Davies, A. G., & Ribberink, J. S. (2008). *Acceleration skewness on rough bed oscillatory boundary layer flow.* Paper presented at the 31st International Conference on Coastal Engineering.

Van der Werf, J. J., Schretlen, J. L. M., Ribberink, J. S., & O'Donoghue, T. (2009). Database of full-scale laboratory experiments on wave-driven sand transport processes. [doi: DOI: 10.1016/j.coastaleng.2009.01.008]. *Coastal Engineering, 56*(7), 726-732.

Van Rijn, L. C. (1993). *Principles of sediment transport in rivers, estuaries and coastal seas*. The Netherlands: Aqua Publications.

Van Rijn, L. C. (2000). *General view on sand transport by currents and waves*. Delft, The Netherlands: Delft Hydraulics.

Van Rijn, L. C. (2007a). Unified View of Sediment Transport by Currents and Waves. I: Initiation of Motion, Bed Roughness and Bed-Load Transport. *Journal of Hydraulic Engineering, 133*(6), 649-667.

Van Rijn, L. C. (2007b). Unified View of Sediment Transport by Currents and Waves. II: Suspended Transport. *Journal of Hydraulic Engineering, 133*(6), 668-689.

Van Rijn, L. C., Ruessink, B. G., Grasmeijer, B., Van der Werf, J. J., & Ribberink, J. S. (2007). *Wave related transport and nearshore morphology*. Paper presented at the Coastal Sediments.

Van Rijn, L. C., Tonnon, P. K., & Walstra, D. J. R. (in preparation). Erosion and accretion of plane sloping beaches at different scales and efficiency of beach nourishments. Deltares.

Van Rijn, L. C., Tonnon, P. K., & Walstra, D. J. R. (submitted). Erosion and accretion of plane sloping beaches at different scales and efficiency of beach nourishments. Deltares.

Van Rijn, L. C., Walstra, D. J. R., & Van Ormondt, M. (2007). Unified View of Sediment Transport by Currents and Waves. IV: Application of Morphodynamic Model. *Journal of Hydraulic Engineering, Vol. 133*(No. 7), pp. 776-793.

Van Thiel de Vries, J. S. M. (2009). *Dune erosion during storm surges.* Doctoral Thesis. Delft University of Technology, Delft.

Walstra, D. J. R. (2000). *Unibest-TC Userguide*. Delft.

Walstra, D. J. R., Roelvink, J. A., & Groeneweg, J. (2000). *Calculation of wave driven currents in a 3D mean flow model.* Paper presented at the 27th International Conference on Coastal Engineering, Sydney.

Walstra, D. J. R., Van Rijn, L. C., Van Ormondt, M., Brière, C., & Talmon, A. M. (2007). *The effects of slope and wave skewness on sediment transport and morphology*. Paper presented at the Coastal Sediments 2007, May 13-17.

Wong, W. H. (2010). *Master thesis: A Comparison of Practical Wave-Dominated Cross-shore Sand Transport Models.* University of Twente, Enschede.

List of Symbols

Subscripts

b	bed
c	current
cr	critical
s	suspended
tot	total
w	wave
wc	combination wave-current
w,c	wave crest
w,t	wave trough

* For practical reasons and due to the different definitions of SANTOSS and TR2004 sometimes exceptions are made. If so, this is mentioned in the context.

Roman symbols

A_w	Amplitude of the horizontal orbital displacement
As	Acceleration skewness (Asymmetry)
B	total non-linearity
D_{50}	Median grain size diameter
D_{ss}	Grain size diameter of suspended sediment
D_*	Dimensionless particle diameter
D_f	Energy dissipation due to bottom friction
D_w	Energy dissipation due to breaking
H_w	Wave height
L	Wave length
P_c / P_t	Phase lag parameter for the wave crest / trough
Q_b	Fraction of breaking waves
R	Velocity skewness (Skewness)
S_{ij}	Radiation stress
Sk	Velocity skewness (Skewness)
Ur	Ursell number
U_w	Characteristic orbital velocity amplitude
$U_{\delta,cw}$	Near bed velocity due to combined currents and waves
T_c / T_t	Wave crest / trough period
T_{cu} / T_{tu}	Period of accelerating part of wave crest / trough
T_p	Peak wave period
V_r	Representative depth-averaged velocity based on the velocity in the lowest computational layer (assuming logarithmic profile)
a_w	Acceleration of the near bed orbital flow velocity
c	Suspended sediment concentration
c_a	Reference concentration at lowest computational point (z=a)
c_g	Wave group velocity
c_w	Wave propagation velocity
f_{pl}	Phase lag factor (TR2004)
f_w / f_c	Wave- / current-related friction factor
g	Gravitational acceleration
h_d	Water depth
k	Wave number

Roman symbols

k_s	Bed roughness height
q_b	Bed load transport component (TR2004)
$q_{s,w}$ / $q_{s,c}$	Wave- / current-related suspended load component
$q_{SANTOSS}$	Transport within the wave boundary layer (SANTOSS)
q_t	Total transport load
s	Sediment specific gravity
u_w	Near bed orbital flow velocity
v_{tide}	Tidal alongshore velocity
w_s	Sediment fall velocity
z_b	Bed level

Greek symbols

Φ	Non-dimensional sediment transport
Ω_{ij}	Sediment load entrained under half-cycle i and transported under half-cycle j (the same half-cycle or the next one)
K	Von Karman constant
α_b	Dissipation coefficient
β	Acceleration skewness (Asymmetry)
β_{sl}	Longitudinal slope
β_r	Slope of the wave front
γ	Wave breaker parameter
γ_{sl}	Lateral slope
δ_w	Wave boundary layer thickness
ε_s	Sediment mixing coefficient
η	Water level
η_{ripple}	Ripple height
θ	Shields parameter
θ_{wave}	Wave propagation direction at boundary (angle with shore normal)
λ	Ripple length
μ_c / μ_w	Current / wave efficiency factor
ν	Kinematic viscosity coefficient
ξ	Irribarren number
ρ_s / ρ_w	Density sediment / water
τ	Shear stress
φ	Angle between direction of mean current and the direction of wave propagation
φ_r	Natural angle of repose of sediment grains
ψ	Mobility number
ω	Angular frequency
ϕ_d	Damping parameter

List of Figures and Tables

List of Tables

Table 3-1: Comparison of the performance of TR2004 and SANTOSS on large amount of sand transport measurements (Ribberink, et al., 2010; Wong, 2010) 17
Table 5-1: Input for the intercomparison of the sand transport models 34
Table 6-1: Input for the morphological runs 49

List of Figures

Figure 1-1: The morphodynamic loop 1
Figure 2-1: Simple example of a cross-shore profile + terminology................................. 5
Figure 2-2: Free-stream velocity under skewed (a) and asymmetric (forward leaning) wave (b) compared to a sine wave. 6
Figure 2-3: Relation between the wave form parameters using the formula of Abreu et al. (2010, see par.4.4 and Appendix B): (a) skewness R and Sk for skewed (non-asymmetric) waves; (b) asymmetry β and As for asymmetric (non-skewed) waves. 6
Figure 3-1: Velocity time series in wave direction. Tc and Tt are respectively the crest and trough periods, Tcu and Ttu are the crest and trough acceleration time lengths. The current shifts the time series up or down and affects both the maximum velocities and the periods (Ribberink, et al., 2010). 16
Figure 3-2: Illustration of wave and current velocity vectors $\vec{u}_w(t)$ and $\vec{u}_\delta$. The vector $\vec{u}_c$ is the resultant velocity vector at maximum velocity under the crest of the wave (Ribberink, et al., 2010). 16
Figure 4-1: Comparison of three near-bed orbital velocity theories: Elfrink et al. (2006) adjusted with Abreu et al. (2010); Ruessink & Van Rijn (in preparation) adjusted with Abreu et al. (2010) amplitude based on linear wave theory; and Van Thiel de Vries (2009). Plots are based on a depth of 2 meters. On the left side the influence of a change in L/h_d is visible and on the right side the influence of a change in H_{rms}/h_d. 28
Figure 5-1: (a) Correlation between Hrms and Tp between 1997 and 2001 (De Leeuw, 2005). (b) Wave height evolution and probability of occurrence at different depths (Al-Salem, 1993). 33
Figure 5-2: Orbital velocity characteristics: SWASYM = 6: RvR2: Ruessink & Van Rijn (in prep.), amplitude based on Grasmeijer & Ruessink (2003). Depth h_d = 4 m. 35
Figure 5-3: Current velocity aspects under breaking waves: (a) Part of breaking waves, (b) near bed mean velocity, (c) thickness wave boundary layer according to Sleath (1989) and (d) mean velocity at the edge of the wave boundary layer. h_d = 4 m, SWASYM = 6 and D_{50} = 0.2 mm 35
Figure 5-4: Current velocity aspects under non-breaking waves: (a) Part of breaking waves (breaking waves are excluded), (b) near bed mean velocity, (c) thickness wave boundary layer according to Sleath (1989) for D50 = 0.2 mm and (d) mean velocity at the edge of the wave boundary layer. h_d = 4, SWASYM = 6 and D_{50} = 0.2 mm. 35
Figure 5-5: Ripple height according to the SANTOSS formulations for different sediment grain sizes. Depth h_d = 4 meters. SWASYM = 6... 35
Figure 5-6: Vertical profiles of the wave-averaged cross-shore current (a), wave-averaged suspended sand concentration (b) and current-related suspended

sediment transport (c) in cross-shore direction for D_{50}=0.1mm (solid), D_{50}=0.2mm (dashed), D_{50}=0.3mm (dotted) and D_{50}=0.4mm (dashed-dotted lines). 37
Figure 5-7: Predicted transport rates in cross-shore direction for changing sediment grain sizes: the bed load (a), the wave-related suspended load (b), the bed load + wave-related suspended load (c), current-related suspended load (d) and total load transport rates (e) by TR2004 (solid black line) and SANTOSS (solid blue line). Option added in figure: excluding phase lag effects (dashed lines) and excluding surface wave effects (dotted lines). 37
Figure 5-8: Vertical profiles of the wave-averaged cross-shore current (a), wave-averaged suspended sand concentration and current-related suspended sediment transport (c) in cross-shore direction for T_p = 4 s (solid lines),T_p = 6 s (dashed lines), T_p = 8 s (dotted lines) and T_p = 10 s (dashed-dotted lines)..........................39
Figure 5-9: Predicted transport rates in cross-shore direction for changing wave period: the bed load (a), the wave-related suspended load (b), the bed load + wave-related suspended load (c), current-related suspended load (d) and total load transport rates (e) by TR2004 (solid black line) and SANTOSS (solid blue line). Options added in figure: excluding asymmetry effects (dash-dotted lines); excluding phase lag effects (dashed lines); and excluding breaking of waves (dotted lines, effect only shown for current-related suspended load transport: goes to zero). 39
Figure 5-10: Vertical profiles of the wave-averaged cross-shore current (a), wave-averaged suspended sand concentration and current-related suspended sediment transport (c) in cross-shore direction for H_{rms} =0.4 m (solid lines), H_{rms}=0.8 m (dashed lines), H_{rms}=1.2 m (dotted lines) and H_{rms}=1.6 m (dashed-dotted lines)....41
Figure 5-11: Predicted transport rates in cross-shore direction for changing wave heights: the bed load (a), the wave-related suspended load (b), the bed load + wave-related suspended load (c), current-related suspended load (d) and total load transport rates (e) by TR2004 (solid black line) and SANTOSS (solid blue line). Options added in figure: excluding asymmetry effects (dotted lines), excluding phase lag effects (dashed lines) and excluding breaking of waves (dash-dotted lines). 41
Figure 5-12: Orbital velocity characteristics based on the different orbital velocity theories for h_d = 4m. R&vR1: amplitude based on linear wave theory, R&vR2: amplitude modified based on Grasmeijer and Ruessink (2003) 43
Figure 5-13: Predicted transport rates in cross-shore direction for changing wave heights under non-breaking waves: the bed load (a), the wave-related suspended load (b), the bed load + wave-related suspended load (c), the transport within the wave boundary layer predicted by the SANTOSS model (d), current-related suspended load (e) and total load transport rates (e) by TR2004 (black lines) and SANTOSS (blue line).In each figure the results are shown using different orbital velocity theories: Elfrink (dotted lines), vTdV (solid lines) , R&vR1 (dashed lines) and R&vR2 (dash-dotted lines). 44
Figure 5-14: Same as Figure 5-13 but for breaking waves 45
Figure 6-1: Test 1B: Bed profile + measurement locations 52
Figure 6-2: Test 1B: wave height evolution + measurements...52
Figure 6-3: Test 1B: mean water level η...52
Figure 6-4: Test 1B: Part of wave breaking Qb 52
Figure 6-5: Test 1B: Ripple height predicted by SANTOSS..52
Figure 6-6: Test 1B: Velocity (upper plots, lines = Eulerian velocities, dashed = Lagrangian velocities) and concentration profiles (lower plots) 54
Figure 6-7: Test 1B: Elfrink, significant on- and offshore orbital velocities and Skewness vs Asymmetry 53
Figure 6-8: Test 1B: R&vR1, significant on- and offshore orbital velocities and Skewness vs Asymmetry 53

Figure 6-9: Test 1B: R&vR2, significant on- and offshore orbital velocities and Skewness vs Asymmetry 53
Figure 6-10: Test 1B: vTdV, significant on- and offshore orbital velocities and Skewness vs Asymmetry 54
Figure 6-11: Test 1B SANTOSS: Rv&R2, asymmetry effects on, phase lag effects on (x-axes are scaled different) 55
Figure 6-12: Test 1B TR2004: Rv&R2, asymmetry effects on, phase lag effects off 55
Figure 6-13: Test 1C: Bed profile + measurement locations 56
Figure 6-14: Test 1C: Elfrink, wave height evolution + measurements 56
Figure 6-15: Test 1C: set-up η....................56
Figure 6-16: Test 1C: Breaking waves Qb 56
Figure 6-17: Test 1C: Ripple height predicted by SANTOSS 56
Figure 6-18: Test 1C: Velocity (upper plots, lines = Eulerian velocities, dashed = Lagrangian velocities) and concentration profiles (lower plots) 58
Figure 6-19: Test 1C: Elfrink, significant on- and offshore orbital velocities and Skewness vs Asymmetry 57
Figure 6-20: Test 1C: R&vR1, significant on- and offshore orbital velocities and Skewness vs Asymmetry 57
Figure 6-21: Test 1C: R&vR2, significant on- and offshore orbital velocities and Skewness vs Asymmetry 57
Figure 6-22: Test 1C: vTdV, significant on- and offshore orbital velocities and Skewness vs Asymmetry 58
Figure 6-23: Test 1C SANTOSS: Rv&R2, asymmetry effects on, phase lag effects on 59
Figure 6-24: Test 1C SANTOSS: Rv&R2, asymmetry effects off, phase lag effects on 59
Figure 6-25: Test 1C SANTOSS: Rv&R2, asymmetry effects on, phase lag effects off 59
Figure 6-26: Test 1C TR2004: Rv&R2, asymmetry effects on, phase lag effects off 60
Figure 6-27: Test 1C TR2004: Rv&R2, asymmetry effects off, phase lag effects off 60
Figure 6-28: Test 1C TR2004: Rv&R2, asymmetry effects on, phase lag effects on 60
Figure 6-29: Test 1C Elfrink: left = SANTOSS (asymmetry on, phase lags on), right = TR2004 (asymmetry on, phase lags off) 61
Figure 6-30: Test 1C R&vR1: left = SANTOSS (asymmetry on, phase lags on), right = TR2004 (asymmetry on, phase lags off) 61
Figure 6-31: Test 1C vTdV: left = SANTOSS (asymmetry on, phase lags on), right = TR2004 (asymmetry on, phase lags off) 61

Content Appendices

A. UNIBEST-TC with TR2004 and SANTOSS 1
A.1. UNIBEST-TC: General user-defined input and boundary conditions 1
A.1.1. General user-defined input 1
A.1.2. Boundary conditions 1
A.1.3. Implemented input switches for (possible) analysis SANTOSS code 2
A.2. UNIBEST-TC: Wave module 3
A.2.1. User-defined input 3
A.2.2. Energy balance equations 3
A.2.3. Breaking waves 5
A.2.4. Solving the differential equations 6
A.3. UNIBEST-TC: Current profile module 7
A.3.1. User-defined input 7
A.3.2. Mean momentum balance 7
A.3.3. Vertical structure of the eddy viscosity 8
A.3.4. Specification of eddy viscosity distribution 9
A.3.5. Specification of eddy viscosity distribution 9
A.3.6. TRANSPOR2004: Bed roughness predictor 10
A.4. UNIBEST-TC: Orbital velocity module 12
A.4.1. User-defined input 12
A.4.2. Short wave flow velocity 12
A.4.3. Wave group related amplitude modulation 12
A.4.4. Generation of a time series of a bound long wave 13
A.5. UNIBEST-TC: Sediment transport modules 14
A.5.1. User-defined input 14
A.5.2. TRANSPOR2004: Bed load transport 14
A.5.3. TRANSPOR2004: Suspended load transport 15
A.5.4. SANTOSS sand transport model 18

B. Different orbital velocity theories 23
B.1. Current options and proposed changes to orbital velocity module 23
B.2. Analysis formula Abreu et al. (*2010*) 23
B.2.1. Different wave forms 24
B.2.2. Mean absolute velocity and root-mean-square velocity 24
B.2.3. Relation between (r,φ) and velocity skewness R, acceleration skewness β and wave skewness parameter α 25
B.2.4. Relation between (r,φ) and the Skewness Sk and asymmetry As 26
B.3. Generation of necessary wave form parameters 27
B.3.1. Method Elfrink et al. (2006) 27
B.3.2. Method Ruessink & Van Rijn (*in preparation*) 28

C. Description FORTRAN codes 33

A. UNIBEST-TC with TR2004 and SANTOSS

A.1. UNIBEST-TC: General user-defined input and boundary conditions

A.1.1. General user-defined input

Inputparameter	Symbol	Default	Description
DT	DT	1 day	Time step (day)
DTBOT	DTBOT	1 day	Time interval between update bed profiles (day)
IBOD	IBOD	1	Switch calculation of bed level changes (0:off, 1: on)
NT	NT	5	Number of timesteps
D50	D_{50}	0.200mm	Median grain size bed sediment (m)
D90	D_{90}	0.300mm	Grain size for which 90% is smaller (m)
DVAR	DVAR	0	Switch for cross-shore variation of grain size (0:off, 1: on, multiplication factors FDIA0/1/2 for depth HDIA0/1/2.
SALIN	SA	0.0	Water salinity in $^{0}/_{00}$
TDRY	T_{DRY}	40	Period T_{dry} in (s) determining the minimum depth to become $h_{d,min} = g(T_p/T_{dry})^2$
TEMP	Te	10	Water temperature (°C)
FL_NEG	FL_NEG		Determines alongshore transport gradient (m^2/s)
FL_POS	FL_POS		Determines alongshore transport gradient (m^2/s)

A.1.2. Boundary conditions

Inputparameter	Symbol	Default	Description
A_WAVE	θ_0		Angle of wave incidence at the seaward boundary (°)
A_WIND	θ_{wind}		Wind direction (°)
H0			Mean still water level (m)
HRMS	H_{rms}		Root-mean-square wave height at the seaward boundary (m)
T	T_p		Peak wave period (s)
USTRA			Sediment transport at the shoreward boundary
V_TIDE	v_{tide}		
V_WIND			Wind velocity (m/s)
Z	z(x)		Bed profile
Z_FIX	z_{fix}		Elevation of fixed layer.

A.1.3. Implemented input switches for (possible) analysis SANTOSS code

Nr	Name	TrModel	Possible values	Description
63	TRMODEL	-	1(Default)/2	Choice of formulas of TR2004 or SANTOSS
64	SW_EFF	2	0/1(Default)	Surface waves effect on transport off (0) or on (1)
65	PL_EFF	2	0/1(Default)	Phase lag effect on transport off (0) or on (1)
66	AS_EFF	1/2	0/1(Default)	Asymmetry effect on transport off (0) or on (1)
67	RIPPLE	2	0. /1.(Default)/ other	Ripple prediction off (0.), normal as in SANTOSS (1.) or ripple dimensions based on maximum orbital velocity times defined factor (other),
68	SFLT_SETT	2	1(Default)/2	Sheet flow layer thickness based on formula of (1) Dohmen-Janssen (1999) or (2) Ribberink (2008)
69	SFLT_W_C	2	1(Default)/2	Sheet flow layer thickness based on bed shear stress of only waves (1) or waves+currents (2)
70	WBLT_SETT	2	0./1.(Default)/2...	Wave boundary layer thickness: 0: 0.20m 1,2,... : is factor times wblt according to Sleath (*1987*)
71	SL_EFF	1/2	0/1(Default)	Influence slope off (0) or on (1)
72	SSW	1/2	0/1(Default)	Wave related suspended transport on (1) or off (0).
73	WORB_3Rh	2	0./3.(Default) or other	In case of ripples (Rh>0) the vertical orbital velocity for the calculation of the phase lag parameter is defined at z=worb_3rh*Rh or at z=3*Sflt (0).

A.2. UNIBEST-TC: Wave module

A.2.1. User-defined input

Inputparameter	Symbol	Default	Description
ALFAC	α_b	1.0	dissipation coefficient in the expression for the wave energy dissipation due to breaking. Eq. (A.2.3)
BETD	β_r	0.1	slope of the wave front in the expression for the wave roller energy. Eq. (A.2.7)
BVAR		0	switch on cross-shore variation of β (0:off/1:on)
FWEE	f_w	0.01	friction factor in the expression for the wave energy dissipation due to bottom friction. Eq.(A.2.4)
GAMMA	γ		parameter in the expression for the maximum wave height Eq. (A.2.13); if GAMMA is less or equal zero it is computed using the expressions indicated by VARGAMM
VAR_GAMM		0	Switch on γ-expressions: VAR_GAMM=0: Battjes and Stive (1985) VAR_GAMM=1: Ruessink et al. (*2003*); overrules GAMMA
K_IJL		1	Breaker delay switch (0:off/1:on)
F_LAM	λ	2.0	parameter in the expression for the integration distance in the weighting function (A.2.17), which controls the breaker delay through the reference depth (A.2.16)
P_IJL		1.0	power that determines the shape of the weighting function (A.2.17)
DEEP_V/SHALLOW_V		-/-	seaward and shoreward boundary of zone where λ is reduced by factor $\sin^2 \Theta$ where Θ=0.5π(x-DEEP_V)/(SHALL_V-DEEP_V)
RC	$k_{s,c}$	0.01	Current roughness height (only for wave module) is adapted according to TR2004 in current profile module.
RW	$k_{s,w}$	0.002	Wave roughness height (only for wave module) adapted according to TR2004 in current profile module.

A.2.2. Energy balance equations

The wave propagation model consists of three first-order differential equations, viz. the time-averaged wave energy balance (*Battjes & Janssen, 1978*), the balance equation for the energy contained in surface rollers in breaking waves (*Nairn, et al., 1990*) and the horizontal momentum balance from which the mean water level set-up is computed. The refraction of the waves is computed using Snell's law. The three coupled equations are solved by numerical integration over the cross-shore profile. These equations generate the input required by the local models for the vertical velocity profile, the vertical concentration profile and the bed-load transport.

The energy balance equation for organised wave energy E reads:

$$\frac{d}{dx}\left(Ec_g \cos\theta\right) = -D_w - D_f \tag{A.2.1}$$

where c_g is the wave group velocity, θ the angle of incidence of the wave field, D_w the dissipation of wave energy due to breaking and D_f the dissipation due to bottom friction. The organised wave energy E is defined according to linear wave theory:

$$E = \frac{1}{8}\rho g H_{rms}^2 \tag{A.2.2}$$

where ρ is the density of water, g the gravitational acceleration and H_{rms} the root mean square wave height.

Battjes and Janssen *(1978)* use as a closure for this an expression for the dissipation of organised wave energy based on a bore model:

$$D_w = \frac{1}{4}\rho g \alpha f_p H_{\max}^2 Q_b \tag{A.2.3}$$

where $f_p = 1/T_p$ is the peak frequency, H_{max} is the maximum possible wave height, Q_b the fraction of breaking waves and α a dissipation coefficient, which equals 1 in case of a fully developed bore. In paragraph A.2.3 the breaking of waves is explained in more detail.

The wave dissipation D_f due to bottom friction, which is the second sink term in Eq. (A.2.1), is modelled as

$$D_f = \frac{f_w \rho}{\sqrt{\pi}} u_{orb}^3 \tag{A.2.4}$$

where f_w is a user-defined friction factor and u_{orb} the orbital velocity amplitude based on H_{rms} using linear wave theory.

Instead of being dissipated immediately after the breaking point, organized wave energy is converted first to turbulent kinetic energy in the form of a roller at the face of a breaking wave. In this way the dissipation process is delayed and the region of wave set-up is shifted in shoreward direction. The balance equation for the wave roller energy is the second differential equation of the wave model:

$$\frac{\delta}{\delta x}\left(2E_r c \cos\theta\right) = D_w - D_r \tag{A.2.5}$$

where the dissipation of organized wave energy acts as a source term. The factor 2 in Eq. (A.2.5) originates from dissipation of roller energy due to net transfer of water from the wave to the roller. The roller energy E_r represents the amount of kinetic energy in a roller with area A and wave length L, and is defined as:

$$E_r = \frac{1}{2}\rho c^2 \frac{A}{L} \tag{A.2.6}$$

The roller energy balance is concluded by modelling the dissipation of roller energy D_r as the power unit length performed by the shear stress between roller and water surface:

$$D_r = \beta_r \rho g c \frac{A}{L} = 2\beta_r g \frac{E_r}{c} \tag{A.2.7}$$

where β_r is the slope of the wave face (user-defined, normally in the range 0.05-0.10).

The third differential equation is the cross-shore momentum equation:

$$\frac{\partial \bar{\zeta}}{\partial x} = -\frac{1}{\rho g h}\frac{\partial S_{xx}}{\partial x} \tag{A.2.8}$$

In this equation ς is the water level, the bed shear stress and wind stress are neglected. S_{xx} is the cross-shore radiation stress defined as:

$$S_{xx} = \left(n + n\cos^2\theta - 0.5\right)E + 2E_r\cos^2\theta \tag{A.2.9}$$

where $n = c_g/c$, which is the ratio between the group velocity and the wave propagation velocity. The wave direction θ is defined as the angle between the x-axis (perpendicular to the shoreline, positive landwards) and the propagation direction, and is found from Snell's law.

$$\frac{\sin\theta}{\sin\theta_0} = \frac{c}{c_0} \tag{A.2.10}$$

Where the subscript 0 refers to values at the seaward boundary of the model.

Finally the propagation speed c is defined as:

$$c = \frac{\omega}{k} \tag{A.2.11}$$

Where $\omega=2\pi/T_p$ is the angular frequency and k is the wave number which is solved from the dispersion relation:

$$\omega^2 = gk\tanh(kh) \tag{A.2.12}$$

A.2.3. Breaking waves

The model applies a so-called clipped Rayleigh through the surf zone, assuming that the waves smaller than H_{max} are not breaking and Rayleigh distributed, and that all waves larger than H_{max} are breaking. This maximum wave height H_{max} is defined as a function of the local water depth, according to:

$$H_{\max} = \frac{0.88}{k}\tanh\left(\frac{\gamma k h_r}{0.88}\right) \tag{A.2.13}$$

with k the local wave number, h_r the local reference water depth and γ the wave height-to-depth ratio. The local reference depth h_r at a particular grid point is obtained from the weighted water depths seaward of this computational grid point. Battjes and Stive (1985) assumed γ to be cross-shore constant, but variable in time:

$$\gamma = 0.5 + 0.4\tanh(33 s_0) \tag{A.2.14}$$

However, Ruessink et al. (*2003*) showed that γ is a locally varying parameter that increases linearly with the product of the local wave-number and water depth k*h.

$$\gamma = 0.29 + 0.76 k h_d \tag{A.2.15}$$

In order to improve the prediction of bar morphodynamics, Roelvink et al. (*1995*) introduced their concept of breaker delay. The dissipation of organised wave energy as computed from Eq. (A.2.3) and (A.2.13) is only based on local water depth, and disregards the fact that waves need a distance in the order of one wave length to actually start or stop breaking. For that reason they suggest to take into account the bottom elevation some distance seaward of the computational point when determining the water depth h_r to be applied in Eq. (A.2.13). To that end they define a reference depth h_r obtained from weighting water depths seaward of the computational point via a weighing function W(ξ):

$$h_r(x) = \frac{\int_{x-X}^{x} W(x-x')h(x')dx'}{\int_{x-X}^{x} W(x-x')dx'} \tag{A.2.16}$$

In this expression, *h* is the local water depth and *X* is the integration distance. The weighting function *W* is given by:

$$W(\xi) = (X-\xi)^p \tag{A.2.17}$$

where *p* is a user defined parameter which determines the shape of the weighting function. The integration distance *X* is taken proportional to the local peak wave length L_p.

$$X = \lambda L_p \tag{A.2.18}$$

where λ (F_LAM) is a user defined coefficient of order one.

The fraction of breaking waves Q_b reflects the percentage of waves larger than H_{max} and is computed iteratively from:

$$\begin{aligned} \frac{1-Q_b}{\ln(Q_b)} &= -\left(\frac{H_{rms}}{H_{\max}}\right)^2 \quad \text{for } \frac{H_{rms}}{H_{\max}} < 1 \\ Q_b &= \left(\frac{H_{rms}}{H_{\max}}\right)^2 \quad \text{for } \frac{H_{rms}}{H_{\max}} > 1 \end{aligned} \tag{A.2.19}$$

A.2.4. Solving the differential equations

In order to solve the system for the three unknown E, E_r and η, boundary conditions for E, E_r, η and θ and a bottom profile $z_b(x)$ are needed. The boundary value of E is computed from Eq. (A.2.2) via a user defined wave height at the upwave boundary. In addition, θ and $z_b(x)$ should be given at the up-wave boundary, while η is set to zero which is reasonable if the up-wave boundary is located outside the surf zone. The roller energy E_r at the seaward boundary is estimated from Eq. (A.2.7), assuming that D_r equals D_w. Coefficient values must be given for α (default value 1), β (optimum value between 0.05 and 0.10) and λ (value of order 1).

A.3. UNIBEST-TC: Current profile module

A.3.1. User-defined input

Inputparameter	Symbol	Default	Description
FACDEL	α_δ	20	multiplication factor in the expression for the wave boundary layer thickness (α_w=1 for regular waves, α_w=20 for irregular waves)
FCVISC	α_b	0.1	coeffcient in the depth-averaged eddy viscosity generated by wave breaking
SWGLM		0	Switch of method to account for wave-induced mass flux. SWGLM = 0: Eulerian velocity (default). SWGLM>0: Generalized Lagrangian Method.
FACKS		1.0	Factor for the RC and RW values calculated with the TR2004 formulations.

A.3.2. Mean momentum balance

The mean current profile model computes the vertical distribution of the wave-averaged mean current in both long-shore and cross-shore direction accounting for wind shear stress, wave breaking, bottom dissipation in the wave boundary layer and the slope of the free surface. The vertical distribution of the alongshore and cross-shore mean current is determined by solving the horizontal momentum balance. Three layers are defined:

- Surface layer above the wave trough level
- Middle layer between the wave trough level and the top of the wave boundary layer
- The wave boundary layer itself.

Neglecting the advective acceleration terms, the mean momentum balance in i-direction (i = x or y) reads:

$$\frac{\partial \tau_i}{\partial \sigma} = \begin{cases} R_i & \text{for } \sigma > \delta_w \\ R_i + \rho \frac{\partial}{\partial \sigma}\left(\langle u_i(t) w_i(t) \rangle\right) & \text{for } \sigma < \delta_w \end{cases} \tag{A.3.1}$$

where σ = z/h, R_i the forcing and δ_w the non-dimensional wave boundary layer thickness given by:

$$\delta_w = 0.36 \alpha_\delta A_w \left(\frac{A_w}{k_{s,w}}\right)^{-0.25} \tag{A.3.2}$$

Where A_w is the peak orbital excursion based on significant wave height H_s, $k_{s,w,r}$ is the wave-related roughness height and α_δ (FACDEL) is the multiplication factor for the wave boundary layer. In earlier versions of UNIBEST-TC the wave-related roughness height is purely based on the user-defined roughness height. In TR2004 the roughness predictor is used for ripples, mega-ripples and dunes. Because the roughness depends also on the current velocity the roughness is calculated using several iteration steps. Formulations of the roughness heights can be found at the end of this paragraph. In the first call the user-defined roughness height is used.

It is assumed that the forcing is dominated by the pressure gradient and that depth variation can be neglected:

$$R_i = \rho g h \frac{\partial h}{\partial x_i} \tag{A.3.3}$$

The time-averaged stress is given by:

$$\rho \frac{\partial}{\partial \sigma}\left(\left\langle u_i(t) w_i(t)\right\rangle\right) = -\frac{1}{\delta_w}\frac{D_f k_i}{\omega} \tag{A.3.4}$$

Vertical integration of Eq. (A.3.1) gives:

$$\tau_i = \begin{cases} \tau_{s,i} - R_i(1-\sigma) & \text{for } \sigma > \delta_w \\ \tau_{s,i} - R_i(1-\sigma) + \dfrac{D_f k_i}{\omega}\dfrac{\delta_w - \sigma}{\delta_w} & \text{for } \sigma < \delta_w \end{cases} \tag{A.3.5}$$

Where $\tau_{s,I}$ is the surface stress applied at the top of the middle layer, which accounts for the wind stress and the breaking wave stress $\tau_{s,w}=D_r/c$. The shear stress is related to the velocity gradients by:

$$\tau_i = \frac{\rho v_t}{h}\frac{\partial u_i}{\partial \sigma} \tag{A.3.6}$$

Where v_t is the eddy viscosity.

A.3.3. Vertical structure of the eddy viscosity

The vertical distribution of the eddy viscosity has a parabolic shape and includes additional turbulence in the wave boundary layer. It is given by:

$$v_t = \begin{cases} \phi_s \bar{v}_t \sigma(\sigma_s - \sigma) & \text{for } \sigma > \delta_w \\ \phi_s \bar{v}_t \sigma(\sigma_s - \sigma) + \phi_b \bar{v}_{tb}\sigma(\delta_w - \sigma) & \text{for } \sigma < \delta_w \end{cases} \tag{A.3.7}$$

The definition of the σ-parameters is illustrated in Figure_Apx A-1. Note that this sketch of the shape of the eddy viscosity is a tentative one. The resulting eddy viscosity distribution strongly depends on the relative magnitudes of δ, σ_s,v_{tb} and v_t.

The parameter φ_s follows from the parameter σ_s and the condition:

$$\int_0^1 \phi_s \sigma(\sigma_s - \sigma)\, d\sigma = 1 \quad \rightarrow \quad \phi_s = \frac{1}{\frac{1}{2}\sigma_s - \frac{1}{3}} \tag{A.3.8}$$

In the wave boundary layer the eddy viscosity is increased to account for the increased turbulence in the boundary layer. This eddy viscosity increase is assumed to have a parabolic distribution throughout the boundary layer and is zero at σ=0 and σ=δ. This yields for the eddy viscosity distribution in the boundary layer. The parameter φ_b is determined by the condition:

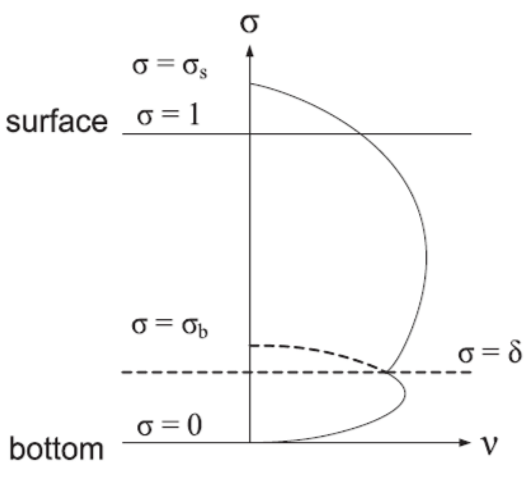

Figure_Apx A-1: Definition of σ –parameters (Bosboom, et al., 2000)

$$\frac{1}{\delta}\int_0^{\delta}\phi_b\sigma(\delta-\sigma)d\sigma = 1 \quad\rightarrow\quad \phi_b = \frac{6}{\delta^2} \tag{A.3.9}$$

A.3.4. Specification of eddy viscosity distribution

The velocity profile is obtained by integrating Eq. (A.3.6). The analytical solution for the current profile is:

$$u_i = \begin{cases} A_b\left[\frac{B_{b,i}}{\sigma_b}\ln\left(\frac{\sigma}{\sigma_0}\right)-\left(\frac{B_{b,i}}{\sigma_b}+C_{b,i}\right)\ln\left(\frac{\sigma_b-\sigma}{\sigma_b-\sigma_0}\right)\right] & \text{for} \quad e\sigma_0 < \sigma < \delta_w \\ u_{\delta_w,i}A\left[\frac{B_i}{\sigma_s}\ln\left(\frac{\sigma}{\delta_w}\right)-\left(\frac{B_i}{\sigma_s}+C_i\right)\ln\left(\frac{\sigma_s-\sigma}{\sigma_s-\delta_w}\right)\right] & \text{for} \quad \sigma > \delta_w \end{cases} \tag{A.3.10}$$

Below σ = $e\sigma_0$ linear velocity decay towards the bed is assumed. The coefficients A_b, $B_{b,i}$, $C_{b,i}$, A, B_i and C_i are expressed in known parameters. The second integration results in a direct relation between the depth-mean velocity $\bar{u}_i$, the depth-dependent forcing R_i, the surface shear stress $\tau_{s,i}$ and streaming term ($[D_f k_i]/\omega$):

$$\bar{u}_i = (H_b + H - G_b - G)R_i + (G_b + G)\tau_{s,i} + \left(G_b - \frac{H_b}{\delta_w}\right)\left(\frac{D_f k_i}{\omega}\right) \tag{A.3.11}$$

where the coefficients G, G_b, H and H_b are expressed through known parameters.

The mass flux in the surface layer is assumed to consist of two parts: due to the progressive character of waves and due to the surface roller in breaking waves:

$$\bar{u}_x = \frac{(E + 2E_r)\cos\theta}{\rho c h} \tag{A.3.12}$$

As the mass flux in the surface layer must be compensated by the mean flow in the middle and bottom layer, the unknown forcing R_x can be determined from Eq. (A.3.11) (in an iterative way, since R_x and $\bar{v}_t$ are coupled through the water surface slope which is not known in the cross-shore direction). Subsequently, the current profile can be computed using Eq. (A.3.10). To compute the forcing Ry, the alongshore surface slope must be known. There are two options to do this: (i) user-defined dh/dy, (ii) user-defined depth-averaged velocity v at reference depth from which the water surface slope is determined using:

$$\bar{v}_{tide} = -C\frac{\partial h}{\partial y}\sqrt{\frac{h}{|\partial h/\partial y|}} \tag{A.3.13}$$

With C = 18log(12h/$k_{s,c}$)

A.3.5. Specification of eddy viscosity distribution

The depth-averaged viscosity is:

$$\bar{v}_t = \sqrt{\bar{v}_{t,current}^{\,2} + \bar{v}_{t,wind}^{\,2} + \bar{v}_{t,breaking}^{\,2}} \tag{A.3.14}$$

With the depth-averaged viscosity for a purely slope-driven (s) current:

$$\bar{v}_{t,current} = \frac{1}{6}\kappa h\sqrt{gh|s|} \tag{A.3.15}$$

With s is the slope, h is the local water depth and κ is the Karman constant = 0.4. The depth-averaged viscosity for a purely wind-driven current:

$$\bar{v}_{t,wind} = \frac{1}{3}\kappa h\sqrt{\frac{|\tau_{s,wind}|}{\rho_w}} \tag{A.3.16}$$

And the depth-averaged viscosity generated by wave breaking:

$$\bar{v}_{t,breaking} = \alpha_b \left(\frac{D_r}{\rho} \right)^{1/3} H_{rms} \tag{A.3.17}$$

In which α_b is a user-defined coefficient (optimum results were obtained with α_b between 0.05 and 0.10(default)).

Parameter σ_s determines the shape of the eddy viscosity and is computed using:

$$\sigma_s = \frac{\bar{v}_t - \frac{1}{3}\bar{v}_{t,surf}}{\bar{v}_t - \frac{1}{2}\bar{v}_{t,surf}} \tag{A.3.18}$$

Where the eddy viscosity at the water surface is only defined by the wind and wave contributions:

$$\bar{v}_{t,surf} = \frac{3}{2}\sqrt{\bar{v}_{t,wind}^2 + \bar{v}_{t,breaking}^2} \tag{A.3.19}$$

The turbulence in the wave boundary layer is increased due to the orbital motion and the bed friction. It follows from:

$$\bar{v}_{tb} = \frac{f_w^3 \hat{u}_w^2}{4\omega} \tag{A.3.20}$$

With f_w the friction factor given by:

$$f_w = 1.39\left(\frac{33A_w}{k_{s,w,r}} \right) - 0.52 \qquad f_{w,\max} = 0.3 \tag{A.3.21}$$

Where A_w is determined by linear wave theory based on the root-mean-square wave height and ω the angular frequency corresponding to the peak wave period.

A.3.6. TRANSPOR2004: Bed roughness predictor

Van Rijn (2007a) distinguishes several bed roughness predictors: a grain roughness ($k_{s,grain}$ = $1d_{90}$); wave-related bed form roughness ($k_{s,w}$); current-related bed form roughness ($k_{s,c}$) and the apparent bed roughness (k_a). These roughnesses depend on both the grain sizes as the near bed velocities, which is why they are related to the mobility number:

$$\psi = \frac{U_{wc}^2}{(s-1)gd_{50}} \tag{A.3.22}$$

In which $U_{wc}^2 = U_w^2 + u_c^2$; U_w = peak orbital velocity near the bed = $\pi H_s/[T_r \sinh(2kh)]$; u_c = depth averaged current velocity; H_s = significant wave height; k = 2π/L; L = wave length derived from $(L/T_p \pm u_c)^2 = gL\tanh(2\pi h/L)$; T_r = relative wave period; T_p = peak wave period; h = water depth.

TR2004 predicts the current-related bed roughness ($k_{s,c}$) for coastal seas using the roughness height for the ripples ($k_{s,c,r}$) and mega-ripples ($k_{s,c,mr}$) according to:

$$k_{s,c} = \left[k_{s,c,r}{}^2 + k_{s,c,mr}{}^2 \right]^{0.5} \tag{A.3.23}$$

In which the different bed roughness heights are predicted using the mobility parameter ψ. The roughness height induced by dunes ($k_{s,c,d}$) should only be applied for rivers and estuaries. The roughness heights are defined as follows:

Current-related bed roughness due to ripples:

$$k_{s,c,r} \begin{cases} 150d_{50} & \text{for} \quad \psi \le 50 \\ 20d_{50} & \text{for} \quad \psi \le 250 \\ (182.5 - 0.65\psi)d_{50} & \text{for} \quad 50 < \psi \le 250 \end{cases} \tag{A.3.24}$$

$$k_{s,c,r,\max} = 0.075$$

Wave-related bed roughness due to mega-ripples:

$$k_{s,c,mr}\begin{cases} 0.0002\psi h & \text{for} \quad \psi \le 50, h>1 \\ 0 & \text{for} \quad \psi \le 250, h>1 \\ (0.011-0.00002\psi)h & \text{for} \quad 50<\psi \le 250, h>1 \end{cases} \tag{A.3.25}$$

$$k_{s,c,mr,\max} = 0.2$$

The wave-related bed roughness height ($k_{s,w}$) of a movable bed is only affected by the presence of small ripples, because only the bed forms with a length scale of the order of the wave orbital diameter (A_w) near the bed are relevant. The length scale of the mega-ripples, ridges and sand waves is too large to contribute to the wave-related roughness. The wave-related bed roughness height is therefore assumed to be: $k_{s,w,r}$ = $k_{s,c,r}$.

The current-related bed roughness $k_{s,c}$ is adapted when the current is superimposed by surface waves. This adapted roughness height k_a can become much higher than $k_{s,c}$:

$$k_a = k_{s,c}\exp\left[\frac{\gamma U_{\delta,r}}{V_R}\right]$$

$$k_{a,\max} = 10k_{s,c} \tag{A.3.26}$$

$$\gamma = 0.8+\varphi-0.3\varphi^2$$

With $U_{\delta,r}$ = $[0.5*U_{on}^3 + 0.5*U_{off}^3]^{1/3}$, V_R is the overall current vector (mean current + undertow) and φ is the angle in radians between the wave and current direction.

A.4. UNIBEST-TC: Orbital velocity module

A.4.1. User-defined input

Inputparameter	Symbol	Default	Description
SWASYM		1	Choice between different short wave flow velocity theories: short description is given below
SWLONG		1	Switch on how to account for bound long wave 1: full bound long wave and wave group effect 2: stirring by constant short wave, advection by bound long waves 3: no bound long wave and wave group effect
C_R	C_r	0.25	Correlation coefficient that determines the phase difference between the long wave flow velocity and the short wave envelope.

The near bed velocity signal consists of three components to have the same characteristics as a natural random wave field.

- A short wave flow component induced by each short wave.
- A flow component induced by bound infra-gravity waves which are induced by wave groups.
- A current component.

The first two orbital velocity components is discussed in this appendix. The component of the mean velocity is discussed in the next chapter.

A.4.2. Short wave flow velocity

All the different short wave theories that were already implemented in UNIBEST-TC are based on the 2 or more order theories consisting of cosines or a combination of cosines and sines:

$$\tilde{u}_r(t) = \sum_{j=1}^{n} A_j \cos(j\omega t) + B_j \sin(j\omega t) \tag{A.4.1}$$

In the case of SWASYM = 2 (*Ruessink & Van Rijn, in preparation*) the short wave orbital wave velocity is based on a second-order theory with a phase difference between the first-order and second-order cosine.

A.4.3. Wave group related amplitude modulation

Due to the combination of different waves wave groups are formed and a wave envelope is visible. To include this effect in the orbital velocity module a new time series is composed of several waves who show a wave group and have the same skewness as the short wave velocity time series as described by one of the chosen theories above:

$$\tilde{u}_{sw}(t) = \sum_{j=1}^{n} \cos(j\omega t)\varepsilon^j = \sum_{j=1}^{n} \cos(j\omega t)\left[\frac{1}{2} + \frac{1}{2}\cos(\Delta\omega t)\right]^j \tag{A.4.2}$$

Where Δω = ω/m, m being the number of waves in one wave group which is set to 7 in UNIBEST-TC. Next the magnitude of this time series is corrected to have the same third momentum of velocities (and thus same skewness) as defined by the chosen theory of the single wave orbital flow velocity.

$$\tilde{u}_{sw\,corr}(t) = \left(\frac{\frac{1}{T}\int_0^T \tilde{u}_r\,dt}{\frac{1}{mT}\int_0^{mT} \tilde{u}_{sw}\,dt} \right)^{1/3} \tilde{u}_{sw}(t) \qquad \text{(A.4.3)}$$

It must be clear that this way only the skewness of the short wave has been recreated. The asymmetry included in the short wave time series of eq. (A.4.1) is not represented by this time series.

A.4.4. Generation of a time series of a bound long wave

The next step is the modelling of the bound long wave. In case of a random wave field the grouping of the short waves generates bound long wvaes. The long wave velocity $u_{lw}(t)$ is computed according to Roelvink and Stive (*1989*) who assume that the wave-group related features of a random wave filed may be represented by a bichromatic wave train with equal amplitudes a_m and a_n, and an accompanying bound long wave with amplitude ξ_a. Using a long wave approximation (shallow water conditions) , the velocity time series $u_{lw}(t)$ due to the long wave component is described by:

$$\tilde{u}_{lw}(t) = \hat{u}_l \cos(\omega_l + \varphi) \qquad \text{(A.4.4)}$$

Where

$$\hat{u}_l = \xi_a \frac{\sqrt{gh}}{h} \qquad \omega_l = \frac{\omega}{m} \qquad \text{(A.4.5)}$$

And ξ_a is found according to the method of Sand, see Bosboom et al. (*2000*)

Then angle φ represents the phase shift between the long-wave and the short-wave envelope, which equals –π in the case of a complete bound long wave situation. In reality however, it appears that the cross-correlation coefficient is only slightly negative as long as we stay offshore from the surf zone, and that it changes into a positive correlation as we enter the surf zone. Cos(φ) has been correlated to the ratio of local wave energy and the incident wave energy as expressed by the squared ratio of the local wave height over the deep water wave height. In UNIBEST-TC the empirical relationship is included via:

$$\cos(\varphi) = C_r \left[1 - 2\left(\frac{H_{rms}}{H_{rms,0}} \right)^2 \right] \qquad \text{(A.4.6)}$$

where C_r is a user-defined correlation coefficient, which is 0.25 according to Roelvink and Stive (*1989*). Finally, the near-bed orbital velocity is described by:

$$\tilde{u}(t) = u_{sw,cor}(t) + \hat{u}_{lw}(t) \qquad \text{(A.4.7)}$$

A.5. UNIBEST-TC: Sediment transport modules

A.5.1. User-defined input

Inputparameter	Symbol	Default	Description
ASFAC	γ_w	0.1	Factor in the expression for the wave-related suspended transport
FACQB		0	Reduction factor on fraction of breaking waves; wave-induced transport is multiplied with (1-FACQB*QB)
TR_MODEL		1	Switch on transport model (1: TR2004, 2: SANTOSS)
TANPHI1	Tan ϕ_r	0.03	Natural angle of repose in ° at location XF1 in (m)
TANPHI2	Tan ϕ_r	0.10	Natural angle of repose in ° at location XF2 in (m)
ZDRY		0	Switch on method to extrapolate sand transport over dry part of the profile (0: no extrapolation, 1: horizontal, 2: vertical, 3: vertical + wave run-up

A.5.2. TRANSPOR2004: Bed load transport

Bed load transport formula

TR2004 relates the bed load transport rates (q_b) to the instantaneous bed shear stress due to both currents and waves ($\tau_{b,wc}$):

$$q_b = \frac{1}{2}\rho_s f_{silt} D_{50} D_*^{-0.3}\left[\frac{\tau_{b,wc}(t)}{\rho_w}\right]^{0.5}\left[\frac{\tau_{b,wc}(t)-\tau_{b,cr}}{\tau_{b,cr}}\right]\frac{U_{\delta,cw}}{\left|U_{\delta,cw}\right|} \tag{A.5.1}$$

In which $\tau_{b,cw}$ is related to the free-stream velocity near the bed and the grain friction coefficient, ρ_s = sediment density, ρ_w = water density, f_{silt} = silt factor = d_{sand}/d_{50} with f_{silt} = 1 for $d_{50} > d_{sand}$ (d_{sand} = 62 μm) and D_* = the dimensionless particle size = $d_{50}[(s-1)g/v^2]^{1/3}$. To compensate for the effects of progressive surface waves, phase lag effects and wave asymmetry, Van Rijn expanded his formula with processes described by earlier research. These processes are described further below.

Bed shear stress

Van Rijn (2007a) relates the instantaneous grain-related bed-shear stress to both currents and waves following:

$$\tau_{b,cw}(t) = 0.5\rho_w f'_{cw}\left(u_{\delta,cw}(t)\right)^2 \tag{A.5.2}$$

With $u_{\delta,cw}(t)$ = near bed velocity due to waves (free-stream orbital velocity outside wave boundary layer) and the currents velocity at the edge of the boundary layer defined as:

$$u_{\delta,cw}(t) = u_{\delta,w}(t) + u_{\delta,c} \tag{A.5.3}$$

The friction factor f'_{cw} is the <u>grain friction</u> coefficient due to currents and waves and is defined as:

$$f'_{wc} = \alpha\beta f'_c + (1-\alpha) f'_w$$

$$\alpha = \frac{u_c}{u_c + U_w} \quad \text{and} \quad \beta = 0.25\left[\frac{-1+\ln\left(30h/k_{s,c}\right)}{\ln\left(30\delta/k_{s,c}\right)}\right] \tag{A.5.4}$$

in which α = coefficient related to relative strength of wave and current motion; u_c = depth-averaged current velocity; U_w = peak orbital velocity = $\pi H_s/[T\sinh(2kh)]$ (according to linear wave theory); β = coefficient related to vertical structure of velocity profile. The wave-related (f'_w) and the current-related grain friction coefficient are defined as:

$$f'_{w,grain} = \exp\left[-6 + 5.2\left(A_w/k_{s,grain}\right)^{-0.19}\right]$$
$$f'_{c,grain} = \frac{8g}{18\log\left(12h/k_{s,grain}\right)} \tag{A.5.5}$$

In which $k_{s,grain}$ is the grain roughness ($k_{s,grain} = 1d_{90}$).

Critical bed shear stress

The initiation of motion depends on the next formula for the critical Shields parameter under cohesionless conditions:

$$\theta_{cr} = 0.115(D_*)^{-0.5} \quad \text{for} \quad D_* > 4$$
$$\theta_{cr} = 0.14(D_*)^{-0.64} \quad \text{for} \quad 4 \le D_* < 10 \tag{A.5.6}$$

In which $D_* = d_{50}[(s-1)g/v^2]^{1/3}$ and $s = \rho_s/\rho_w$ = relative sediment density, d_{50} = median diameter. When the $\theta > \theta_{cr}$, sediment particles start to move. The critical bed-shear stress for cohesionless particles is defined by $\tau_{cr,0} = \theta_{cr}(\rho_s - \rho_w)gd_{50}$. Van Rijn also gives a solution to take into account the effects of cohesive particle-particle interaction effects including clay coating effects, the packing effects, and the biological and organic material effects, but this is not part of this research.

Wave asymmetry

Van Rijn (2007a) recommends to use the method of Nielsen and Callaghan *(2003)* to include acceleration when determining the bed shear stress. Nielsen defines a sediment mobilizing velocity $u_\theta(t)$, which is generated with weightings of drag forces (free flow velocity) and of pressure gradient (acceleration) which are respectively cosine and sine of the angle φ_t (between 0° and 90°):

$$u_\theta(t) = \cos\varphi_t \cdot u_{\delta,wc}(t) + \sin\varphi_t \cdot \frac{du_{\delta,wc}(t)}{dt} \tag{A.5.7}$$

Van Rijn (2007) recommends to use the angle φ_t = 40° (in contrary to Nielsen *(2006)*, who used φ_t = 51°).

Surface wave effects

Van Rijn (2007) defines a wave-induced streaming component u_δ which is included in the near bed orbital velocity. This wave-induced streaming at the edge of the wave boundary layer is positive or negative (against wave propagation direction) as a function of relative roughness $A_w/k_{s,w}$. The streaming velocity is calculated following from:

$$u_{\delta,s} = \begin{cases} 0.75U_w^2/c & \text{for} \quad A_w/k_{s,w} \ge 100 \\ \left(-1 + 0.875\log\left(A_w/k_{s,w}\right)\right)U_w^2/c & \text{for} \quad 1 < A_w/k_{s,w} < 100 \\ -U_w^2/c & \text{for} \quad A_w/k_{s,w} \le 1 \end{cases} \tag{A.5.8}$$

Van Rijn does not take into account the Lagrangian effect on the experienced transport periods.

The Quasi-3D approach of Reniers et al. (*2004*) is implemented in the mean current-module of UNIBEST-TC in which the near-bed streaming is already included, so the effect is noticeable on the imposed current velocity. This part of the TR2004 formulations has therefore not been implemented.

A.5.3. TRANSPOR2004: Suspended load transport

Suspended sediment size and fall velocity

The suspended sediment size d_s is defined as:

$$d_s = \max\left[d_{10}, \left(1+0.0006\left(d_{50}/d_{10}-1\right)\left(\psi-550\right)\right)d_{50}\right] \quad \text{for } \psi < 550$$
$$d_s = d_{50} \qquad \text{for } \psi \geq 550 \tag{A.5.9}$$

The fall velocity of suspended sediment in a fluid sediment mixture is defined as:

$$w_{s,0} = \frac{(s-1)gd_s}{18\upsilon} \qquad \text{for} \quad 65\mu m < d_s \leq 100\mu m$$
$$w_{s,0} = \frac{10\upsilon}{d_s}\left[\left(1+\frac{0.01(s-1)gd_s^{\,3}}{\upsilon^2}\right)^{0.5}-1\right] \quad \text{for} \quad 100\mu m < d_s \leq 1000\mu m \tag{A.5.10}$$
$$w_{s,0} = 1.1\left[(s-1)gd_s\right] \qquad \text{for} \quad 1000\mu m < d_s$$

Current-related and wave-related suspended transport.

The suspended-load transport formulations in TR2004 are based on a time-averaged approach and divide the suspended-load into current-related transport and wave-related transport. The current-related suspended-load transport is based on the time-averaged vertical distribution of the concentration and fluid velocities:

$$q_{s,c} = \frac{\int_a^{h+\eta} \bar{U}\bar{C}dz}{(1-p)\rho_s} \tag{A.5.11}$$

In which $q_{s,c}$ is the current-related suspended load transport (m^2/s), $\bar{U}$ (z) is the local time-averaged velocity at height z, $\bar{C}$ (z) is the local time-averaged sediment concentration at height z (kg/m^3), p is the porosity (=0.4) and ρ_s is the sediment density (kg/m^3).

The wave-related suspended sediment transport is defined as the transport of the sediment particles by the oscillating fluid component and is based on the amount of sediment in the suspension layer above the bed and a velocity skewness factor.

$$q_{s,w} = \lambda f_{pl} \frac{\left[U_{w,c}^4 - U_{w,t}^4\right]}{\left[U_{w,c}^3 + U_{w,t}^3\right]} \frac{\int_a^{\delta} \bar{C}dz}{(1-p)\rho_s} \tag{A.5.12}$$

where the term $[(U_{w,c})^4-(U_{w,t})^4]/[(U_{w,c})^3+(U_{w,t})^3]$ = the velocity skewness factor. $U_{w,c}$ and $U_{w,t}$ are the peak orbital velocities under respectively the crest and the trough. δ is the thickness of suspension layer near the bed (=3 x thickness of the wave boundary layer) and λ=0.1 and f_{pl} = a phase lag factor (between +1 and -1), which predicts the reduce in the wave-related suspended transport due to phase lag effect or even change the direction into offshore. The phase lag factor is defined as (*Van Rijn, Ruessink, et al., 2007*):

$$f_{pl} = -\tanh\left[100\left(P-P_{cr}\right)\right] \quad P = \frac{k_{s,w,r}}{w_s T_p} \quad P_{cr} = 0.1 \tag{A.5.13}$$

But in most models this parameter is defined as an input parameter (default f_{pl} = 1), because the effect seems to be small and it is hard to predict which effect it has on the transport rates.

Reference concentration c_a (at z=a)

The reference concentration c_a close to the bed is defined by:

$$c_a = 0.015\frac{d_{50}}{a}\frac{T^{1.5}}{D_*^{0.3}} \qquad c_a \leq 0.05 \tag{A.5.14}$$

Where $D_* = d_{50}/[(s-1)g/v^2]^{1/3}$ = dimensionless particle diameter; T = dimensionless bed-shear stress parameter; a = reference level (m), where a is defined as the maximum value of half the wave-related and half the current-related bed roughness values: $a = \max(0.5 * k_{s,c,r}, 0.5k_{s,w,r})$ with a minimum value of 0.01 m.

The dimensionless bed shear stress parameter T is defined as:

$$T = \frac{\left(\tau'_{b,cw} - \tau_{b,cr}\right)}{\tau_{b,cr}} \tag{A.5.15}$$

Where $\tau_{b,cw}'$ = time-averaged effective bed-shear stress (N/m^2) and $\tau_{b,cr}$ = time-averaged critical bed-shear stress according to Shields (N/m^2).

The magnitude of the time-averaged bed-shear stress (independent of the angle between the wave- and current direction) is given by:

$$\tau'_{b,cw} = \tau'_{b,c} + \tau'_{b,w} \tag{A.5.16}$$

Where $\tau_{b,c}' = \mu_c \alpha_{cw} \tau_{b,c}$ = effective current-related bed-shear stress and $\tau_{b,w}' = \mu_w \tau_{b,w}$ = effective wave-related bed-shear stress; μ_c and μ_w = current- and wave-related efficiency factors and α_{cw} = wave-current interaction factor. The current efficiency factor is defined as:

$$\mu_c = f_c' / f_c \tag{A.5.17}$$

With f_c'= grain-related friction coefficient based on $1d_{90}$; and f_c = current-related friction coefficient based on predicted bed roughness values.

The wave efficiency factor is defined as:

$$\mu_w = 0.7/D_* \qquad \begin{array}{l} \text{with } \mu_{w,\min} = 0.14 \text{ for } D_* \geq 5 \\ \text{with } \mu_{w,\max} = 0.35 \text{ for } D_* \leq 5 \end{array} \tag{A.5.18}$$

Concentration profile

To compute the time-averaged concentration profile a convection-diffusion equation is applied which computes the equilibrium concentration profile in steady flow:

$$w_{s,m} \cdot c + \phi_d \varepsilon_{s,cw} \frac{dc}{dz} = 0 \tag{A.5.19}$$

In which $w_{s,m}$ = the fall velocity of suspended sediment in a fluid sediment mixture (m/s), c = the time-averaged volume concentration at height z (-) and $\varepsilon_{s,cw}$ = sediment mixing coefficient for combined steady and oscillatory flow (m^2/s). The parameter ϕ_d takes into account the damping of the turbulence due to the presence of high sediment concentrations in the near-bed layer:

$$\phi_d = 1 + \left(\frac{c}{c_0}\right)^{0.8} - 2\left(\frac{c}{c_0}\right)^{0.4} \tag{A.5.20}$$

The sediment mixing coefficient is modelled as:

$$\varepsilon_{s,cw} = \left[\varepsilon_{s,c}{}^2 + \varepsilon_{s,w}{}^2\right]^{0.5} \tag{A.5.21}$$

Where $\varepsilon_{s,c} = \beta_c \varepsilon_{f,c}$ = the current-related mixing coefficient due to main current (m^2/s); the effect of the sediment particles. $\beta_c = 1+2(w_s/u_{*,c})^2$ with $\beta_c < 1.5$ = takes into account the effect of the sediment particles on the mixing of fluid momentum. $\varepsilon_{s,w} = \beta_w \varepsilon_{f,w}$ = the wave-related mixing coefficient (m^2/s);

For the current-related mixing coefficient the next maximum is defined:

$$\varepsilon_{s,c,\max} = 0.25 \cdot \kappa \cdot u_{*,c} \cdot h_d \cdot \beta_c \qquad \text{for } z > 0.5h_d \tag{A.5.22}$$

For z < 0.5 h_d a negative parabolic function is used to define the current-related mixing coefficient. The wave-related mixing coefficient has the next minimum and maximum:

$$\varepsilon_{s,w,\max} = 0.035 \cdot \frac{\gamma_{br} h_d H_s}{T_p} \qquad \text{for } z > 0.5h_d \qquad \varepsilon_{s,w,\max} \le 0.05 m^2/s \tag{A.5.23}$$

$$\varepsilon_{s,w,bed} = 0.018 \cdot \gamma_{br} \beta_w \delta_m U_{b,r} \qquad \text{for } z < \delta_m \tag{A.5.24}$$

In which $U_{b,r}$ = representative near-bed orbital velocity based on significant wave height. β_w = wave coefficient = $1+2(w_s/u_{*,w})^2$ with $\beta_w<1.5$, w_s = fall velocity of suspended sediment $u_{*,w}$ = wave-related bed shear velocity.

The thickness of the sediment mixing layer near the bed reads as:

$$\delta_m = 2\gamma_{br}\delta_w \qquad 0.1 < \delta_m < 0.5m \tag{A.5.25}$$

Where δ_m = thickness of effective near-bed sediment mixing layer; δ_w = thickness of wave boundary layer:

$$\delta_w = 0.36 A_{w,sig} \left(\frac{A_{w,sig}}{k_{s,w,r}} \right)^{-0.25} \tag{A.5.26}$$

$A_{w,sig}$ = peak orbital excursion based on significant wave height H_s; $k_{s,w,r}$ = wave-related bed roughness; and γ_{br} = 1 + $(H_s/h_d-0.4)^{0.5}$ = empirical coefficient related to wave breaking (γ_{br} = 1 for H_s/h_d < 0.4).

A.5.4. SANTOSS sand transport model

An important aspect of the SANTOSS sand transport formula is that less input data about the near bed orbital velocity is needed (see Table_Apx A-1)

Description input characteristic	**Symbol**
Local flow depth	h [m]
Grain size characteristics	d_{50}, d_{90} [m]
Peak wave period	T
Crest and trough period	$T_{w,c}$, $T_{w,t}$
Acceleration period of wave and trough	$T_{w,cu}$, $T_{w,tu}$
Peak orbital flow velocity near bed for crest and trough	$\hat{u}_{w,c}$ and $\hat{u}_{w,t}$ [m/s]
Depth-averaged current velocity	u_c [m/s]
Angle between wave direction and current direction	φ [radians]

Table_Apx A-1: Input parameters for the SANTOSS-model

Transport formula

Ribberink et al. (2010) uses another approach and determines the sediment transport under the crest and the trough separately. For both half-cycles the representative bed shear stress is determined (which not only depends on the free-stream velocity and the friction but also additional processes are included, further described below) and the amount of sediment ($\Omega_{wc,c}$ and $\Omega_{wc,t}$) that is stirred up according to:

$$\Omega_{wc,i} = \begin{cases} 0 & \text{if} \quad |\theta_{wc,i}| \le \theta_{cr} \\ 9.41\left(|\theta_{wc,i}| - \theta_{cr}\right)^{1.2} & \text{if} \quad |\theta_{wc,i}| \le \theta_{cr} \end{cases} \quad \text{with} \quad i = c,t \tag{A.5.27}$$

In which θ_{cr} is the critical Shields parameter (see further below). Because a proportion of the sediment that is stirred up during one half-cycle, is transported during the next half cycle the sediment loads Ω_{cc}, Ω_{tc}, Ω_{tt} en Ω_{ct} are determined using the phase lag parameters P_c and P_t (see in the paragraph about phase lag effects) in which:

- Ω_{cc} and Ω_{tt} represent the sand loads that are entrained during respectively the wave crest and trough period and transported during the same half-cycle,

- Ω_{ct} and Ω_{tc} represent the sand loads that are entrained during respectively the wave crest and trough period and transported during the next half-cycle.

The total sediment transport in the wave boundary layer is calculated according to:

$$\Phi_b = \sqrt{|\theta_c|}\frac{T_c}{T}\left(\Omega_{cc} + \frac{T_c}{2T_{cu}}\Omega_{tc}\right)\frac{\vec{\theta_c}}{|\theta_c|} + \sqrt{|\theta_t|}\frac{T_t}{T}\left(\Omega_{tt} + \frac{T_t}{2T_{tu}}\Omega_{ct}\right)\frac{\vec{\theta_t}}{|\theta_t|} \qquad \text{(A.5.28)}$$

In which Φ_b is the non-dimensional sediment transport = $q_b/[(s-1)gD_{50}^3]^{0.5}$, s = relative density = ρ_s/ρ_w and g is the gravitational acceleration. The travel distance of the sediment loads under the crest and trough are defined by the square roots of the corresponding Shields parameters and the periods, while also a wave asymmetry factor is used to correct the travel distance for the sediment that is still in the water column beyond the phase of flow reversal.

Bed shear stress

Ribberink et al. (2010) do not use the whole time series of flow velocities at the wave boundary, but use the half-cycle approach to define the Shields parameter (representative non-dimensional bed shear stress for each half-cycle). The flow parameters that are used are the maximum crest and trough velocity at the edge of the boundary layer (vectors $u_{wc,c}$ and $u_{wc,t}$ respectively) consisting of a combination of the maximum orbital velocity and the current velocity:

$$\begin{aligned} \vec{u}_{wc,c} &= u_{w,c} + \vec{u}_c \\ \vec{u}_{wc,t} &= -u_{w,t} + \vec{u}_c \end{aligned} \qquad \text{(A.5.29)}$$

The non-dimensional bed shear stresses under wave crest and trough (θ_c and θ_t) are defined as follows:

$$\vec{\theta}_i = \frac{f_{wc,i}\left|u_{wc,i}\right|\vec{u}_{wc,i}}{(s-1)gd_{50}} \quad \text{with} \quad i = c,t \qquad \text{(A.5.30)}$$

The combined wave-current friction factor at crest and trough are calculated as the linear combination of the wave friction factor (at crest and trough) and the current friction factor:

$$\begin{aligned} f_{wc,i} &= \alpha f_c + (1-\alpha) f_{w,i} \quad &&\text{with} \quad i = c,t \\ \alpha &= \frac{3|u_c|}{3|u_c| + \hat{u}_w} \quad &&\text{with} \quad \hat{u}_w = \sqrt{\frac{1}{2}u_{w,c}^{\,2} + \frac{1}{2}u_{w,t}^{\,2}} \end{aligned} \qquad \text{(A.5.31)}$$

$\hat{u}_w$ is the characteristic orbital velocity amplitude. The wave friction factor at crest and trough is defined as:

$$\begin{aligned} f_{w,i} &= 0.00251\exp\left[5.21\left(\frac{\left(\frac{2T_{iu}}{T_i}\right)^2 \hat{A}_w}{k_{s,w}}\right)^{-0.19}\right] \quad &&\text{for} \quad \frac{\hat{A}_w}{k_{s,w}} > 1.587 \\ f_{w,i} &= 0.3 \quad &&\text{for} \quad \frac{\hat{A}_w}{k_{s,w}} \le 1.587 \end{aligned} \quad \text{with} \quad i = c,t \quad \text{(A.5.32)}$$

With A_w is the characteristic orbital excursion amplitude. The factors $[2T_{cu}/T_c]^2$ and $[2T_{tu}/T_t]^2$ are needed to include the wave asymmetry effects (see paragraph below for further clarification). The current friction factor is computed using a logarithmic velocity profile:

$$f_c = 2\left[\frac{0.4}{\ln(30\delta/k_{s,c})}\right] \qquad \text{(A.5.33)}$$

With δ is the level on which the current velocity is imposed. The roughness heights include additional roughness for the ripple form roughness (an additional suspended sediment transport component may exist in the wave boundary layer) and an increased wave roughness for fine sands with d_{50}<0.20 using factor μ:

$$k_{s,c} = \max\left\{3d_{90}, d_{50}\left[\mu + 6\left(\langle|\theta|\rangle - 1\right)\right]\right\} + \frac{0.4\eta^2}{\lambda}$$
$$k_{s,w} = \max\left\{3d_{50}, d_{50}\left[\mu + 6\left(\langle|\theta|\rangle - 1\right)\right]\right\} + \frac{0.4\eta^2}{\lambda} \quad (A.5.34)$$

With η = ripple height; λ = ripple length and with:

$$\mu = \begin{cases} 6 & \text{if} \quad d_{50} \le 0.15\text{mm} \\ \left[6 + \left(10^3 d_{50} - 0.15\right)\frac{(1-6)}{(0.20-0.15)}\right] & \text{if} \quad 0.15\text{mm} < d_{50} < 0.20\text{mm} \\ 1 & \text{if} \quad d_{50} \ge 0.20\text{mm} \end{cases} \quad (A.5.35)$$

And with the mean Shields parameter according to:

$$\langle|\theta|\rangle = \frac{0.5 f_c |u_c|^2}{(s-1) g d_{50}} + \frac{0.25 f_w u_w^{\,2}}{(s-1) g d_{50}} \quad (A.5.36)$$

Critical bed shear stress

Ribberink et al. (2010) uses the formula of Soulsby (1997) for the critical Shield parameter:

$$\theta_{cr} = \frac{0.3}{1 + 1.2D_*} + 0.055\left(1 - \exp\left(-0.02D_*\right)\right) \quad (A.5.37)$$

The sand transport models use different formulations for the critical shields parameter, which give the same results for d_{50}<0,5 mm, but with differences for the larger sediment grain sizes (d_{50} > 0,5 mm). The influences of clay coating, packing effects and organic material effects are not taken into account.

Phase lag effects

The SANTOSS model computes their phase lag parameter on a slightly different way and again for the crest and trough separately. The phase-lag parameters for the crest and the trough determine which proportion of the entrained sediment during that half-cycle is transported during the next half-cycle (in the opposite direction). Especially during the acceleration period, the flow in the boundary layer is very turbulent, while during the deceleration the turbulence near the bed is very low:

$$P_i = \begin{cases} 9.3\dfrac{\eta}{2(T_i - T_{iu})w_s} & \text{if} \quad \eta > 0 \quad (\text{ripple-regime}) \\ 8.0\dfrac{\delta_{si}}{2(T_i - T_{iu})w_s} & \text{if} \quad \eta = 0 \quad (\text{sheetflow-regime}) \end{cases} \quad \text{with} \quad i = c,t \quad (A.5.38)$$

The parameter depends on:

- The height to which the sediment is taken into suspension during the acceleration period. To make an approximation of this height the ripple height η is used in the ripple regime and the sheet flow layer thickness (δ_{sc} or δ_{st}) in the sheet flow regime.
- The period in which the sediment particles can settle down is given by the period of that half-cycle, but because the settling of deceleration until the flow changes direction ($T_c - T_{cu}$ for under the crest and $T_t - T_{tu}$ for under the trough) is used as approximation of the settle time.

- Fall velocity of suspended sediment which depends on the sediment grain size. The settling velocity is also affected by the vertical orbital velocity, which is present under surface waves (see paragraph about surface wave effects below). Without the vertical orbital velocity, the fall velocity is determined by:

$$w_s = \frac{v}{0.8d_{50}}\left(\sqrt{10.36^2 + 1.049D_s^{*3}} - 10.36\right) \quad (A.5.39)$$

$$D_s^* = \left(\frac{(s-1)g}{v^2}\right)^{1/3} 0.8d_{50} \quad (A.5.40)$$

The different sediment loads becomes:

$$\begin{aligned}
&\text{if} \quad P_c \le 1 \quad \Omega_{cc} = \Omega_c && \text{and} \quad \Omega_{tc} = 0 \\
&\text{if} \quad P_c > 1 \quad \Omega_{cc} = \frac{1}{P_c}\Omega_c && \text{and} \quad \Omega_{tc} = \frac{(P_c - 1)}{P_c}\Omega_c \\
&\text{if} \quad P_t \le 1 \quad \Omega_{tt} = \Omega_t && \text{and} \quad \Omega_{ct} = 0 \\
&\text{if} \quad P_t > 1 \quad \Omega_{tt} = \frac{1}{P_t}\Omega_t && \text{and} \quad \Omega_{ct} = \frac{(P_t - 1)}{P_t}\Omega_t
\end{aligned} \quad (A.5.41)$$

Wave asymmetry

Sand transport rates not only depend on the crest and trough periods and the corresponding flow velocities (both are accounted for because of velocity skewness) because the bed shear stress and the phase lag effects (which both have large influence on the transport rates) are also influenced by the wave asymmetry:

- Acceleration skewness leads to a higher bed shear stress (and thus more entrained sediment) at the strongly accelerating half-cycle and a lower bed shear stress (thus less entrained sediment) at the weakly accelerating half cycle. Magnitudes of the total bed shear stress under the wave crest and the trough (calculated trough the Shields parameter $|\theta_c|$ or $|\theta_t|$) are compensated for acceleration skewness. The relative period of acceleration compared to the corresponding half cycle period is related to the wave friction factor: see equation(A.5.32).
- The phase lag parameters for the crest and the trough (P_c and P_t respectively) are based on the settling distance of sediment grains and thus the settling period. When the period of acceleration is shorter, the settling period (period of deceleration) is longer. Of the amount of sediment entrained during that half cycle more is settled and less is transported during the following half cycle: see equation (A.5.38).
- For the proportion of the sediment that is entrained during one half cycle, but which is also transported in the next half cycle in the other direction (phase lag effect), the velocities directly after the velocity-direction-change are of importance for the settling distance. The wave asymmetry is in this case also included in equation (A.5.28) to take the acceleration into account in the travel distance of sediment that is entrained in the previous half-cycle.

In case of forward-leaning waves (acceleration skewness of β>0.5, As<0) all effects of acceleration skewness leads to a higher onshore-directed sediment transport rate.

Surface wave effects

Real surface waves have several effects on the near bed velocity and the transport in the boundary layer. The differences between the circumstance under real waves and in the oscillating flow tunnels are recognized and taken into account by the SANTOSS transport model. These are listed below:

- Additional (positive) wave Reynolds stress in the direction of the wave. This enhances the crest x-component and reduce the trough x-component of the bed shear stress. The y-components (perpendicular to the wave propagation direction) are unchanged.

$$\theta_{cx,sw} = \theta_{cx} + \theta_{w\mathrm{Re}} \quad \text{and} \quad \theta_{tx,sw} = \theta_{tx} + \theta_{w\mathrm{Re}}$$
$$\theta_{w\mathrm{Re}} = \frac{\tau_{w\mathrm{Re}}}{\rho(s-1)gd_{50}} \quad \text{with} \quad \tau_{w\mathrm{Re}} = \rho \frac{f_{w\mathrm{Re}}}{2c}\frac{4}{3\pi}u^3 \tag{A.5.42}$$

- The friction factor used here is the combined friction factor of currents and waves given in equation (A.5.31), although for the wave friction factor the total wave friction factor is used.
- Lagrangian motion: The extension/reduction ΔT of the half-cycle period depends on the ratio of the wave propagation velocity c and the horizontal grain displacement d_g during the half wave-cycle:

$$T_{c,sw} = T_c + \Delta T_c \quad \text{with} \quad \Delta T_c = \frac{d_g}{c} = \left[\frac{c}{0.55u} - 2\right]^{-1} T$$
$$T_{t,sw} = T_t - \Delta T_t \quad \text{with} \quad \Delta T_t = \frac{d_g}{c} = \left[\frac{c}{0.55u} + 2\right]^{-1} T \tag{A.5.43}$$

- Presence of vertical orbital velocity leads to another asymmetry between crest and trough. the vertical orbital velocity is directed downward under the 2nd half of the crest period (which enhances the fall velocity) and directed upward under the 2nd half of the trough period (which reduces the fall velocity). This way it has also influence on the phase lag parameters of equation (A.5.38) and results in higher onshore transport.

The surface wave effects included in the SANTOSS model all enhance the onshore transport.

B. Different orbital velocity theories

B.1. Current options and proposed changes to orbital velocity module

In the near-bed orbital velocity module of UNIBEST-TC 4 different orbital velocity theories were already implemented:

- SWASYM=0: Stream function theory by Rienecker & Fenton (*1981*): 8-order theory which shows only skewness.
- SWASYM=1: Second-order Stokes wave theory by Grasmeijer and Van Rijn (*1998*) based on the theory of Isobe & Horikawa (*1982*): shows only skewness and wobbles under high non-linear waves
- SWASYM=2: Theory by Ruessink & Van Rijn (*in preparation*) which is also applied by Van Rijn et al. (*Van Rijn, et al., submitted*): shows both skewness and asymmetry but also wobbles under high non-linear waves. Root-mean-square velocity is based on linear wave theory.
- SWASYM=-1: Combination of the stream function theory of Rienecker & Fenton and the theory of Ruessink & Van Rijn by Van Thiel de Vries (*2009*): shows both skewness and asymmetry and no unrealistic wobbles.
- SWASYM=-2: Approach of Van Thiel de Vries applied to the second-order Stokes wave theory of Grasmeijer & Van Rijn (*1998*): shows both skewness and asymmetry but unrealistic wobbles.

Only SWASYM 2, -1 and -2 show both skewness and asymmetry and only SWASYM -1 shows no unrealistic wobbles. Two versions of another theory and an updated version of SWASYM 2 is implemented:

- SWASYM=3: Theory of Elfrink et al. (*2006*): shows both skewness and asymmetry but small discontinuities in acceleration.
- SWASYM=4: Theory of Abreu et al. (*2010*) used to modify the theory of Elfrink et al. (*2006*): shows skewness and asymmetry and no discontinuities or unrealistic wobbles.
- SWASYM=5: Theory of Abreu et al. (*2010*) used to modify the theory of Ruessink & Van Rijn (*in preparation*): shows skewness and asymmetry and no discontinuities or unrealistic wobbles. Amplitude based on linear wave theory.
- SWASYM=5: Theory of Abreu et al. (*2010*) used to modify the theory of Ruessink & Van Rijn (*in preparation*): shows skewness and asymmetry and no discontinuities or unrealistic wobbles. Amplitude based Grasmeijer and Ruessink (*Grasmeijer & Ruessink, 2003*).

To explain the last two implemented theories the formula of Abreu et al. (*2010*) is analysed below in more detail and also how it is used during the implementation.

B.2. Analysis formula Abreu et al. (*2010*)

The very promising oscillating flow velocity formula of Abreu et al. (2010) has been analysed extensively for use in the UNIBEST-TC module to generate the near-bed-orbital velocity time series. First some characteristics of the formula are given and then it is explained how it is applied together with other theories.

The formula of Abreu et al. (*2010*) for the near bed orbital velocity is based on the work of Drake and Calantoni (*2001*) and is defined as follows:

$$u(t) = U_w f \frac{\left[\sin(\omega t) + \dfrac{r \sin\phi}{1+\sqrt{1-r^2}}\right]}{\left[1 - r\cos(\omega t + \phi)\right]} \tag{B.2.1}$$

In which U_w is the amplitude of the orbital velocity (defined as $(U_c+U_t)/2$); the variable f is a dimensionless factor allowing the velocity amplitude to be equal to Uw ($f = (1-r^2)^{0.5}$; ω the angular frequency; r an index of non-linearity and φ a phase which determines if the non-linearity consists of skewness or asymmetry. The acceleration of the function is given by:

$$a(t) = U_w \omega f \frac{\cos(\omega t) - r\cos(\phi) - \dfrac{r^2}{1+\sqrt{1-r^2}}\sin\phi\sin(\omega t+\phi)}{\left[1 - r\cos(\omega t+\phi)\right]^2} \tag{B.2.2}$$

B.2.1. Different wave forms

4 different wave forms can be distinguished and are shown in Table_Apx B-1. In practice most (not all) of the waves are positive skewed and lean forward the wave form displayed right at the top in Table_Apx B-1. Waves that are purely skewed (As = 0, β=0.5) have a phase of φ = -1/2*π. Waves that are not skewed but only asymmetric (Sk = 0, R = 0.5) are found with a phase of φ = 0 (forward leaning) or φ = -π (backward leaning).

B.2.2. Mean absolute velocity and root-mean-square velocity

The formula of Abreu et al. (*2010*) uses a amplitude of the orbital velocity which is defined as $(U_c+U_t)/2$. This means that the mean absolute velocity and the root-mean-square velocity are not the same for the ranges for r (range is: -1 < r < +1) and φ (range is: -π < φ < 0). This means that if theories want to generate a time series with a certain mean absolute velocity or root-mean-square velocity the formula has to be adapted.

shows (a) the mean absolute velocity and (b) the root-mean-square velocity for the case of U_w = 1 m/s. The root-mean-square velocity of the time-series seems to depend only on the non-linearity index r. After basic fitting the root-mean-square velocity can be estimated using:

$$U_{rms} = \frac{1}{2}\sqrt{2}\cdot U_w \cdot \left[-0.3|r|^3 + 0.087|r|^2 - 0.045|r| + 1\right] \tag{B.2.3}$$

The mean absolute velocity also depends mainly on the non-linearity index r, although

	-π < φ < -0.5π	-0.5π < φ < 0
1 > r > 0	Positive skewed (Sk>0, R>0.5) Backward leaning (As>0, β<0.5) 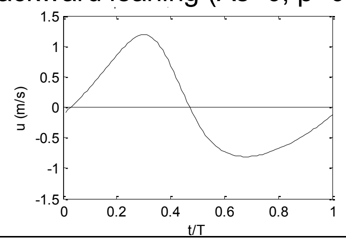	Positive skewed (Sk>0, R>0.5) Forward leaning (As<0, β>0.5) 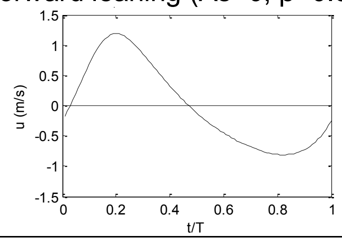
0 > r > -1	Negative skewed (Sk<0, R<0.5) Backward leaning (As<0, β>0.5) 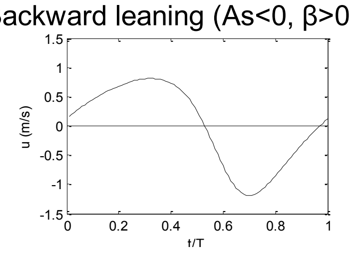	Negative skewed (Sk<0, R<0.5) Forward leaning (As>0, β<0.5) 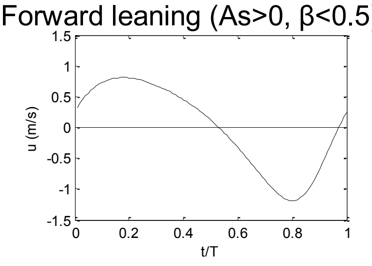

Table_Apx B-1: Different wave forms

for skewed waves (φ = -π/2) the effect seems to be larger than for asymmetry waves (φ = -π or φ = 0).

B.2.3. Relation between (r,φ) and velocity skewness R, acceleration skewness β and wave skewness parameter α

Abreu et al. *(2010)* already described the relationship between an arbitrary (r,φ)-combination and a (R,β)- or (R,α) combination:

$$R = \frac{u_{max}}{u_{max} - u_{min}} \qquad \beta = \frac{a_{max}}{a_{max} - a_{min}} \qquad \alpha = \frac{2 \cdot T_{cu}}{T} \tag{B.2.4}$$

Abreu et al. (*2010*) developed a code to find the values of the (r,φ)-combination belonging to all possible (R,α)-combinations shown in Figure_Apx B-2. For different φ-values (from –π to 0 with steps of 1/8*π) approximations for R(r) and α(r) are given from

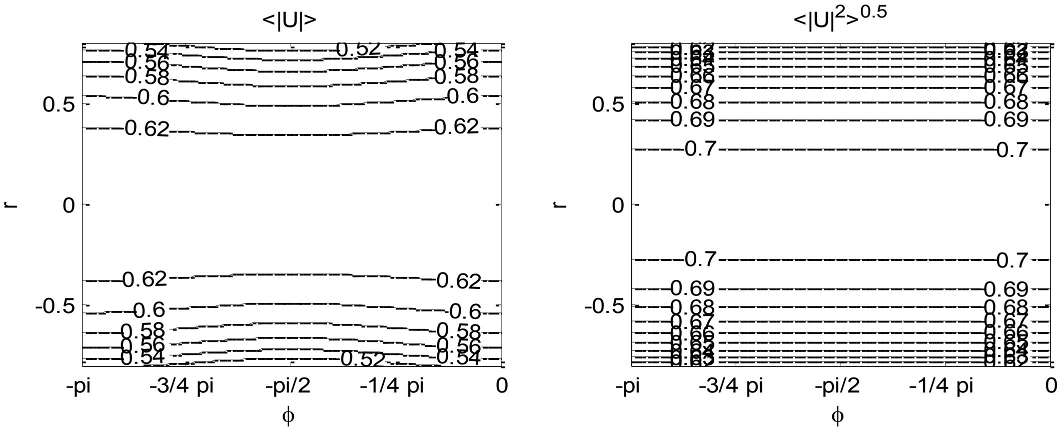

Figure_Apx B-1: Mean absolute velocity and root-mean-square velocity for all (r,φ)-combinations (U_w = 1)

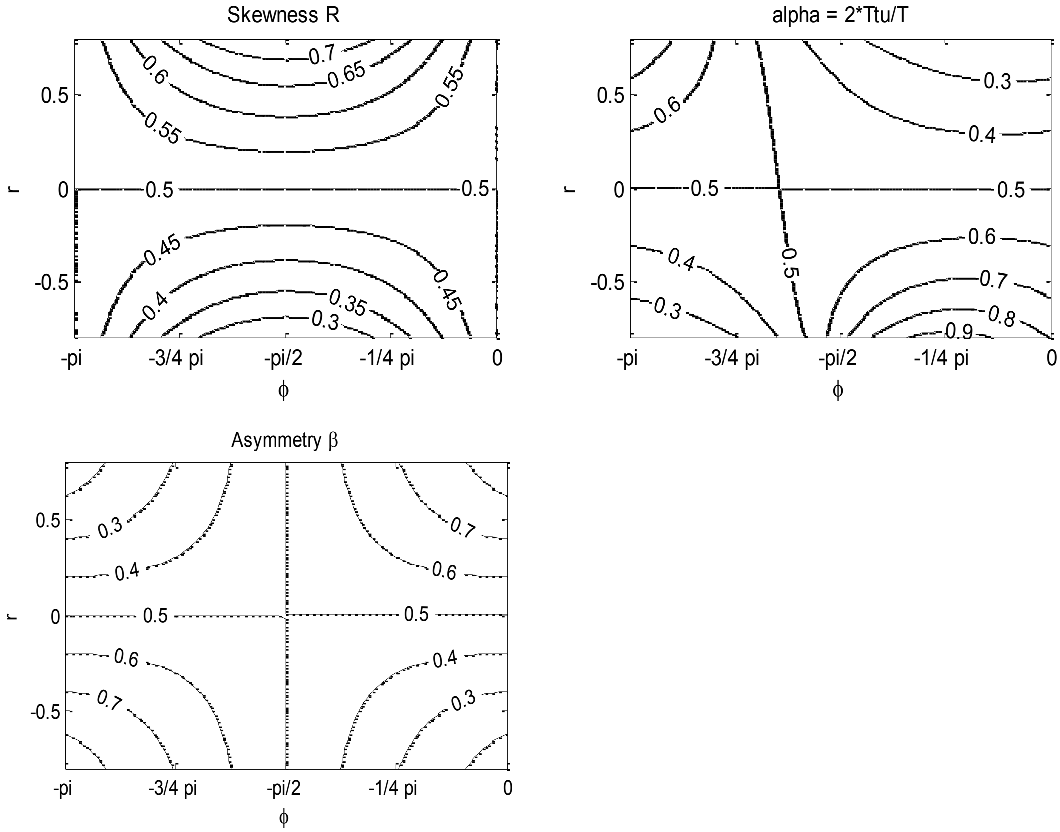

Figure_Apx B-2: Skewness R, skewness parameter α and asymmetry β for all (r,φ)-combinations which the final (r,φ)-combination can be iteratively generated. This extensive code has been made available by Mr. Abreu (code in Visual Basic). The code is translated in FORTRAN 77 language and extensively tested.

B.2.4. Relation between (r,φ) and the Skewness Sk and asymmetry As

Although this is not mentioned by Abreu et al. *(2010)* there seems to be a strong relationship between the (r-φ) combinations and the related combination of skewness Sk and asymmetry As:

$$Sk = \frac{\left\langle u_w^{\,3} \right\rangle}{\left\langle u_w^{\,2} \right\rangle^{1.5}} \quad As = \frac{\left\langle H\left(u_w\right)^3 \right\rangle}{\left\langle u_w^{\,2} \right\rangle^{1.5}} \tag{B.2.5}$$

The relation between the wave form parameters (for -1<r<1 and –pi/2<φ<0) and the skewness and asymmetry is shown in Figure_Apx B-3. It shows that the parameter r and φ of Abreu et al (*2010*) have a clear relation with the skewness Sk and asymmetry As. The phase φ determines the distribution of the amount of non-linearity between skewness Sk and asymmetry As:

$$\tan(\phi) = \frac{Sk}{As} \tag{B.2.6}$$

$$\text{with} \quad -\pi < \phi < 0 \tag{B.2.7}$$

Figure_Apx B-4 shows the nonlinearity B given by:

$$. B = \sqrt{Sk^2 + As^2} \; . \tag{B.2.8}$$

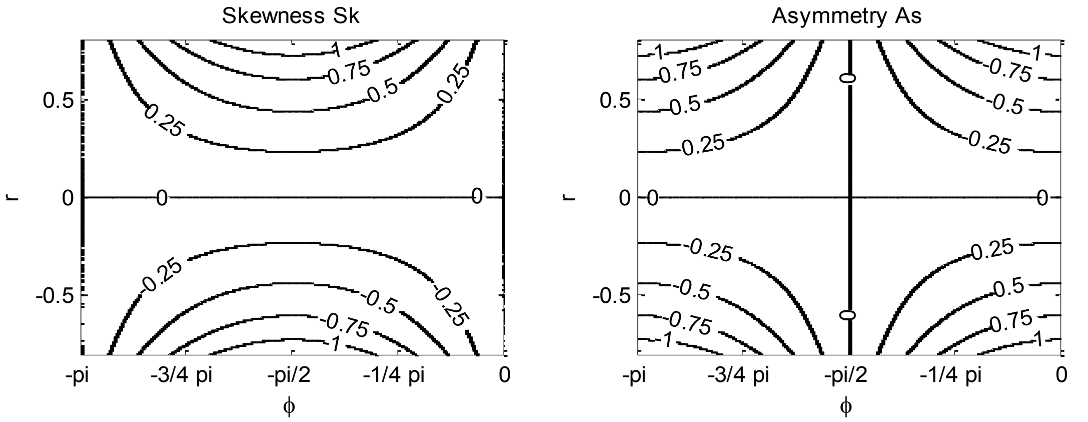

Figure_Apx B-3: (a) Skewness Sk and (b) Asymmetry As for all (r,φ)-combinations

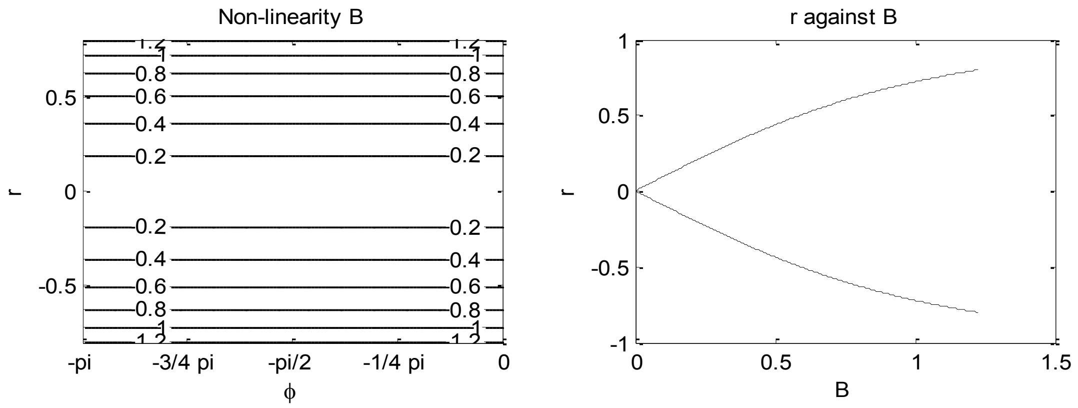

Figure_Apx B-4: (a) Non-linearity B for all (r,φ)-combinations and (d) the relation between the two non-linearity indices r and B.

It is clear that the total non-linearity does not depend on φ and only on the other non-linearity index r. Basic fitting using quadratic functions leads to the following relationship between r and B (RMSE = 0.0053 for 0<r<0.95):

$$|r| = -0.2926 \cdot B^2 + 1.015 \cdot B \quad \text{with } B = \sqrt{Sk^2 + As^2} \tag{B.2.9}$$

B.3. Generation of necessary wave form parameters

In this paragraph the different ways are presented which are used to determine the wave form parameters. The first method presented is the method of Elfrink et al. (*2006*) and focuses on generation of the maximum flow velocities and the half-cycle and acceleration periods. The second method is the method of Ruessink & Van Rijn (*in preparation*) who generate the skewness Sk and asymmetry As.

B.3.1. Method Elfrink et al. (2006)

Elfrink et al. (*2006*) used field measurements at Terschelling (the Netherlands, NOURTEC project), Duck (USA, SandyDuck97 experiments) and Egmond aan Zee (the Netherlands, Coast3D project) of in total to determine the characteristic velocity parameters (partial periods and peak velocities) based on 3 independent dimensionless wave parameters: normalized wave height H*, wave length L* and the local Irribarren number ξ.

$$H^* = \frac{H}{h_d} \quad L^* = \frac{L}{h_d} \quad \xi = \frac{\tan\beta}{\sqrt{H/L_0}} \tag{B.3.1}$$

In which H is the local wave height, h_d is the local depth, L is the local wave length, β the average slope over the length of 2 local wave length offshore of the point and L_0 is the wave length at deep water. Elfrink et al. (*2006*) empirical expressions to calculate the peak orbital velocities (for crest $U_{w,c}$ and trough $U_{w,t}$) and the partial periods (half-cycle periods T_c and T_t and the acceleration periods $T_{w,cu}$ and $T_{w,tu}$). From these wave characteristics the values of R and α can be calculated which leads to the (r-φ) combination (according to method describe above). The other 2 input parameters for the formula of Abreu et al. (*2010*) (see equation (B.2.1)) can be easily derived ($U_w = (U_{w,c} + U_{w,t})/2$ and $\omega = 2*\pi/T$).

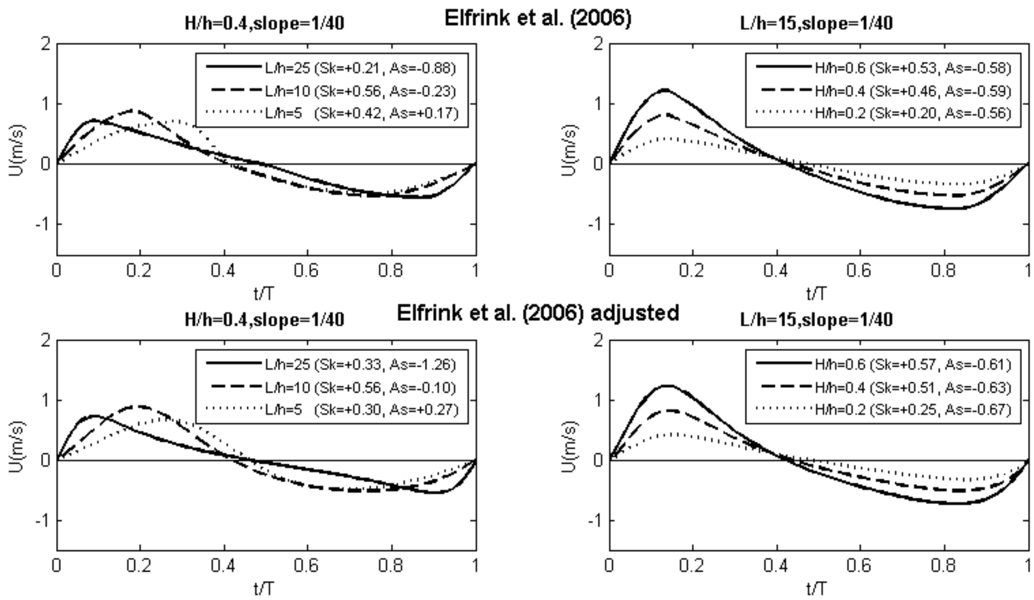

Figure_Apx B-5: Theory of Elfrink et al. (2006, upper two figures) compared to the adjusted version using the formula and approach of Abreu et al. (2010, lower two figures).

It has to be mentioned that Elfrink et al. (*2006*) also developed their own theory to develop a time series for the orbital flow velocity. This solution is only a simplification and just combines the defined points under the conditions that the average velocity is kept zero. The result is a time series that shows discontinuities in acceleration. The two methods are compared in Figure_Apx B-5, where the improvements by using the new approach of Abreu et al. (*2010*) are especially visible for asymmetric waves. Next to a smooth time series it is now also easier to extract the wave form parameters for skewness (R or Sk) and asymmetry (β or As)

B.3.2. Method Ruessink & Van Rijn (*in preparation*)

The method developed by Ruessink & Van Rijn (*in preparation*) is already implemented in UNIBEST-TC but the way they generate a orbital velocity time series from the wave form parameters leads to a time series with wobbles and is not well enough for use by the SANTOSS model. They parameterized the wave skewness S_k and wave asymmetry A_s as a function of the Ursell number defined as:

$$Ur = \frac{3}{8}\frac{H_s k}{\left(kh_d\right)^3} \tag{B.3.2}$$

In which H_s = 1.41*H_{rms}, k = the local wave number and h_d the depth. The parameterization is optimized by applying a nonlinear least square fit procedure to more than 30.000 measurements at Egmond aan Zee and Terschelling several measurement campaigns. They calculate the total non-linearity B and phase φ by:

$$B = \frac{0.7939}{1+\exp\left[\frac{-0.6065-\log(Ur)}{0.3539}\right]} \tag{B.3.3}$$

$$\phi = -\pi + \frac{\pi}{2}\tanh\left(\frac{0.6373}{Ur^{0.5995}}\right) \tag{B.3.4}$$

Using equation (B.2.9) the non-linearity r can be estimated based on B. According to Ruessink & Van Rijn (*in preparation*) orbital velocity time series need to have the same root-mean-square velocity as defined by linear wave theory:

$$U_{rms} = \frac{\pi H_{rms}}{\sqrt{2}\cdot T\sinh\left(k\cdot h_d\right)} \tag{B.3.5}$$

This means that the parameter U_w of equation (B.2.1) needs to be defined using equation (B.2.3):

$$U_w = \frac{\sqrt{2}\cdot U_{rms}}{\left[-0.3|r|^3+0.087|r|^2-0.045|r|+1\right]} \tag{B.3.6}$$

Figure_Apx B-6 shows the improvements by using the adjusted method of Ruessink & Van Rijn (*in preparation*) using the formula of Abreu et al. (*2010*). Unrealistic wobbles are disappeared but the maximum velocities are still about the same. This last point is important while these maximum orbital velocities are used as input for the suspended load transport (both current-related and wave-related).

The third figure shows a version where the root-mean-square velocity is not any more equal to that of linear wave theory. Grasmeijer & Ruessink (*2003*) found analysing field and experimental data, that the orbital amplitude is not always equal to that of linear wave theory but must be adjusted using:

$$U_w = \frac{U_{w,c} + U_{w,t}}{2} = r \cdot U_{orb,linear} \tag{2.3.7}$$

$$r = -0.4\frac{H_w}{h_d} + 1 \tag{2.3.8}$$

This leads to smaller orbital velocity amplitudes especially for high relative wave heights. This result is also shown in Figure_Apx B-6.

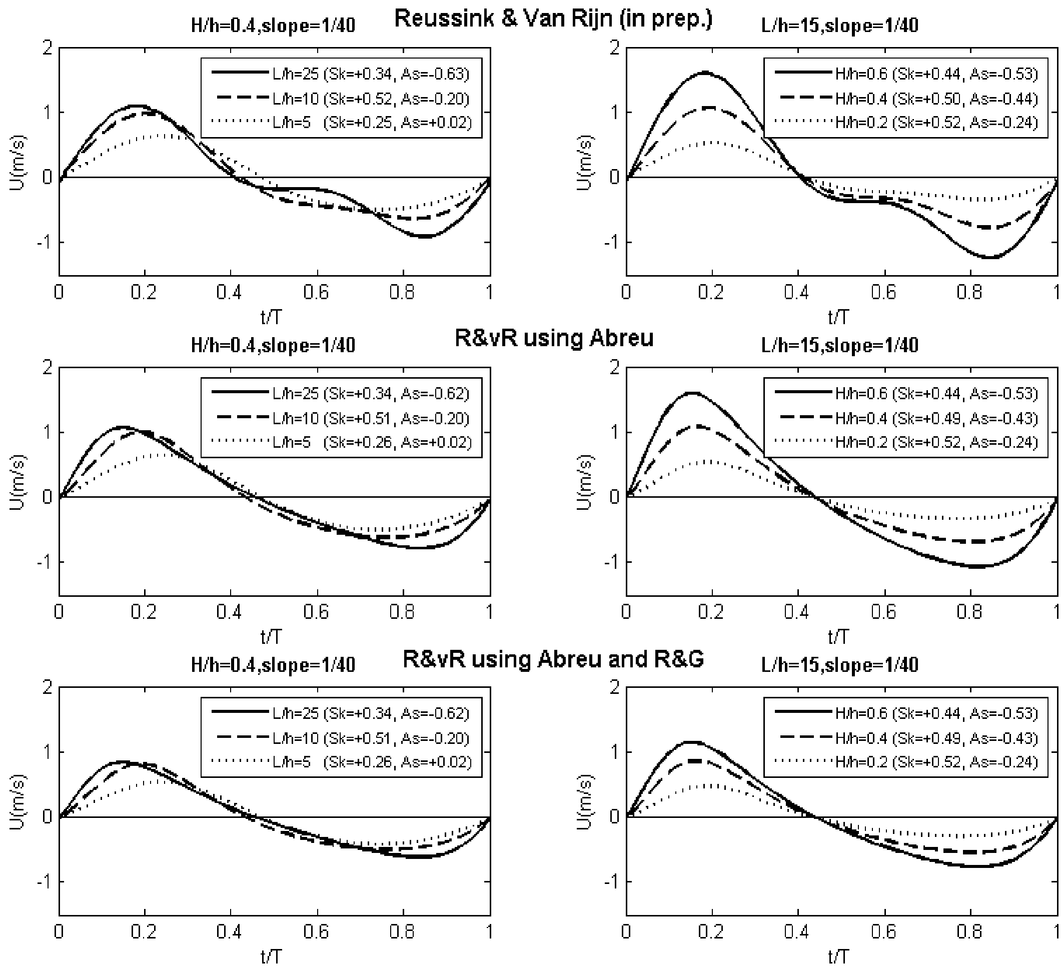

Figure_Apx B-6: Theory of Ruessink & Van Rijn (in preparation, upper two figures) compared to the adjusted version using the formula of Abreu et al. (2010, middle two figures) and to the second adjusted version using the formula of Abreu et al. (2010) and the formula of Ruessink & Grasmeijer (2003) for the amplitude definition.

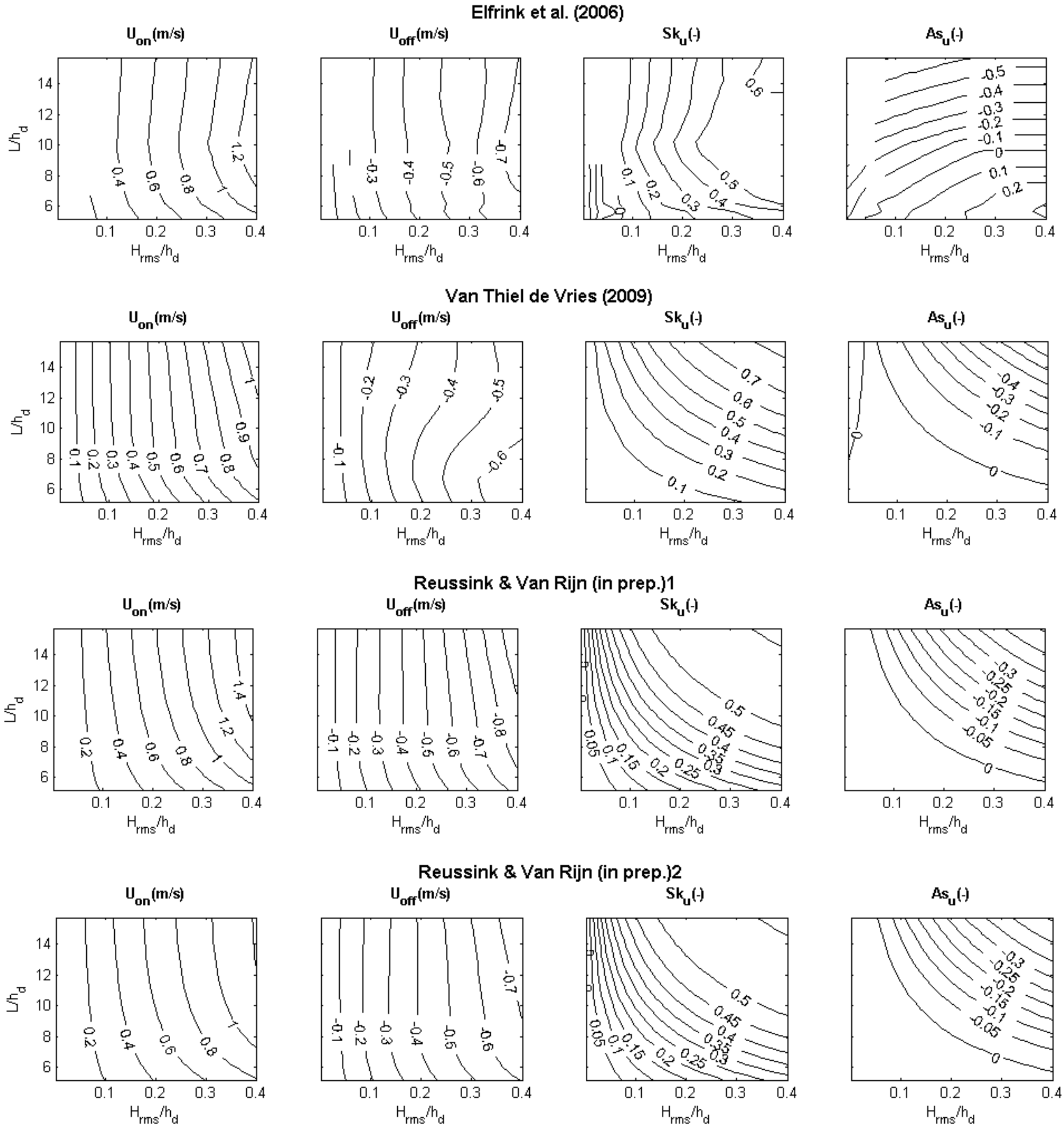

Figure_Apx B-7: Orbital velocity characteristics based on the different orbital velocity theories for depth h_d = 4 m. Comment: R&vR1: amplitude based on linear wave theory, R&vR2: amplitude modified based on Grasmeijer and Ruessink (2003)

B.3.3. Measurements of Skewness and Asymmetry in the field

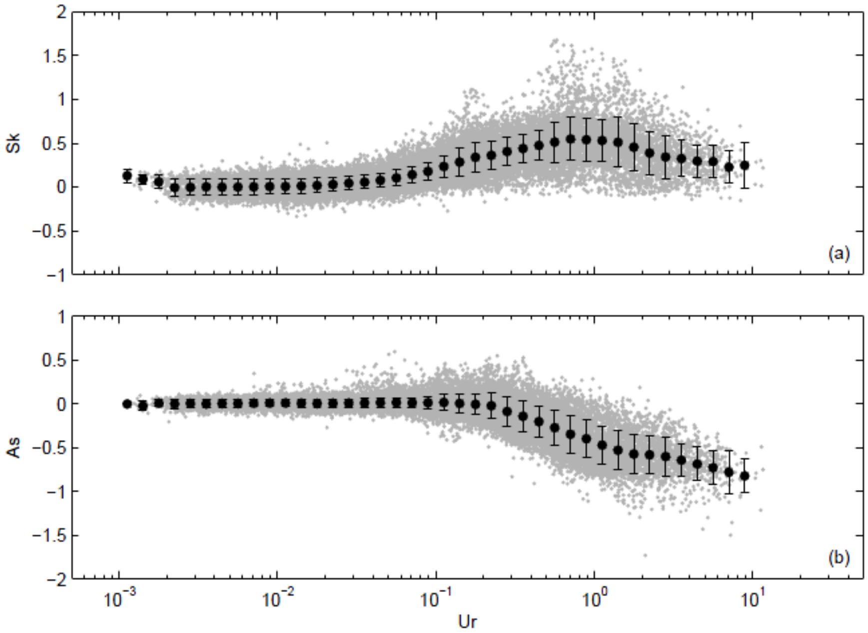

Figure_Apx B-8: (a) Skewness Sk and (b) asymmetry As as a function of the Ursell number Ur. The grey dots are the 30.617 individual estimates, the filled circles are class-mean values based on binning the individual estimates according to log(Ur) +/- 0.05. The vertical lines represent one standard deviation in each bin (Ruessink & Van Rijn, in preparation).

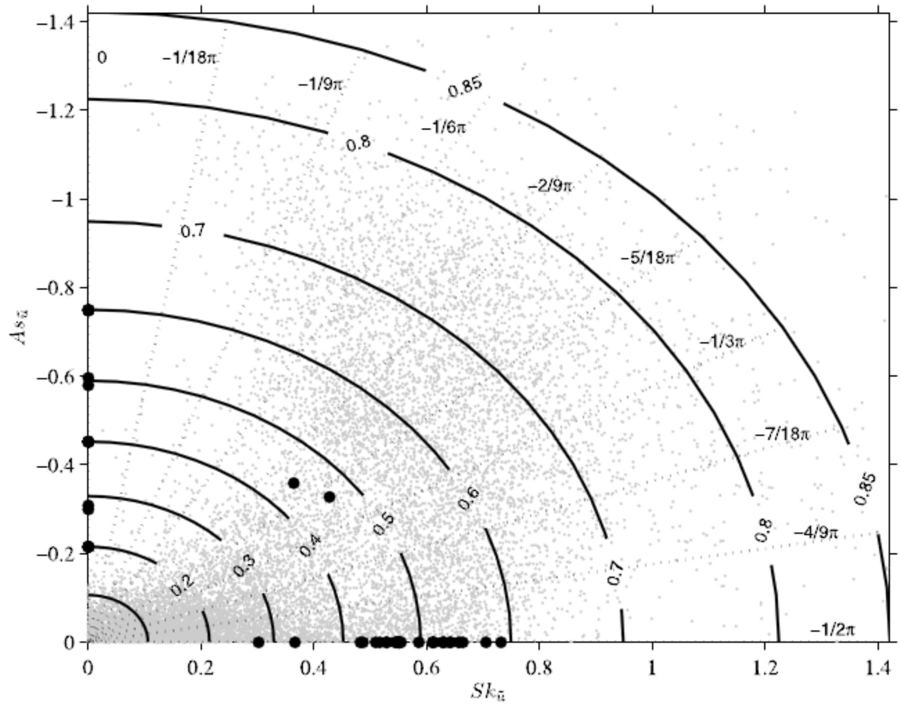

Figure_Apx B-9: Scatterplot of observed velocity asymmetry As versus velocity skewness Sk, the solid (dotted) black lines are r_{Abreu} (φ_{Abreu}) contours (Ruessink, et al., 2009).

C. Description FORTRAN codes

In this appendix a description is given of the different FORTRAN files of the SANTOSS model. Changes to the original matlab code and important assumptions are clearly described. The SANTOSS code is subroutine of the subroutine TRANSP.FOR in the UNIBEST-TC code. Next to these codes, also some changes are made to the subroutines for the orbital velocities and a new subroutine is generated for the new developed orbital velocity theories.

SANT207.for (several changes)

This is the main code of the SANTOSS-model which converts the input, calls all the subroutines and converts the output.

Input	Output
rnu (kin. viscosity), H, D50, D90, rhos, rhow, hw, tp, theta, uxmean, uymean, Zref, Pcr, g, deltabl, dzbdcs, dzbdls, n, m, nt, tanphi, ubotx, uboty, u1, Keys: SWLONG, PL_EFFECTS, SW_EFFECTS, AS_EFFECTS, RIPPLE_PRED, DELTABL_SETT, SFLT_SETT, SFLT_W_C	Qs_cs (cross-shore transport), Qs_ls (longshore transport), deltabl (wave boundary layer thickness)

Wave orbital velocity characteristics

The wave orbital velocity is represented by a time serie which might represent:

- A wave group of 7 irregular waves (SWLONG = 1 → Amplitude modulation, plus bound long wave).
- 7 regular waves (SWLONG = 3 → No amplitude modulation, no bound long wave)

The chosen time series is given as input by the components u_{botx} and u_{boty}. The time series u1 (regular waves) is in any case needed to calculate the ripple characteristics and the current velocity at the edge of the boundary layer.

In the original SANTOSS code the near bed orbital velocity characteristics for crest and trough are used including the skewness R and asymmetry β. The skewness and asymmetry are used to calculate the (partial) periods. In this case the orbital velocity characteristics are extracted from the orbital velocity time series using the subroutine **SANTorb.for** (which is used instead of the function **wctp.m** in the original SANTOSS code.

First the characteristics of the regular and irregular waves are defined:

- The subroutine **SANTorb.for** is called to determine the maximum orbital velocities of u1 (regular waves). These maximum crest and trough velocities are used to determine the characteristic orbital velocity amplitude and the characteristic orbital excursion amplitude.
- The subroutine **SANTorb.for** is called to determine the maximum orbital velocities of ubot (irregular waves or regular waves) for each crest and trough. For each crest and trough the characteristic orbital velocity amplitude, the excursion amplitude and the wave height are rescaled.

Because the ripple characteristics do not instantaneously react on the wave characteristics, but will adjust slowly to the average characteristics. This is why the the maximum crest and trough velocities of regular waves are used to compute the wave height and wave length (**SANTripple.for**).

To calculate the Shields parameter first the current velocity at the edge of the wave boundary layer will be calculated. Because the wave boundary layer and the friction coefficients will continuously change under the irregular waves, the characteristics of the regular waves (horizontal displacement diameter **aw**) are used to calculate one representative current velocity at a representative wave boundary layer thickness (**SANTbss1.for**).

The subroutine **SANTorb.for** is now called with both the wave orbital velocity time series and the mean near bed velocity to calculate the final near bed orbital wave + current characteristics.

Now for each measured crest and trough in the time series, the friction coefficients and the (representative and peak) Shields parameters are calculated:

- The subroutine **SANTbss1.for** is called to define the friction coefficients for every separate crest and trough using the rescaled characteristic orbital velocity (uw), horizontal displacement diameter (aw) and wave height (hw).
- The subroutine **SANTbss2.for** is called two times per crest and trough to define the representative Shields Stress and the peak Shields stress. Also the influence of the surface waves on the by the sediment grain experienced (partial) periods is calculated.

Several variables are now defined

- The slopes per crest and trough are defined using the direction of the representative Shields stresses and the slopes in cross-shore and long-shore direction. The slopes and the angle of natural bank are used to define per crest and trough the influence factors for the critical shear stress and the entrained sediment load.
- The critical bed shear stress is defined using the formula of Soulsby (1997) and corrected by the slope influence factor per crest and trough.
- The subroutine **SANTsflt.for** is called to calculate the sheet flow layer thickness based on the theories of Dohmen-Janssen (1999).
- The fall velocity of suspended sediment is calculated using the formula of Soulsby (1997).

The subroutine **SANTcore.for** is called to define per crest and trough the phase lag parameter, the sediment loads and the transport rates.

The output (transport rates) need to be converted to the right coordinate system (transport rates in cross-shore and long-shore direction)

SANTorb.for (completely new)

Input	**Output**
Ubot, m, n, unet, ang	dum_periods, uc, ut, ucx, utx, ucy, uty, ucrepr, utrepr, ucxrepr, utxrepr, ucyrepr, utyrepr, Tc, Tt, Tcu, Ttu, Tcd, Ttd

In this code the time series of the near-bed orbital velocity that is given by UNIBEST-TC will be analyzed and several elements will be extracted. The time serie is m wave peak periods long with n values per wave period.

The option is added to include the mean velocity. In this case the vector component of the mean velocity in the direction of the wave propagation direction is added to the time serie (so ubot(t) = u(t) + umean*cos(ang), with ang is the angle between the wave propagation direction and the direction of the mean flow velocity).

From the time serie the next elements are extracted.

- Local maximum and local minimum velocities and the corresponding time moments.
- Negative-positive and positive-negative zero-crossing moments in time.
- Periods (Tc and Tt) and partial periods (Tcu, Tcd, Ttu and Ttd) are defined using the zero-crossings moments and the moments at which the maximum velocities are reached.
- For each half cycle (crest and trough) the representative (rms) near bed velocity has been defined.

A local maximum in the time series corresponds to a crest period which should be found around that maximum. However, when the velocity is still negative (off-shore directed) this means that no crest can be really defined. To make a representative model as possible, in this case a crest period will be added at the maximum with a period of T_c = 0 seconds. This means in principle that there will be two consecutively troughs (for an example see Figure_Apx C-1)

This code will be used 3 times at each location for every time step:

- To define the near bed orbital velocity parameters for regular waves
- To define the near bed orbital velocity parameters for the wave group of 7 irregular waves.
- To define the orbital velocity parameters for the 7 irregular waves including the net velocity.

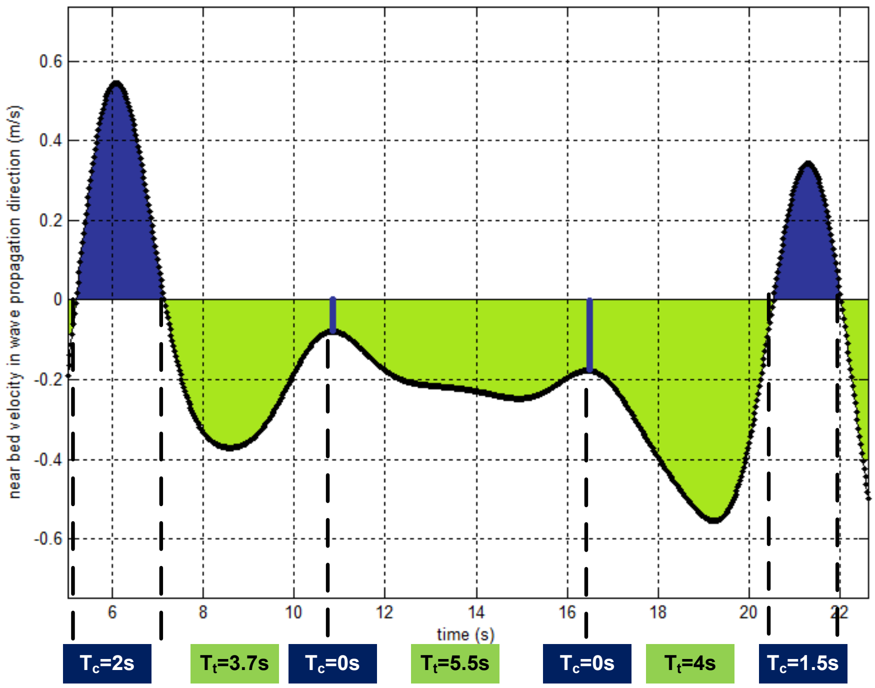

Figure_Apx C-1: Practical application of half-cycle approach when crest and trough are not always visible.

SANTripple

Input	Output
D50, Delta, aw, uwc, uwt Key: RIPPLE_PRED	Rh, Rl

This is the code which calculates the ripple height and length. Because ripple react slowly on the change in waves, the characteristics of the regular wave time serie (uwc_reg, uwt_reg and aw_reg) are used to calculate the height and length of the ripples. If option RIPPLE_PRED = 0 then Rh = 0 and Rl = 0.

SANTbss1.for (small changes)

This is the first part of the bed shear stress function of the original matlab code with the goal to calculate the wave friction coefficient (excluding acceleration effect), the current friction coefficient and the mean velocity at the edge of the wave boundary layer.

Input	Output
H, D50, D90, Delta, rhos, rhow, aw, uw, Unet, Ang, Zref, Rh, Rl Keys: DELTABL	ksw, ksc, fc, fw, fcw, unet_deltabl, alpha

- Initial roughness sheet flow regime + current roughness
- Additional roughness if wave-averaged total Shield stress parameter > 1
- While-loop to find real Shields parameter
- Additional roughness in case of ripples (k_{sw}, k_{sc} and f_w and f_{cc} are defined)
- Added option of calculation of the wave boundary thickness (DELTABL = 1/0): Option DELTABL = 0: edge of wave boundary layer is estimated at 20 cm above the bed. Option DELTABL = 1: Definition of the thickness of the wave boundary layer using Sleath (1987).
- Calculation of the current velocity at the edge of the wave boundary layer

Because in the case of a wave group the irregularity in time will lead to always changing friction coefficients and boundary layer thicknesses, the current velocity at the edge of the boundary layer will change too. This code will be used 1 time with the parameters of the regular waves to make an estimate of the current velocity at the edge of the wave boundary layer. This current velocity will after that used to redefine the near bed velocity characteristics (using SANTorb.for). **Later this code will be used to calculate the friction coefficient per individual crest and trough. The horizontal displacement diameter (A_w) will be rescaled per crest and trough (with a minimum value to prevent A_w = 0 m)**

SANTbss2.for (small changes)

This is the second part of the bed shear stress function of the original matlab code with the goal to include the effect of asymmetry on the friction factors, the resulting bed shear stress and the additional wave Reynolds stress and finally the calculation of the (partial) periods that are experienced by the sediment grains.

Input	Output
pi, H, D50, D90, Delta, rhos, rhow, g, T, Tc, Tt, Tcu, Ttu, Tcd, Ttd, uw, aw, uw_c, uw_t, aw_c, aw_t, unet_deltabl, ang, alpha, uwc, uwt, ucx, utx, ucx, ucy, utx, uty, uc, ut, ksw, fc, fcw. Keys: SW_EFFECTS, AS_EFFECTS	c, Swc, Swt, Sc, St, Scx, Scy, Stx, Sty, Tc_exp, Tt_exp, Tcu_exp, Ttu_exp, Tcd_exp, Ttd_exp

The script has been runned twice per crest and trough: using the peak and the representative velocities resulting in peak stresses and representative stresses:

Steps in script:

- Acceleration effect on the friction coefficient has been calculated for each crest and trough individually.
- Shields parameters are calculated using the friction coefficient and the velocities **(if crest or trough period is zero seconds, the Shields parameter is 0).**
- The additional wave Reynolds stress in the direction of wave propagation is calculated using the wave height **(wave height is rescaled per crest and trough based on characteristic orbital velocities)**.
- The calculation of the experienced periods is a little bit changed by estimating the wave period as being twice the concerned half-cycle period (so 2Tc or 2Tt).

SANTsflt.for (no modifications on code)

Input	Output
D50, Sc, St, Swc, Swt Keys: SFLT_SETT, SFLT_W_C	SFLTc, SFLTt

This code calculates the sheet-flow layer thickness for the crest and the trough using the method of Dohmen-Janssen (1999) or the method of Ribberink (2008) and the option to use the Shields parameters based on only waves (SFLT_W_C = W) or waves and currents (SFLT_W_C = WC).

SANTcore.for (several modifications)

Input	Output
pi, g, D50, H, Rhos, rhow, Delta, tp, m, r, hw_c, hw_t, Tc_exp, Tt_exp, Tcu_exp, Ttu_exp, SFLTc, SFLTt, wss, Rh, Scr_c, Scr_t, Screpr, Strepr, Scxrepr, Scyrepr, Stxrepr, Styrepr, fsantoss_n, fsantoss_m, fsantoss_alphas, fsantoss_alphar, fsl_omega_c, fsl_omega_t, dum_periods, Pcr Keys: SW_EFFECTS, PL_EFFECTS, AS_EFFECTS, SWLONG	Pc, Pt, Oc, Occ, Oct, Ot, Ott, Otc, Qsx, Qsy, Phix, Phiy, Phicx, Phicy, Phitx, Phity

In this code:

- Phase lag parameter defined per crest and trough based on sheet-flow layer thickness or ripple height, deceleration periods and the vertical velocity. **Edit Nomden (2010): vertical wave orbital velocity is defined at the level of 3 times the sheet-flow-layer thickness or (in case of ripples) at 3 times the ripple height (discrepancy between SANTOSS-report and code). Additionally: when a crest or trough period is zero seconds (dummy period) the phase lag parameter cannot be calculated and is defined as 1.**
- Representative Shields stresses per crest and trough are translated into entrained sediment loads **(using critical Shields Stress and slope effects per crest and trough)**.
- Transport components are calculated in normal manner per crest or trough using acceleration effect. When crest or trough period is zero seconds the transport components are also zero. In this case the sediment load coming from the previous half cycle is directed to the next half cycle (so if crest is zero seconds the sediment load coming from the previous trough is directed towards the next trough).

The keys are implemented in the code to exclude (0) or include (1) the surface wave effects (SW_EFFECTS), phase lag effects (PL_EFFECTS) or the asymmetry effects (AS_EFFECTS). Also the options for the calculation of the sheet flow layer are included (SFLT_SETT = D99/R08 and SFLT_W_C = W/WC)